

Methods to assess the coronary circulation by guidewire-mounted sensors

Citation for published version (APA):

Geven, M. C. F. (2007). *Methods to assess the coronary circulation by guidewire-mounted sensors*. [Phd Thesis 1 (Research TU/e / Graduation TU/e), Biomedical Engineering]. Technische Universiteit Eindhoven. <https://doi.org/10.6100/IR629343>

DOI:

[10.6100/IR629343](https://doi.org/10.6100/IR629343)

Document status and date:

Published: 01/01/2007

Document Version:

Publisher's PDF, also known as Version of Record (includes final page, issue and volume numbers)

Please check the document version of this publication:

- A submitted manuscript is the version of the article upon submission and before peer-review. There can be important differences between the submitted version and the official published version of record. People interested in the research are advised to contact the author for the final version of the publication, or visit the DOI to the publisher's website.
- The final author version and the galley proof are versions of the publication after peer review.
- The final published version features the final layout of the paper including the volume, issue and page numbers.

[Link to publication](#)

General rights

Copyright and moral rights for the publications made accessible in the public portal are retained by the authors and/or other copyright owners and it is a condition of accessing publications that users recognise and abide by the legal requirements associated with these rights.

- Users may download and print one copy of any publication from the public portal for the purpose of private study or research.
- You may not further distribute the material or use it for any profit-making activity or commercial gain
- You may freely distribute the URL identifying the publication in the public portal.

If the publication is distributed under the terms of Article 25fa of the Dutch Copyright Act, indicated by the "Taverne" license above, please follow below link for the End User Agreement:

www.tue.nl/taverne

Take down policy

If you believe that this document breaches copyright please contact us at:

openaccess@tue.nl

providing details and we will investigate your claim.

**Methods to assess the coronary
circulation by
guidewire-mounted sensors**

A catalogue record is available from the Eindhoven University of Technology Library

ISBN: 978-90-386-1104-4

Copyright ©2007 by M.C.F. Geven

All rights reserved. No part of this book may be reproduced, stored in a database or retrieval system, or published, in any form or in any way, electronically, mechanically, by print, photoprint, microfilm, or any other means without prior written permission of the author.

Cover design: Oranje Vormgevers, Eindhoven, The Netherlands

Printed by Universiteitsdrukkerij TU Eindhoven, Eindhoven, The Netherlands.

This research was financially supported by the Dutch Technology Foundation STW, project EPG 5454. The financial support of Radi Medical Systems, and Stichting Vrienden van het Hart Zuidoost-Brabant was gratefully acknowledged.

Methods to assess the coronary circulation by guidewire-mounted sensors

PROEFSCHRIFT

ter verkrijging van de graad van doctor
aan de Technische Universiteit Eindhoven,
op gezag van de Rector Magnificus, prof.dr.ir. C.J. van Duijn,
voor een commissie aangewezen door het College voor Promoties
in het openbaar te verdedigen op
donderdag 4 oktober 2007 om 16.00 uur

door

Maartje Cornelia Francisca Geven

geboren te Geldrop

Dit proefschrift is goedgekeurd door de promotoren:

prof.dr.ir. F.N. van de Vosse

en

prof.dr. N.H.J. Pijls

Copromotor:

dr.ir. M.C.M. Rutten

Contents

Summary	ix
1 Introduction	1
1.1 General introduction	1
1.2 (Patho)physiology of the coronary arterial system	2
1.3 Mathematical and experimental models describing the coronary circulation	4
1.4 Clinical diagnosis of coronary disease	6
1.5 Diagnostic methods	6
1.5.1 Coronary angiography	6
1.5.2 Physiologic indices of coronary disease	8
1.5.3 Proposed methods for flow assessment	10
1.6 Aim and outline of the thesis	11
2 A physiologically representative <i>in-vitro</i> model of the coronary circulation	13
2.1 Introduction	14
2.2 Materials and methods	15
2.2.1 Modelling conditions	15
2.2.2 The lumped parameter mathematical model	16
2.2.3 The <i>in-vitro</i> experimental model	19
2.3 Results	22
2.3.1 The lumped parameter mathematical model	22
2.3.2 The <i>in-vitro</i> experimental model	25
2.4 Discussion	26
2.4.1 Modelling: physiological basis	26
2.4.2 The lumped parameter mathematical model	27
2.4.3 The <i>in-vitro</i> experimental model	27
2.4.4 Limitations	27
2.4.5 Extended applications	28
2.5 Conclusions	28
2.6 Acknowledgements	28

3	From bedside to bench: a physiologically representative <i>in-vitro</i> model to evaluate catheter-based intracoronary diagnostic techniques	29
3.1	Introduction	30
3.2	Materials and methods	31
3.2.1	<i>In-vitro</i> experimental model	31
3.2.2	Background of the clinical indices FFR and IMR	32
3.2.3	FFR and IMR measurement in this study	35
3.2.4	Statistical analysis	36
3.3	Results	36
3.4	Discussion	37
3.5	Limitations	42
3.6	Conclusion	42
3.7	Acknowledgements	42
4	Continuous infusion thermodilution for assessment of coronary disease: theoretical background and <i>in-vitro</i> validation	43
4.1	Introduction	44
4.2	(Theoretical) background	46
4.2.1	Measurement principle	46
4.3	Methods	48
4.3.1	<i>In-vitro</i> model of the coronary circulation	48
4.3.2	Infusion catheters	49
4.3.3	Procedures	49
4.4	Results	50
4.4.1	Guidewire pullback	50
4.4.2	Flow measurement at fixed position	50
4.4.3	Position of infusion catheter	52
4.5	Discussion	52
4.6	Clinical implications	57
4.7	Conclusions	57
4.8	Acknowledgements	57
5	PressureWire thermoconvection flow measurement: background and experimental evaluation	59
5.1	Introduction	60
5.2	Materials and methods	61
5.2.1	Analytical description: general hot-film models	61
5.2.2	PressureWire®	62
5.2.3	Specific problems in PW application	63
5.2.4	Measurement set-up	63
5.2.5	Characterization of the relation between flow and electrical power	65
5.2.6	Data analysis	66
5.3	Results	67
5.3.1	Overheat variation	67

5.3.2	Small changes in ambient temperature	71
5.3.3	Geometrical boundary conditions	72
5.3.4	Different wires	72
5.3.5	Steady flow: stationary flow and heat transfer	72
5.3.6	Unsteady flow	73
5.3.7	Coronary flow	75
5.4	Discussion	81
5.5	Conclusions	83
6	PressureWire thermoconvection flow measurement: animal validation	85
6.1	Introduction	86
6.2	Methods	86
6.2.1	Physical background of thermoconvection flow measurement	86
6.2.2	Application to the pressure guidewire	87
6.2.3	Animal preparation	87
6.2.4	Measurements in the LAD	88
6.2.5	Data analysis	88
6.3	Results	88
6.3.1	Procedural results and hemodynamic characteristics	88
6.3.2	Raw data: time-based registration of electrical power and reference flow	89
6.3.3	Thermoconvection derived flow versus reference flow	90
6.4	Discussion	90
6.4.1	Limitations	90
6.4.2	Clinical implications	93
6.5	Conclusions	93
6.6	Acknowledgements	93
7	General discussion and conclusions	95
7.1	Modelling of the coronary circulation	95
7.2	Continuous infusion coronary flow measurement	96
7.3	Thermoconvection coronary flow measurement	97
7.3.1	Ethical considerations for the use of the swine model	99
7.4	Thermoconvection or continuous infusion?	99
7.5	Conclusions	99
A	Background of hot-film anemometry	101
A.1	Introduction	101
A.2	Governing equations	101
A.2.1	Conservation of mass, momentum and energy	101
A.2.2	Scaling	103
A.3	Steady flow and heat transfer	105
A.3.1	Boundary layer theory	105
A.4	Analysis of the hot-film anemometer	107
A.4.1	First order approximation	107

A.5 Unsteady flow and heat transfer	108
A.5.1 Partially heated flat plate	108
A.5.2 Substrate-mounted hot-film	109
A.6 Concluding discussion	111
References	113
Samenvatting	121
Dankwoord	125
Curriculum Vitae	127

Methods to assess the coronary circulation by guidewire-mounted sensors

Summary

Disease in the coronary circulation can cause local blood flow impediment anywhere in the vascular system of the heart, from the larger epicardial vessels to the capillaries in the microcirculation. The disease may lead to severely increased resistance to blood flow resulting in myocardial ischemia. In the catheterization laboratory, the initial approach to investigate coronary disease is to perform coronary angiography: by injecting contrast medium the epicardial coronary arteries are made visible on X-ray film. However, in this way only a two-dimensional, qualitative assessment is made, easily over- or underestimating the physiological significance of disease. To obtain direct knowledge on the resistance to flow, quantitative information regarding blood pressure and flow is needed. Pressure and flow can be measured during catheterization by means of sensor-tipped guidewires introduced into the arterial system through the groin. From the practical point of view, it is desirable to have one single sensor-tipped wire equipped to measure both pressure and flow.

The main aim of the study described in this thesis was to develop a method for simultaneous assessment of coronary pressure and flow by a single guidewire, the pressure-temperature sensor-tipped PressureWire (Radi Medical Systems, Uppsala, Sweden). Hereto well-controlled experimental evaluation conditions were mandatory. Practically, *in-vivo* experiments are often limited in controlling relevant parameters and moreover, from the ethical point of view, alternatives for evaluation in animal models or patients are desirable. Therefore a second focus of the work described in this thesis was to design and use an *in-vitro* model of the coronary circulation for well-controlled evaluation circumstances.

The design of the *in-vitro* model was based on physiologically representative functional elements for the relevant components of the circulation, both regarding

their geometry and function. The model consisted of a computer-controlled pump mimicking the left ventricle, a systemic and a coronary circulation. The systemic circulation was used to obtain a physiological aortic pressure, as an input for the coronary circulation. Distal to the epicardial tube representing the coronary artery, the myocardial vascular bed was divided into a subendocardial and subepicardial branch. A collapsible tube, led through the left ventricle and collapsed by the ventricular pressure, represented the variable resistance and volume behaviour of the endocardial part of the myocardium. The evaluation of the model was carried out twofold. First, the pressure and flow signals were found to correspond closely to patterns and values obtained in conscious human. Secondly, two well-validated catheter-based diagnostic techniques as used in the human catheterization laboratory (FFR and IMR, for characterization of epicardial and microvascular disease, respectively) were assessed in the well-controlled *in-vitro* situation. The *in-vitro* model accurately reproduced the indices in accordance with clinical observations. Hence the model's reciprocal usefulness for research and development of coronary diagnostic techniques was confirmed.

Two new methods for coronary flow assessment were introduced and initially evaluated *in-vitro*. The first was continuous infusion coronary flow measurement. When the saline is continuously infused into the coronary artery, blood flow may be calculated from the temperature of the blood, the saline, and the mixture downstream to the infusion site, combined with the known infusion rate. The principle of measurement was evaluated in the *in-vitro* coronary model assessing the boundary conditions for accurate flow measurement by variation of infusion catheter design, infusion rate, and location of infusion and temperature measurement. Using an appropriate catheter and high enough infusion rate, accurate determination of mean coronary flow was possible.

Using continuous infusion the mean coronary blood flow may be derived. However, also the phasic nature of flow is of clinical importance. Furthermore, a clinical methodology should be as little complicated as possible, whereas for continuous infusion an extensive protocol and additional equipment have to be used. To better meet these requirements for clinical application, a second method for flow assessment described in this thesis was the thermoconvection method.

The principle of thermoconvection flow measurement is that of hot-film anemometry. A resistance located at the PressureWire sensor was kept at a constant overheat above ambient temperature. The electrical power needed to maintain the temperature difference was related to the local flow. The theoretical relation between electrical power and flow was used to calibrate the sensor in stationary and mean instationary flow in a glass tube and in the coronary model. Calibration in mean flow was successful: flow could be determined at an accuracy comparable to that of the continuous infusion method. The dynamic response was also determined evaluating flow estimated from the calibration curve over time. The pattern of phasic flow could be clearly recognized, but further research including numerical simulations is needed to determine the direct transfer function between the estimated and real flow.

The thermoconvection method has also been evaluated in an animal study. In three Yorkshire swine instrumented with an epicardial flow meter for reference

flow, the electrical power and reference flow signals were recorded. The *in-vitro* determined calibration curves were found to be appropriate for *in-vivo* application and accuracy of mean flow determination was found to be comparable to that of the *in-vitro* study.

Two novel techniques of coronary flow assessment were developed and evaluated. To facilitate the development process a model of the coronary circulation was designed and used. Continuous infusion involves a complex protocol and careful consideration of boundary conditions, but may directly be applied in the catheterization laboratory for determination of mean flow. Thermoconvection is a very easily applicable method, potentially valuable for clinical assessment of mean and phasic coronary flow. However, thermoconvection requires further numerical, *in-vitro*, and *in-vivo* (clinical) validation studies.

Chapter 1

Introduction

1.1 General introduction

Disease in the coronary circulation can cause local blood flow impediment anywhere in the vascular system of the heart, from the ostium of the epicardial coronary arteries to the microcirculation. Progression of disease can be slow and remain unnoticed until severely increased resistance to blood flow results in myocardial ischemia (Gould, 1999). The nature of the disease can vary from a local epicardial stenosis to more diffusely diseased vessel walls or increased resistance in the myocardial microvasculature.

The current initial approach to investigate coronary disease in the catheterization laboratory is to perform coronary angiography. By injecting contrast medium the epicardial coronary arteries are made visible on X-ray film, a methodology already available since the 1960's (Sones and Shirey, 1962; Judkins, 1967). A drawback of this method is that it is a qualitative morphological diagnostic tool, while quantitative information regarding physiological parameters such as blood pressure and flow is needed to come to a more accurate diagnosis and treatment (Little et al., 1988; Gould et al., 1990). Pressure and flow can be measured during catheterization by means of sensor-tipped guide-wires introduced into the arterial system through the groin. To obtain direct knowledge on the resistance to blood flow, pressure and volumetric flow should be determined simultaneously. The resistance equals the ratio of the pressure difference and flow rate (De Bruyne et al., 1996; Meuwissen et al., 2002). From the practical point of view, it is desirable to have one single sensor-tipped wire equipped to measure both pressure and flow. In previous studies wires combining pressure sensors and Doppler flow probes were used (Siebes et al., 2004). A drawback to these wires is that it is difficult to obtain a high-quality Doppler signal and that flow rate needs to be derived from flow velocity by an estimate of the luminal area from the angiogram.

The main aim of the study described in this thesis is to develop a method for simultaneous assessment of coronary pressure and direct flow by a single guidewire, the pressure-temperature sensor-tipped PressureWire (Radi Medical Systems, Uppsala,

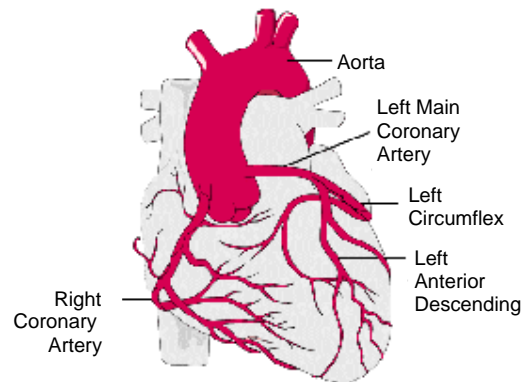


Figure 1.1: The coronary arteries (after Putz and Pabst, 1994)

Sweden). Hereto well-controlled evaluation conditions are mandatory. Practically, *in-vivo* experiments are often limited in controlling haemodynamic conditions and possibilities for calibration measurement of relevant parameters. Moreover, from the ethical point of view, alternatives for *in-vivo* evaluation in animal models or patients are desirable. Because for the studies on combined pressure and flow measurement as described above multiple and repeated testing under controlled conditions were mandatory, at first a suitable representative model of the coronary circulation had to be developed. Therefore a second focus of the work described in this thesis is to design and use such an *in-vitro* model of the coronary circulation. In the following sections, a background is given on the (patho)physiology of the coronary arterial system, the clinical diagnostic pathway for coronary disease, and diagnostic methods currently used in the catheterization laboratory. Furthermore, the work described in this thesis will be introduced: the novel methodologies for flow measurement, and the modelling of the coronary circulation.

1.2 (Patho)physiology of the coronary arterial system

The contractions of the heart are vital for the circulation of blood through the lungs to exchange carbon dioxide and oxygen, to supply the entire body with oxygen and nutrients and dispose of metabolic waste products, and to regulate body temperature. However, the heart itself is a muscle and needs to be perfused as well as any other organ. Although the endocardium is in continuous contact with blood flowing through the heart, endocardial exchange is insufficient: the heart receives its nutritional blood supply almost entirely from the coronary circulation. This

circulation (figure 1.1) consists of the coronary arteries, originating from the aorta near the aortic root and having a typical diameter of approximately 3 mm, branching into smaller arteries and arterioles, and eventually into an interconnected network of small capillaries (\varnothing 5 μ m) forming the coronary microvasculature perfusing the myocardium. Here the actual exchange of oxygen, nutrients and metabolic waste products occurs. After passing the myocardium the blood flows back to the right atrium via the coronary veins and through the coronary sinus.

In a healthy coronary circulation the resistance of the larger coronary vessels is negligible compared to the resistance of the microcirculation (Pijls et al., 1995). The arterioles, the smaller arteries forming the transition between the larger vessels and the microvasculature, contain smooth muscle cells and can regulate the resistance of the vascular bed according to the oxygen demand. During exercise the oxygen demand increases, and the myocardial resistance can be decreased by relaxation of the arterioles such that the myocardial flow can increase up to four to six times the value in resting (baseline) conditions in healthy humans (White, 1993).

Characteristically, coronary flow to the left ventricle predominantly occurs in diastole (the relaxation phase of the cardiac cycle), while it is primarily driven by aortic pressure. Already in early years an explanation for this phenomenon has been found in the influence of left ventricular contraction on the subendocardial myocardium, resulting in an increase in the resistance to flow during the systolic (contraction) part of the cardiac cycle (Porter, 1898). Typical values for systolic and diastolic pressure are 120 and 80 mmHg, respectively. Baseline flow in the left anterior descending artery (LAD) is in the range of 50 ml/min, the flow rate during diastole about twice as high as during systole. During hyperemia, flow in a main epicardial coronary artery may increase up to 250-300 ml/min (figure 1.2).

In a normal coronary artery, under normal physiological circumstances, coronary blood flow is primarily determined by variations in arteriolar resistance, keeping flow constant over a large range of blood pressure and adapting blood flow in case of increased demand. This mechanism is called autoregulation. If a stenosis (narrowing) develops in an epicardial coronary only, relaxation of the arterioles can partly compensate for an increased epicardial resistance due to such coronary stenoses (figure 1.3). Hence sufficient myocardial perfusion in rest can be sustained. However, part of the autoregulatory reserve is already consumed, so during exercise perfusion can become insufficient, resulting in angina pectoris. Another mechanism to counteract the consequences of severe epicardial narrowings is the recruitment and growth of collaterals. Collaterals are vessels interconnecting the coronary arteries and bypassing obstructed areas, so that the total myocardial flow becomes the sum of epicardial coronary and collateral flow. Collaterals generally develop when a stenosis becomes functionally significant and are associated with repeated episodes of myocardial ischemia (Schaper et al., 1988).

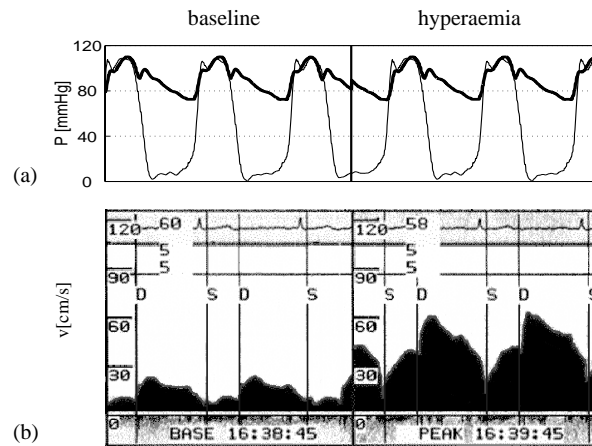


Figure 1.2: Pressure (a) and Doppler flow velocity (b) registrations in human, during baseline and hyperemia. (a) Aortic (bold) and left-ventricular pressure. Signals were subsequently obtained from one patient and the signal was copied to allow both baseline and hyperemic comparisons. (b) Doppler flow-velocity registration of left coronary artery (LCA), not taken from the same patient as in (a).

1.3 Mathematical and experimental models describing the coronary circulation

The characteristic features of the coronary system, such as the phase difference between pressure and flow, the arteriolar autoregulation and collateral contribution to myocardial flow play an important role in the implementation and understanding of diagnostic methods to assess coronary artery disease and should be incorporated in models of the coronary circulation.

Several mathematical models have been proposed in literature to explain coronary flow patterns by describing the relations between intramyocardial pressure, volume and resistance to flow. The earliest models were based on the waterfall principle (Downey and Kirk, 1975), in which the vascular bed is assumed to collapse when intramyocardial pressure exceeds intravascular pressure. This approach can describe the systolic decline in coronary flow. However, a total collapse of the vascular bed is unlikely to occur, since the coronary perfusion volume is too small to empty and refill the coronary vasculature completely in one heart beat (Arts and Reneman, 1985). Moreover, during maximum coronary hyperemia, as encountered during exercise or pharmacological stimuli and associated with increased intramyocardial pressure, a systolic flow component becomes apparent in the left coronary artery. In the intramyocardial pump model, flow variations between systole and diastole are not directly coupled to variable resistance as in the waterfall model, but to intramyocardial volume variations, by introducing the capacitance of the coronary vasculature (Spaan et al., 1981; Arts and Reneman, 1985), later adjusted to

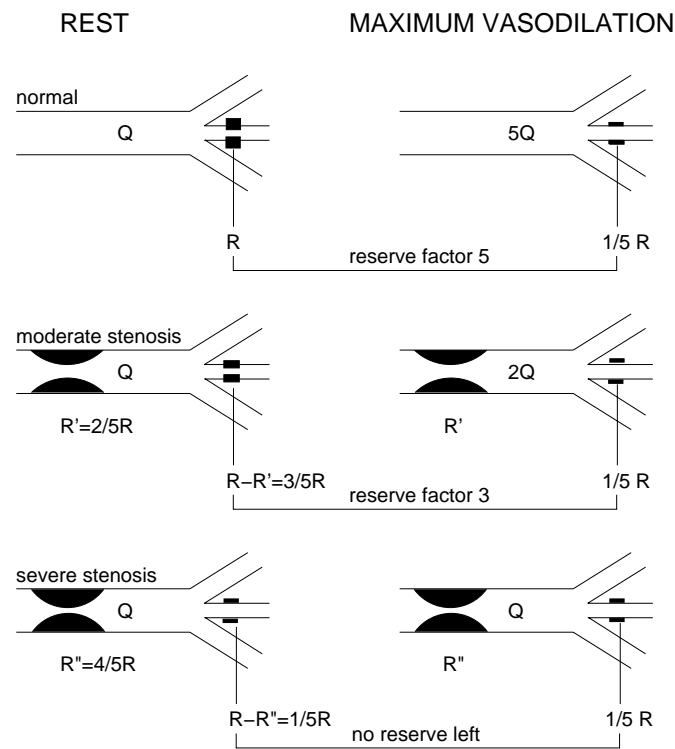
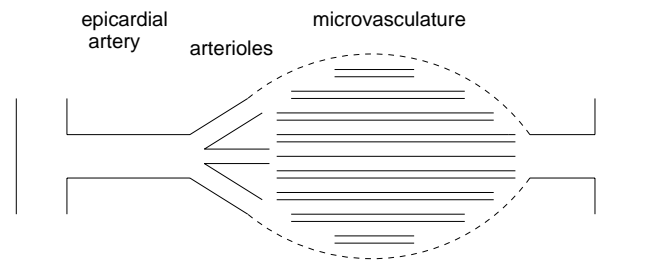


Figure 1.3: Functional compensation of increased epicardial coronary resistance by decreased arteriolar resistance.

resistances and capacitances dependent on intramyocardial pressure (Bruinsma et al., 1988). With these models correct phasic patterns of coronary artery flow could be obtained. Another approach was taken by Krams et al. (1989a; 1989c), applying the time-varying elastance model introduced by Suga et al. (1973) to the coronary circulation. He suggested relating intramyocardial volume changes to increased myocardial stiffness during the cardiac cycle. The validity of this model under low left ventricular pressure conditions was shown *in-vivo* (Krams et al., 1989a,b,c). A more extended mechanical model, incorporating the functional relation of active myocardial mechanics, perfusion and across-capillary mass transport, was introduced by Zinemanas et al. (1994). Interactions between these aspects influencing the coronary flow pattern can be properly evaluated by this model. A less complex model describing the interaction between coronary flow and cardiac mechanics with only a few parameters has been proposed by Bovendeerd et al. (2006).

Only a few *in-vitro* measurements evaluating clinical diagnostic techniques based on these models have been reported up to now (Segers et al., 1999; Matthys et al., 2001). In these set-ups the coronary circulation is driven by prescribed aortic pressure and myocardial resistance. This is a restriction on the value of these models in mimicking physiological conditions.

1.4 Clinical diagnosis of coronary disease

The clinical pathway for patients suffering from angina pectoris initially involves functional testing such as bicycle or treadmill testing, echocardiography during (pharmacological) stress, or myocardial perfusion scintigraphy, to estimate the presence and severity of inducible myocardial ischemia. Although a wide range of typical and atypical disease characteristics can be found, there are generally two possibilities for further diagnosis and treatment. Mild ischemia in a restricted area of the myocardial tissue can be treated by medication alone. Patients diagnosed with more severe ischemia or a larger area at risk, causing angina pectoris in everyday life during (minor) exercise, and insufficiently responding to medical treatment, often undergo cardiac catheterization to directly investigate the pathology of the coronary arterial system. During catheterization the interventionalist can choose for direct treatment to restore coronary conductance by balloon angioplasty (pushing the plaque aside and increasing the luminal diameter, mostly combined with the placement of a stent to prevent elastic recoil of the dilated artery). Or, in case of severe multi-vessel disease, the patient may be referred to a cardiac surgeon for bypass surgery.

1.5 Diagnostic methods

1.5.1 Coronary angiography

During catheterization, coronary angiography using contrast agent is the standard diagnostic method. The condition of the coronary arterial system is visually assessed



Figure 1.4: Angiogram of a stenosed coronary artery.

through the two-dimensional projection of the vascular system filled with contrast agent. Several limitations to this diagnostic method are well-known. The severity of an irregularly shaped stenosis may easily be over- or underestimated, as explained in figure 1.5 and confirmed in several studies on pathological findings during autopsy (Grondin et al., 1974; Isner et al., 1981). Or a large inter- and intra observer variability in the visual determination of disease is found (Beauman and Vogel, 1990). Apart from these limitations, and even more important, not only the anatomy of the stenosed vessel is of importance for diagnostics, but also functional factors such as the extent of the myocardial perfusion area of the diseased artery, the presence of collateral flow, and the resistance of the microvascular bed (Gould et al., 1990).

Hence, the severity of disease cannot only be characterized by even a reliable representation of the anatomy of the vascular system, but should also be characterized by its functional, physiological implications. For the decision whether or not a coronary artery stenosis needs to be treated, the most important parameter is the limitation of the maximum achievable blood flow as a result of that stenosis (Pijls et al., 1991), and hence the extent of inducible ischemia when the patient is sufficiently stressed (Pavin et al., 1997; Beller and Zaret, 2000).

Besides the analysis of stenosis severity by functional significance, the determination of the vulnerability of a plaque (the risk of plaque rupture) is considered to be an important issue in diagnosis and treatment of disease (Falk et al., 1995). Vulnerable plaque is generally believed to represent a mild luminal stenosis (Shah, 2003), and hence may not be characterized by assessment of maximum achievable blood flow, but by other detection techniques such as intravascular ultrasound (IVUS) (Falk et al., 1995). On the contrary, studies indicate that the overall prognosis and risk for acute myocardial infarction is related to minimum lumen area (Abizaid et al., 1999) and the presence of inducible ischemia (Boyne et al., 1997), and in a recent retrospective study plaque rupture was even found to be more often associated with presence of a severe stenosis (Frøbert et al., 2007). Direct assessment of the coronary plaque other than based on functional characteristics remains outside the scope of the work described in this thesis.

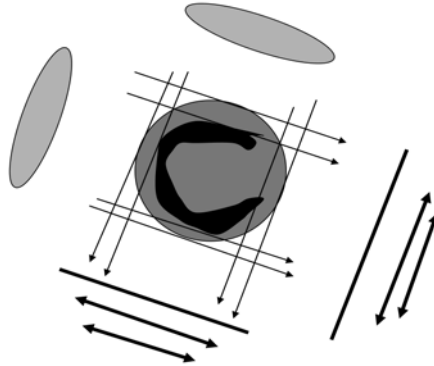


Figure 1.5: 2D projection in coronary angiography may lead to misjudgement of the functional importance of an epicardial coronary stenosis (Aarnoudse (2006)).

1.5.2 Physiologic indices of coronary disease

Because the resistance of the components of the myocardial bed (epicardial arteries, arterioles, microvasculature) cannot be directly derived due to the lack of simultaneous measurement methods of pressure and flow, indirect indices have been developed.

The vasodilatory reserve of the coronary circulation is characterized by the index referred to as the Coronary Flow Reserve (CFR), defined as mean hyperaemic flow divided by mean resting flow (Gould et al., 1990), and represents the relative decrease in resistance of the total myocardial bed between resting and hyperaemic conditions when perfusion pressure is constant.

$$\text{CFR} = \frac{Q_{max}}{Q_{rest}} \quad (1.1)$$

CFR is limited by several factors: its dependency on resting coronary blood flow, age, heart rate, arterial pressure, the broadness of the range for CFR to be considered normal, and because it does not discriminate between the microvascular and epicardial segments in the coronary circulation. To overcome these limitations, the additional concept of Fractional Flow Reserve (FFR) was developed. FFR is defined as the maximum achievable mean myocardial blood flow in presence of a stenosis (Q_{max}), divided by the maximum mean myocardial blood flow if no stenosis were present (Q_{max}^N). The main prerequisite for determining FFR is that maximum hyperemia is present, in other words, that the resistance downstream of the epicardial arteries (R) is minimal and constant. In that case blood flow is directly proportional to perfusing pressure. Consequently, the ratio of mean flows may be represented by a

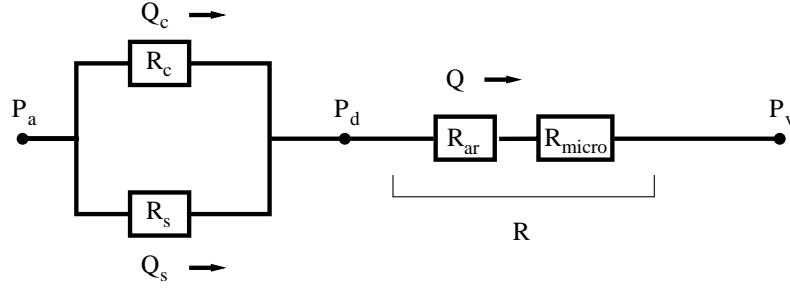


Figure 1.6: Linearized representation in resistances of the main components of the coronary circulation.

ratio of mean pressures. When the central venous pressure (P_v) is assumed equal to zero, FFR may be represented by the ratio of the mean pressure distal in the epicardial artery (P_d) and the mean main arterial pressure (P_a):

$$\text{FFR} = \frac{Q_{max}}{Q_{max}^N} = \frac{(P_d - P_v)/R}{(P_a - P_v)/R} \approx \frac{P_d}{P_a} \quad (1.2)$$

As indicated above, FFR is based on mean values for pressure and flow, and although the coronary circulation is a non-linear dynamic system, this approach was shown to be valid for quantification of the severity of coronary stenoses (Bech et al., 2001). This allows for the resistive modelling of the coronary circulation as depicted in figure 1.6. Henceforth, we will assume mean values used in indices, unless stated differently.

CFR characterizes the entire coronary vascular bed, FFR the epicardial coronary arteries, and recently, a separate index for assessment of the of the microvasculature has been developed: Index of Microcirculatory Resistance (IMR) (Fearon et al., 2003, 2004; Aarnoudse et al., 2004b; Ng et al., 2006). The resistance of the microcirculation is defined as the ratio of the perfusion pressure and the myocardial flow. For the determination of IMR the thermodilution method is used: flow is represented by the inverse mean transit time $1/T_{mn}$ of a bolus of cold saline injected into the coronary ostium. It has been shown *in-vitro* and *in-vivo* that coronary flow is inversely proportional to T_{mn} (De Bruyne et al., 2001b; Pijls et al., 2002). When a severe epicardial stenosis is present, the recruitment of collaterals implies that myocardial flow does not equal coronary flow, but the sum of coronary and collateral flow. During catheterization coronary wedge pressure can be determined at epicardial occlusion to characterize collateral flow. Hence IMR is defined as

$$\text{IMR} = (P_d - P_v)T_{mn} \frac{Q_{cor}}{Q_{myo}} = P_a T_{mn} \frac{(P_d - P_w)}{(P_a - P_w)} \quad (1.3)$$

If no stenosis is present, P_d equals P_a and IMR is simplified to $P_d T_{mn}$. The indices CFR, FFR, and IMR describe the myocardial vasculature. However, due to the lack of methods for determination of absolute flow, no direct determination of the resistances in the system is possible. As mentioned before, one of the goals of this thesis is to

assess blood flow in the coronary circulation quantitatively, enabling calculation of absolute resistance. In this thesis, two novel methods for flow measurement by the pressure-sensor tipped guidewire will be evaluated: thermodilution by continuous infusion and thermoconvection.

1.5.3 Proposed methods for flow assessment

Continuous infusion thermodilution

In conventional thermodilution a bolus of cold saline is injected into the coronary ostium, and the mean transit time T_{mn} of this bolus, registered by a temperature sensor downstream, is inversely correlated to the local blood flow. The volume of the bolus is not exactly known because part of it is lost into the aorta, introduction of the guiding catheter into the artery would largely increase coronary resistance. Hence the volumetric flow cannot be determined by the area under the thermodilution curve. Using T_{mn} , the volumetric blood flow could also be determined independently of the amount of injected indicator. However, then the vascular volume should be known, which is also not the case in current application of coronary thermodilution.

Alternatively, the saline may also be infused continuously through a small infusion catheter positioned in the artery. Theoretically, absolute blood flow may then be measured in a selective coronary artery from the mixing temperature of a known infusion rate at a known temperature, and the constant temperature of blood. More than 30 years ago continuous infusion has been proposed (Ganz et al., 1971), but was only applied for the measurement of coronary sinus flow due to technical limitations at that time. The main prerequisites for applicability of the continuous infusion method for measurement of absolute coronary blood flow are full mixing of the infusate and blood, accurate measurement of the mixing temperature, and sufficiently small dimensions of the measurement equipment. Studies to apply these principles in selective coronary arteries are described in chapter 4 of this thesis.

Thermoconvection: hot-film anemometry

The principle of thermal anemometry is used for laminar or turbulent flow and shear stress assessment in a wide range of applications (Bruun, 1996). The use of hot-films to measure flow rate in blood was initially described by Seed and Wood (1970b), Clark (1974), and Nerem et al. (1976), but equipment at that time was not miniaturized sufficiently to enable application of such a method in human coronary arteries. A hot-film sensor consists of a variable electrical resistance introduced into the blood flow. It is kept at constant temperature by adjusting the electrical current through the resistance. The electrical power needed to maintain a constant sensor temperature is a measure for the heat convectively transferred to the fluid and flow rate along the resistance. Pedley (1972a; 1972b; 1976) derived analytical solutions for heat transfer of the hot-film anemometer. Using boundary layer theory, the heat transfer from the film is calculated from the velocity gradient normal to the film, on the assumption that the probe resembles a semi-infinite flat plate. Bellhouse and Rasmussen (1968) developed a one-dimensional dynamic heat transfer model,

incorporating the capacitive effect of the backing material of the film on the thermal response. Experimental studies with various flow media were carried out by Clark (1974) and Seed and Wood (1970b) among others. Probes with diameters of order 1 mm were operated at 5°C above fluid temperature. Calibration was done in steady and oscillating flow, both in blood and in water, yielding calibration curves consistent with theory. By using the sensor of a commercially available pressure-temperature sensor-tipped guidewire (the Radi PressureWire) as a hot-film, the application of hot-film anemometry may become technically possible for coronary arteries. Studies on the feasibility of PressureWire hot-film anemometry are described in chapters 5 and 6 of this thesis.

1.6 Aim and outline of the thesis

The aim of the work described in this thesis is the development and validation of the novel thermodilution and thermoconvection measurement methods for coronary flow using the commercially available pressure-temperature sensor-tipped guidewire. The work was carried out within a project combining analytical, *in-vitro*, and clinical aspects of guidewire-based coronary circulation assessment: the clinical evaluation of methodology was outside the scope of this thesis and carried out by Aarnoudse (2006). For the validation of such methods, well-controlled evaluation circumstances are mandatory. Both from the ethical and practical point of view, there is a strong need for alternative evaluation models between the measurement design and validation in animal or patient models. Therefore, as described in chapter 2, a physiologically representative model of the coronary circulation is designed and developed, to allow for well-controlled circumstances in physiological pressure and flow regimes. In chapter 3 the model was tested and validated by an *in-vitro* validation of known clinical indices based on pressure and flow assessment such as FFR and IMR. In chapter 4, the methodology of continuous infusion flow measurement in the coronary arteries is optimized and evaluated using the physiologically representative *in-vitro* model. The clinical testing of the continuous infusion thermodilution is beyond the scope of this thesis and has been described elsewhere (Aarnoudse, 2006). In chapter 5 the development of the thermoconvection flow assessment is described. A resistance of the sensor-tipped guidewire is heated and the dynamic characterization of the relation between the sensor response (electrical power) and the flow is evaluated in flow through a glass tube and in the *in-vitro* model. The background analytical models of the heated sensor in the flow are discussed in appendix A. In chapter 6 the feasibility of hot-film flow measurement by the sensor-tipped guidewire is confirmed in an *in-vivo* study evaluating thermoconvection flow assessment in swine coronary arteries. In the last chapter the most important findings of this thesis are discussed, and a comparison between the two novel methods for coronary flow assessment is made with respect to future clinical application.

Chapter 2

A physiologically representative *in-vitro* model of the coronary circulation

With the development of clinical diagnostic techniques to investigate the coronary circulation in conscious humans, the in-vitro validation of such newly-developed techniques is of major importance. Aim of this study was to develop an in-vitro model that can mimic the coronary circulation in such a way that coronary pressure and flow signals under baseline as well as hyperemic conditions are approximated as realistically as possible and are in accordance with recently gained insights into such signals in conscious humans. In the present in-vitro model the heart, the systemic and coronary circulation are modelled based on the elements of a lumped parameter mathematical model only consisting of elements that can be represented by segments in an experimental set-up. A collapsible tube, collapsed by the ventricular pressure, represents the variable resistance and volume behaviour of the endocardial part of the myocardium. The pressure and flow signals obtained are similar to physiological human coronary pressure and flow, both for baseline and hyperemic conditions. The model allows for in-vitro evaluation of clinical diagnostic techniques.

The contents of this chapter are based on M.C.F. Geven, V.N. Bohté, W.H. Aarnoudse, P.M.J. van den Berg, M.C.M. Rutten, N.H.J. Pijls and F.N. van de Vosse. A physiologically representative *in-vitro* model of the coronary circulation. *Physiological Measurement*, 25:891-904, 2004.

2.1 Introduction

While validating clinical intracoronary diagnostic techniques, an *in-vitro* model of the coronary circulation that properly mimics physiological and pathological behaviour in the coronary circulation is of major importance as it allows testing and validation of these techniques under well-controlled circumstances. Generating flow patterns and pressure curves that closely mimic human coronary flow and pressure, both under resting and hyperemic conditions, is paramount in modelling the coronary circulation.

Aim of this study was to develop a realistic *in-vitro* model of the coronary circulation with physiologically representative elements for relevant components of the circulation, both regarding geometry and function.

Characteristically, coronary flow predominantly occurs in diastole, while it is primarily driven by aortic pressure. As introduced in chapter 1, an explanation for this phenomenon is found in the influence of left ventricular contraction on the subendocardial myocardium, resulting in an increase in the resistance to flow during the systolic part of the cardiac cycle. This influence is considered to be the key element in the modelling of the coronary circulation. It is assumed to be independent of the autoregulation effect of the arteriolar resistances on the mean coronary flow, by which coronary flow is actively varied from baseline to hyperemic levels in response to varying oxygen demand.

Several mathematical models have been proposed in literature to explain coronary flow patterns by describing the relations between intramyocardial pressure, volume and resistance to flow. The earliest models were based on the waterfall principle (Downey and Kirk, 1975), in which the vascular bed is assumed to collapse when intramyocardial pressure exceeds intravascular pressure. This approach can describe the systolic decline in coronary flow. However, a total collapse of the vascular bed is unlikely to occur, since the coronary perfusion volume is too small to empty and refill the coronary vasculature completely in one heart beat (Arts and Reneman, 1985). In the intramyocardial pump model, flow variations between systole and diastole are not directly coupled to variable resistance as in the waterfall model, but to intramyocardial volume variations, by introducing the capacitance of the coronary vasculature (Spaan et al., 1981; Arts and Reneman, 1985), later adjusted to resistances and capacitances dependent on intramyocardial pressure (Bruinsma et al., 1988). With these models correct phasic patterns of coronary artery flow could be obtained. Another approach was taken by Krams et al. (1989a,c), applying the time-varying elastance model introduced by Suga et al. (1973) to the coronary circulation. He suggested relating intramyocardial volume changes to increased myocardial stiffness during the cardiac cycle. The validity of this model under low left ventricular pressure conditions was shown *in-vivo* (Krams et al., 1989a,b,c). A more extended mechanical model, incorporating the functional relation of active myocardial mechanics, perfusion and across-capillary mass transport, was introduced by Zinemanas et al. (1994). Interactions between these aspects influencing the coronary flow pattern can be evaluated properly with this model.

Only a few *in-vitro* measurements evaluating clinical diagnostic techniques based on these models have been reported up to now (Segers et al., 1999; Matthys et al.,

2001). In these set-ups the coronary circulation is driven by prescribed aortic pressure and myocardial resistance, which is a restriction on the value of the model in mimicking physiological conditions.

Our objective was to translate the influence of left ventricular contraction, as described by the models mentioned above, to physical elements for the development of an *in-vitro* model. In the present study a more pragmatic approach was taken, since mathematical elements such as active contractile elements resembling heart muscle, as used in the time-varying elastance model and the model of Zinemanas et al. (1994), are not physically available. The model is primarily based on insights into physiological parameters as obtained by invasive measurements of pressure and flow in the coronary circulation in healthy persons and in patients with coronary artery disease (Wilson et al., 1985; De Bruyne et al., 2001a).

First the modelling conditions were defined and a lumped parameter mathematical model was developed, as a design tool for the *in-vitro* experimental model. Then the elements from the lumped parameter model were translated into physical elements in the *in-vitro* model. Finally, the generated signals from both models were compared to pressure and flow recordings in conscious humans.

2.2 Materials and methods

2.2.1 Modelling conditions

The modelling conditions of both the numerical and the *in-vitro* model are primarily based on knowledge of the relevant physiological conditions. The main consideration is the physiological basis of both the pressure and flow signals in the coronary circulation, which has not been modelled in earlier *in-vitro* models (Segers et al., 1999; Matthys et al., 2001). To model this ventricular contraction or volume change was made the only active input for the *in-vitro* model. Hence the main modelling conditions are as follows:

- (a) Coronary flow is primarily driven by aortic pressure.
- (b) Ventricular contraction determines the phasic systolic/diastolic coronary artery flow pattern.
- (c) The change from baseline to hyperemic flow conditions (autoregulation) is modelled by a decrease of arteriolar resistance only.

A *conditio sine qua non* for the model to be realistic is that at least all pressure and flow signals generated under different physiological and pathological conditions clearly resemble similar signals in conscious humans.

The physiological reference values for mean coronary flow (\bar{q}_{ca}), mean aortic pressure (\bar{p}_{ao}), mean venous pressure (\bar{p}_v), and mean aortic flow (\bar{q}_{ao}) in baseline and hyperemia are given in table 2.1. The physiological modelling conditions were implemented in a lumped parameter model and from this model the *in-vitro* set-up of the systemic and coronary circulation was derived. Care was taken that all parameters and physical dimensions were in accordance with the human coronary circulation.

2.2.2 The lumped parameter mathematical model

Design

The model consists of three parts: a heart, a systemic circulation and a coronary circulation (figure 2.1). The heart consists of the left ventricle (LV) and the mitral and aortic valves. The heart and systemic circulation are of importance to the coronary circulation, as they produce the characteristic aortic pressure pattern (p_{ao}) that drives the coronary circulation. The LV is a single node with a prescribed flow in and out, according to data from Nolan (1976), representing the change of volume of the LV. Flow-dependent variable resistances analogue to electric diodes represent the mitral and aortic valves. A four-element Windkessel as introduced by Stergiopoulos et al. (1999) represents the systemic circulation.

The coronary circulation comprised three primary components: the coronary artery, the arteriolar resistance, and the myocardial vascular bed. The left coronary artery (LCA) was modelled with a LRC segment with L_{ca} , R_{ca} , and C_{ca} based on the material and geometrical properties of a thin-walled linear elastic artery. The whole autoregulation was assumed to be determined by one parameter: the arteriolar resistance R_{ar} . Thus, this resistance will be the sole discriminator between hyperemia and baseline coronary flow ($R_{ar,hyperemia} < R_{ar,baseline}$). The arteriolar resistance was modelled to be low at hyperemia and of the same order of magnitude as the resistance of the LCA: $O(R_{ar,hyperemia}) = O(R_{ca})$.

In the mathematical model the changes in volume and resistance of the myocardial vascular bed were taken as two separate influences: the myocardial contraction was modelled after the intramyocardial pump model by a prescribed change of myocardial volume ΔV_{myo} with the same pattern as the change of volume of the LV (Spaan et al., 1981; Arts and Reneman, 1985; Bruinsma et al., 1988) and a variable myocardial resistance $R_{ma}(t)$ dependent on LV-pressure p_{LV} , (Bruinsma et al., 1988):

$$R_{ma} = \begin{cases} c + b \cdot p_{LV} & \text{in systole} \\ c & \text{in diastole} \end{cases} \quad (2.1)$$

and

$$q_{myo}(t) = a \cdot q_{LV}(t) \quad (2.2)$$

Parameter estimation

The parameters used in the final model are given in table 2.2. The resistance R_{ca} of the coronary artery based on Poiseuille flow conditions can be approximated by

$$R_{ca} \approx \frac{8\eta l}{\pi r^4} = O(10^{-1}) \text{ kPa s/ml} \quad (2.3)$$

where length $l = 0.15$ m, radius $r = 2 \times 10^{-3}$ m, and dynamic viscosity $\eta = 4 \times 10^{-3}$ kg/ms. The inertance L_{ca} is defined as

$$L_{ca} = \frac{\rho l}{\pi r^2} = O(10^{-2}) \text{ kPa s}^2/\text{ml} \quad (2.4)$$

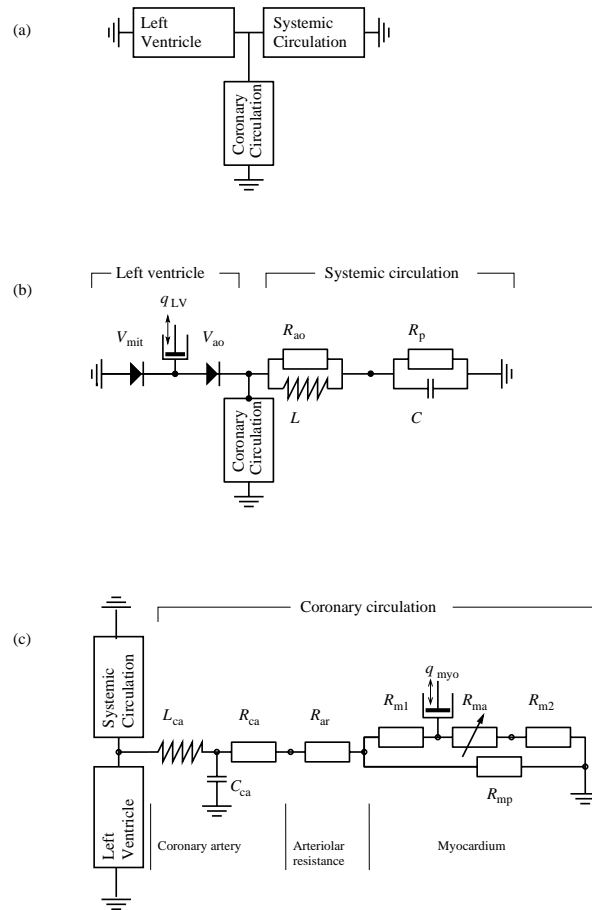


Figure 2.1: Schematic representation of the lumped parameter model, consisting of a left ventricle, systemic circulation and coronary circulation (a). V_{mit} and V_{ao} are the mitral and aortic valves, q_{LV} is the prescribed flow in and out of the left ventricle, R_{ao} , R_p , L , and C are the coefficients of the four-element Windkessel model (b). The model for the coronary circulation (c) comprises the coronary artery (L_{ca} , C_{ca} , R_{ca}), the arteriolar resistance R_{ar} , and the myocardial resistances R_{m1} , R_{ma} , R_{m2} , R_{mp} . The prescribed change of myocardial volume is q_{myo} .

where $\rho = 1 \times 10^3 \text{ kg/m}^3$. The compliance C_{ca} is given by

$$C_{ca} = \frac{2\pi(1 - \mu^2)r^3l}{hE} = O(10^{-3}) \text{ kPa s}^2/\text{ml} \quad (2.5)$$

Here $\mu = 0.5$ denotes the Poisson ratio and $E = 13 \text{ MPa}$ the Young's modulus.

Due to the complex non-linear behaviour of the system, a rigorous analysis to obtain the exact values of the myocardial parameters of the model cannot be given. Initial values can be obtained using the approximate values of arterial and venous flow as depicted in figure 2.2, assuming that duration of systole and diastole is 0.3 s and 0.5 s, respectively, and an order of magnitude stroke volume of 100 ml. Now left ventricular flow can be derived: $q_{LV,\text{systole}} = 100 \cdot 60/0.3 = 20 \times 10^3 \text{ ml/min}$ and $q_{LV,\text{diastole}} = 100 \cdot 60/0.5 = 12 \times 10^3 \text{ ml/min}$: equation (2.2) then yields $a = 8 \times 10^{-3}$.

If subendocardial and subepicardial blood supply are of the same order in both systole and diastole and moreover

$$R_{ma,\text{diastole}} \ll R_{m1} + R_{m2} \quad (2.6)$$

then

$$R_{m1} + R_{m2} = O(R_{mp}) \quad (2.7)$$

Moreover, subepicardial flow is driven by mean aortic pressure, so

$$R_{mp} = O\left(\frac{\bar{p}_{ao}}{\frac{1}{2}\bar{q}_{ca}}\right) \approx 5 \text{ kPa s/ml} \quad (2.8)$$

Systolic flow is at least half the diastolic flow (figure 2.2). This is only possible if we assume the following during systole:

$$R_{m2} + R_{ma,\text{systole}} \gg R_{m1} \quad (2.9)$$

In practice $R_{m2} \approx 3R_{m1}$, and $R_{ma,\text{systole}} \approx 10R_{m1}$ turned out to be a reasonable choice, resulting in $R_{m1} \approx 1.3 \text{ kPa s/ml}$, $R_{m2} \approx 3.8 \text{ kPa s/ml}$ and $R_{ma,\text{systole}} \approx 12.5 \text{ kPa s/ml}$. It then follows that when c (equation (2.1)) is assumed to be small (equation (2.6)), then $b \approx 0.9 \text{ s/ml}$.

Total myocardial resistance (R_{myo}) can be estimated from mean coronary pressure and flow at hyperemia, when arteriolar and coronary artery resistances are assumed to be insignificant. Hence

$$R_{myo} \approx \frac{\bar{p}_{ao}}{\bar{q}_{ca}} \approx 2.7 \text{ kPa s/ml} \quad (2.10)$$

For baseline conditions, when mean coronary flow can easily be as low as a fourth of that at hyperemia, it then follows that

$$R_{ar,\text{baseline}} \approx 3R_{myo} \approx 8.1 \text{ kPa s/ml} \quad (2.11)$$

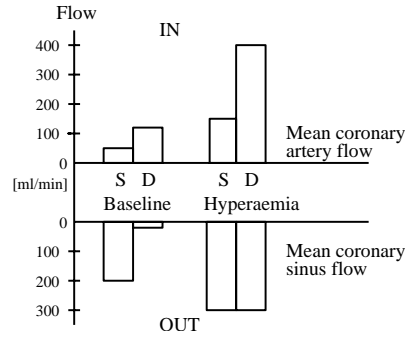


Figure 2.2: Generalized reference values for mean flow rates in the coronary artery (\bar{q}_{ca}) and coronary sinus (\bar{q}_{cs}), enabling estimation of the myocardial volume change ΔV_{myo} . Systole is abbreviated to S and diastole to D.

Solution method

The lumped parameter modelling was performed by solving the following set of equations

$$C\ddot{\mathbf{p}}(t) + R\dot{\mathbf{p}}(t) + L\mathbf{p}(t) = \dot{\mathbf{q}}(t) \quad (2.12)$$

at a finite number of incremental steps in time for the discrete system. Compliances, resistances, and inertances are ordered in the matrices C , R and L respectively. Together with the nodal variable \mathbf{p} (pressure) and the element variable \mathbf{q} (flow) they form the set of second order differential equations. The solution of this set was determined at equidistant steps in time with step size Δt by using the implicit trapezoidal rule as an integration method. The initial conditions were $\mathbf{p}_{t=0} = 0$, $\dot{\mathbf{p}}_{t=0} = 0$, $\ddot{\mathbf{p}}_{t=0} = 0$ and \mathbf{q}_{LV} and \mathbf{q}_{myo} were prescribed at the left ventricular node and the myocardial compression node (figure 2.1), respectively. The system reached a periodic state after approximately 8 'heart cycles', when the difference between two heart cycles was less than a few percent.

2.2.3 The *in-vitro* experimental model

Heart and systemic circulation

The *in-vitro* model consisted of a pump (mimicking the heart), a systemic and a coronary circulation. The *in-vitro* heart included a rigid chamber with a piston inside (figure 2.3), driven by a computer-controlled linear motor (ETB32, Parker) and two artificial valves (a Bjork-Shiley valve for the aortic valve and a St. Jude for the mitral valve, \varnothing 23 mm and 31 mm, respectively). The aorta was modelled as a tube made out of polyurethane (Desmopan 588, Bayer, $E = 13$ MPa, $\mu \approx 0.5$) and connected to a Windkessel, modelling the distal systemic compliance. Two external occluders (or clamps) formed the aortic resistance and the peripheral resistance. The aortic tube had a length of 450 mm, a diameter of 25 mm, a thickness of 0.13 ± 0.01 mm

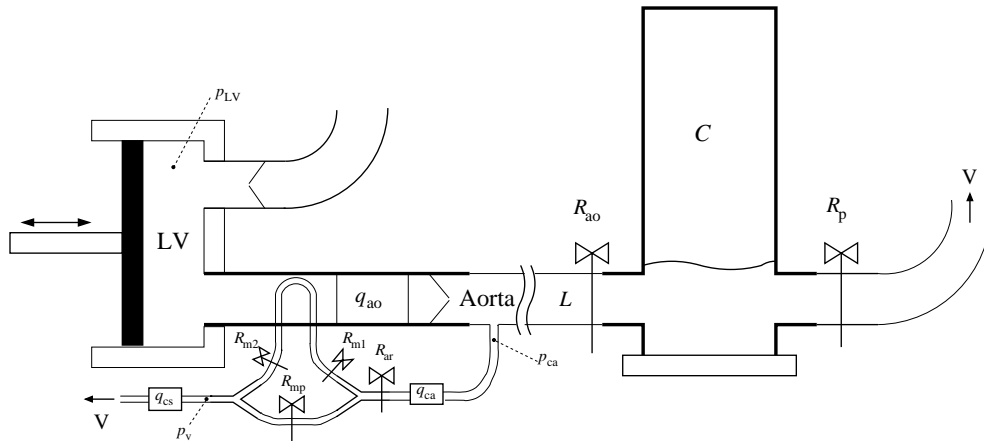


Figure 2.3: Schematic of the in-vitro experimental model. The LV-chamber pumps water through the aortic flow probe and the artificial valve into the aorta and from the aorta into the systemic Windkessel components (with lumped parameters R_{ao} , L , C , and R_p representing aortic resistance, systemic inertance, systemic compliance and peripheral resistance, respectively). A coronary artery branches off the aorta, passes the coronary artery flow probe, the arteriolar resistance R_{ar} , bifurcates into a collapsible tube which is led through the LV and a non-compressible tube and passes the coronary sinus flow probe towards a venous outlet V . Myocardial lumped resistances are indicated by R_{m1} , R_{m2} and R_{mp} . All resistances indicated are manually adjustable clamps. The location of pressure measurements in the left ventricle, coronary venous pressure and coronary artery pressure is indicated by p_{LV} , p_v and p_{ca} , respectively. Flow rates are registered by the electromagnetic flow probes q_{ao} , q_{ca} and q_{cs} .

and a static compliance of 2.7 ml/kPa (0.36 ml/mmHg). Aortic input impedance characterizes the systemic circulation behaviour and sufficed for a physiological aortic pressure pattern, as shown in figure 2.4.

Coronary circulation

The *in-vitro* coronary circulation comprised a coronary epicardial artery, a dual-tubed myocardium and a venous outlet (figure 2.3). The coronary artery tube was modelled with physiological dimensions and capacitance; it was made of the same polyurethane as the aortic tube and had a length of 115 mm, an inner diameter of 4 mm, a thickness of 0.13 ± 0.02 mm and a static compliance of 4×10^{-3} ml/kPa (3×10^{-2} ml/mmHg). The myocardium was modelled as a resistive circuit consisting of two parallel tubes, representing the subepicardial and subendocardial myocardium. Both were formed from rigid tubes with an internal diameter of 4 and 5 mm, and a thick wall (0.5–1.0 mm). The variable resistance and volume of the subendocardial myocardium were represented by a collapsible tube through the LV-chamber as a part of the subendocardial branch. It was made of the same polyurethane as the coronary artery tube and had a length of 100 mm, a diameter of 4 mm and a thickness of 0.13 ± 0.02 mm. A single tube connected the venous myocardial outlet to the venous reservoir and had no additional resistance. It consisted of a rigid tube with an internal diameter of 9 mm and a wall thickness of 1 mm. An external occluder was placed on the subepicardial (non-compressible) myocardial line (R_{mp}). The arteriolar resistance (R_{ar}), crucial for the modelling of autoregulation, was present as a clamp and was placed between the myocardial circulation and the coronary artery tube. An adjustable external occluder on the coronary artery, allowing a wide range of stenosis severity simulations, could mimic an epicardial stenosis. The location of the occluders and clamps was derived from the numerical model and they were all manually controlled. Initially the systemic circulation was tuned to generate physiologically representative pressure and flow signals. Thus appropriate input conditions for the coronary circulation were created and subsequently the coronary resistances were fine-tuned considering coronary pressure and flow patterns and magnitudes.

Left ventricular (p_{LV}) and aortic (p_{ao}) pressures were measured, as these two pressure patterns are considered to be the driving forces of coronary flow (q_{ca}). Aortic flow (q_{ao}) was measured to compute cardiac output. Coronary sinus flow (q_{cs}) was measured to deduce the change of myocardial volume. Coronary venous pressure (p_v) was registered to determine the perfusing pressure difference over the coronary circulation. All flow rates were measured by electromagnetic flow sensors (Transflow 1401, Skalar): directly proximal to the aortic valve (q_{ao}), approximately 30 mm distal to the polyurethane coronary artery (q_{ca}), and 80 mm distal to the myocardial circulation (q_{cs}). Pressures were measured 20 mm distal of the coronary artery-aorta connection (p_{ca}), in the LV-chamber (p_{LV}) and 20 mm distal to the junction of both the myocardial lines on the venous side (p_v), using a PressureWire (PressureWire-4, Radi Medical Systems, Uppsala, Sweden).

As stated in modelling conditions (a) and (b), the only input in the experimental set-up of the circulation was the motion of the piston within the LV-chamber, designed

Table 2.1: Reference values and results for pressure and flow at relevant sites in the circulation.

		Baseline			Hyperemia		
		Reference	Lumped parameter model	<i>In-vitro</i> model	Reference	Lumped parameter model	<i>In-vitro</i> model
\bar{q}_{ca}	[ml/min]	50–75	81	80	250–300	250	279
$\bar{q}_{ca,syst}$	[ml/min]	50	51	50	150	131	185
$\bar{q}_{ca,diast}$	[ml/min]	100	106	99	400	346	339
\bar{q}_{ao}	[l/min]	5–6	5.8	5.2	5–6	5.8	5.1
\bar{p}_{ao}	[kPa]	12.0–13.5	13.6	13.2	12.0–13.5	13.9	13.1
\bar{p}_v	[kPa]	0.00	0.00	-0.23	0.00	0.00	0.21

as a combination of two squared sines; one accounting for a rather steep systolic outflow, the second for a more prolonged diastolic inflow pattern:

$$x(t) = \begin{cases} \sin^2\left(\frac{1}{2 \cdot 0.3}\pi t\right) & \text{for } 0 < t \leq 0.3 \text{ s} \\ \sin^2\left(\frac{1}{2 \cdot 0.5}\pi(0.8 - t)\right) & \text{for } 0.3 < t \leq 0.8 \text{ s} \end{cases} \quad (2.13)$$

Measurements in the *in-vitro* coronary circulation were done at a heart rate (HR) of 75 bpm and at reference values for p_{ao} , p_v and q_{ao} as stated in table 2.1. As HR was 75 bpm, a single heart cycle was 0.8 s and systole and diastole were approximately 0.3 s and 0.5 s, respectively. Water was used as a flow medium and sodium chloride was added to enable electromagnetic flow measurement. Generally, data were recorded for three heart cycles or 2.4 s, and time averages were based on this time period.

The signals acquired at the specified measurement sites in the experimental model and the output of the numerical simulations were compared qualitatively and quantitatively to *in-vivo* pressure and flow registrations as obtained in the coronary circulation of conscious humans.

2.3 Results

As can be observed in figure 2.4 all signals obtained from the numerical simulations and experimental model (p_{LV} , p_{ao} , p_v , q_{ca} , and q_{ao}) closely resembled true physiological signals for both baseline and hyperemic conditions. A strong quantitative agreement was also present (table 2.1). The changes in myocardial volume resembled the values estimated above (figure 2.5).

2.3.1 The lumped parameter mathematical model

The LV-pressure and aortic pressures were physiological, except for the low diastolic pressure of the LV. Coronary flow at baseline and hyperemia were close to or within the predefined ranges (table 2.1). Qualitatively, the decreasing diastolic coronary flow pattern and systolic drop of coronary flow rate are clearly visible; the mean systolic flow was much lower than the mean diastolic flow.

Table 2.2: Parameter values for the lumped parameter model. A slight increase of the systemic peripheral resistance R_p upheld the mean aortic pressure between baseline and hyperemia.

Systemic circulation		
R_{ao}	[kPa s/ml]	7.5×10^{-3}
L	[kPa s ² /ml]	6.8×10^{-4}
$R_{p, \text{baseline}}$	[kPa s/ml]	0.146
$R_{p, \text{hyperemia}}$	[kPa s/ml]	0.153
C	[ml/kPa]	9.2
Coronary circulation		
L_{ca}	[kPa s ² /ml]	8.7×10^{-3}
C_{ca}	[ml/kPa]	4.0×10^{-3}
R_{ca}	[kPa s/ml]	0.2
$R_{ar, \text{baseline}}$	[kPa s/ml]	6.4
$R_{ar, \text{hyperemia}}$	[kPa s/ml]	0.1
R_{m1}	[kPa s/ml]	1.3
a	-	8×10^{-3}
b	[s/ml]	0.9
$R_{ma, \text{diastole}}$	[kPa s/ml]	0.3
$R_{ma, \text{systole}}$	[kPa s/ml]	13.3
R_{m2}	[kPa s/ml]	3.3
R_{mp}	[kPa s/ml]	5.0

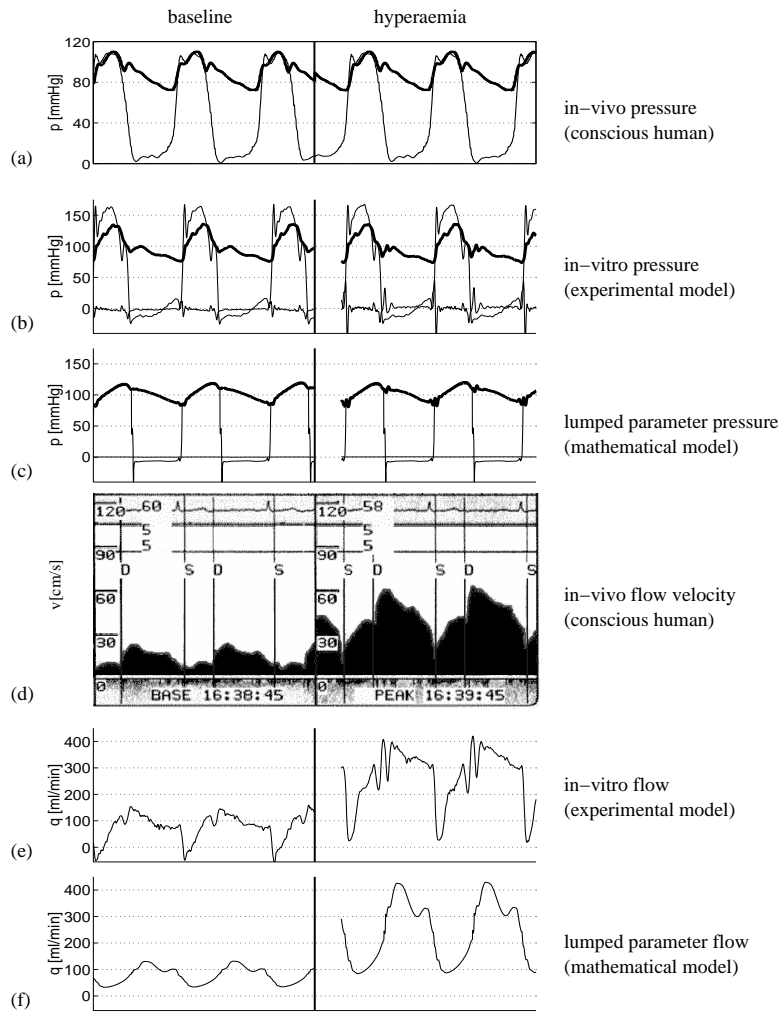


Figure 2.4: Pressure and flow registrations of the lumped parameter and in-vitro modelling at baseline and hyperemic conditions, compared to in-vivo human signals. (a) In-vivo aortic (bold) and left-ventricular pressure. Signals were subsequently obtained from one patient and the signal was copied to allow both baseline and hyperemic comparison. (b) Corresponding pressures measured in the in-vitro experimental model, at baseline and hyperemia, as well as coronary sinus pressure. (c) Corresponding pressures from the lumped parameter model. (d) In-vivo Doppler flow-velocity registration of left coronary artery (LCA), not taken from the same patient as in (a). (e) Coronary flow rate measured in the in-vitro experimental model. (f) Coronary flow rate from the lumped parameter model.

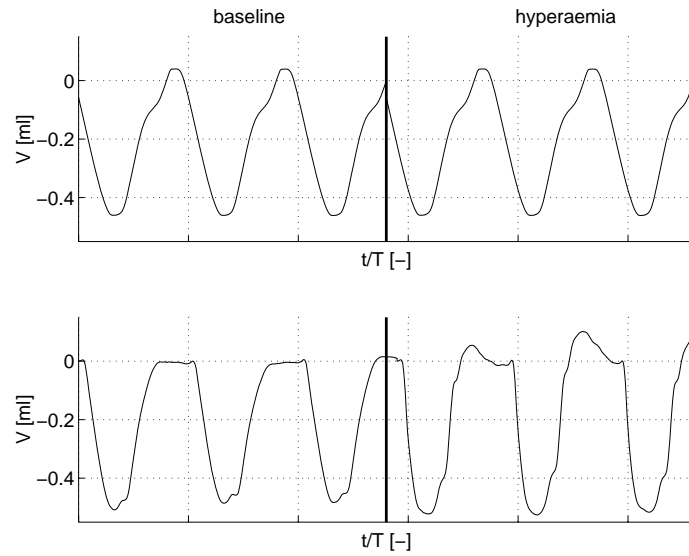


Figure 2.5: Myocardial volume change from lumped parameter and experimental model.

The change from baseline to hyperemic flow conditions was obtained via a decrease in the arteriolar resistance R_{ar} only. A slight increase in the systemic peripheral resistance R_p maintained the mean aortic pressure (table 2.2).

2.3.2 The *in-vitro* experimental model

The aortic pressure pattern (which primarily drives the coronary flow) was physiologically correct, as well as that of the LV, where the gradient during systole was due to the size of the artificial valve used. Strong spikes in coronary sinus pressure at hyperemia occurred around steep increases and decreases in LV-pressure due to the opening and closing effects of the valves.

The coronary flow patterns closely matched *in-vivo* Doppler flow measurements in human coronary arteries. Qualitatively, the characteristic decreasing diastolic flow pattern and systolic drop of flow rate were present. In the pressure signals, the hyperemic early-diastolic flow wave in coronary venous pressure and aortic pressure can also be seen. The change from baseline to hyperemic conditions was mainly obtained by varying R_{ar} , but a small adjustment of the myocardial resistances still was needed. Quantitatively, all flow rates were within the estimated ranges, except mean diastolic and systolic flow at hyperemia, which were slightly low and high, respectively.

The signals obtained from the experimental model are even more physiologically realistic than those from the lumped parameter numerical model and very close to signals measured in conscious humans. Differences from the results of simulations

with the lumped parameter model can be found in the steep increase of systolic flow rate in the second half of systole and a significantly faster change of the myocardial volume (gained by the collapsible tube), while the amount of volume change is the same (figure 2.5).

2.4 Discussion

2.4.1 Modelling: physiological basis

The main requirements for the lumped parameter mathematical model and the *in-vitro* experimental model were the generation of physiological pressure and flow signals through physiologically representative elements, ventricular contraction being the only input for the model (driving aortic pressure and thus coronary flow and acting on myocardial resistance and volume), and the change between baseline and hyperemic flow conditions only dependent on a change in arteriolar resistance. To achieve this in both models physical elements representing parts of the circulation were used.

Concepts from physiological models from literature were taken for the changes in volume and resistance of the myocardial vascular bed: in the mathematical model the myocardial resistance and volume were implemented by separate influences and in the *in-vitro* model a collapsible tube was used for the subendocardial part of the myocardium. In the models described in literature mostly complicated, multilayered structures were used (Spaan et al., 1981; Arts and Reneman, 1985; Bruinsma et al., 1988), as well as mechanisms based on fibre contraction (myocardial stiffening) (Suga et al., 1973; Krams et al., 1989a,c). Although Krams et al. (1989a,b,c) showed in their experiments that coronary flow amplitude is only weakly related to left ventricular pressure, and strongly related to contractility, the collapsible tube approach led to physiologically representative coronary pressure and flow curves. A possible explanation may be found in the low left ventricular pressure during the experiments by Krams et al., resulting in a decreased end-systolic left ventricular volume and hence a large volume change of the wall and large passive stress in the myocardium, increasing the intramyocardial pressure and counterbalancing the effect of decreased left ventricular pressure.

The change between baseline and hyperemic flow conditions was achieved by varying R_{ar} . The small adjustment of the myocardial resistances still needed will probably be unnecessary when the myocardial volume change could be increased. This could be achieved by using a collapsible tube with a larger volume, or an accumulator, connecting the LV with the proximal side of the collapsible tube and containing a membrane, allowing volume change of the subendocardial branch and transmission of LV pressure to the collapsible tube, but not changing myocardial resistance.

The influence of the opening and closure of the valves can be seen in the pressure curves from the *in-vitro* model; the Bjork-Shiley is known to produce significant pressure drops (more than 4 kPa at a cardiac output of 5 l/min).

2.4.2 The lumped parameter mathematical model

The values for the resistance elements of the lumped parameter model were estimated from physiological data. The final values (resembling the estimation closely) were determined iteratively and resulted in physiologically representative pressure and flow signals. The applied myocardial volume change was deduced from generalizations of the mean coronary artery and coronary sinus flow (q_{ca} and q_{cs} , figure 2.2) using clinical experience. Based on the intramyocardial pump model, the myocardial flow pattern was taken linearly related to the left ventricular volume change. Together with the myocardial resistance being partially dependent on left ventricular pressure this leads to physiologically representative pressure and flow signals, despite the possibly incorrect physiological mechanism, as indicated by the experiments of Krams et al. (1989a,b,c).

2.4.3 The *in-vitro* experimental model

As indicated in the description of the physiological models for the mechanics of coronary blood flow, the most crucial element of the *in-vitro* coronary circulation was the modelling of the myocardium. In the lumped parameter model a combination of the influence of the left ventricular pressure on the myocardial resistance and volume change linearly related to that of the left ventricle was used. This approach was extended to the *in-vitro* model by using a collapsible tube led through the left ventricle. Another non-compressible branch was connected parallel outside the left ventricle, representing the subendocardial and subepicardial part of the myocardium, respectively. The collapsible tube occludes during systole; both branches are uncompressed at diastole. In this way, using the collapsible tube principle from the waterfall model (Downey and Kirk, 1975), the physiological compression of the subendocardial part of the myocardial vascular bed can be mimicked.

2.4.4 Limitations

The exact resistive behaviour, exact point of collapse and the direction of the expelled fluid of the collapsible tube are not known. Placement of the collapsible tube in the aortic ejection stream of the left ventricle lowered the predictability of its behaviour even further. Nevertheless, the collapsing behaviour was stable, as may be concluded from the periodic coronary flow patterns. The amount of retrograde and antegrade flow and the fully occluded time period of the collapsible tube are unknown. Therefore, it is likely that the flow through the collapsible tube was lower than deduced from the end-diastolic resistance assessment.

In the set-up, water was used as a medium instead of blood. Viscosity is the main parameter in which blood and water differ; it is roughly three times as high for blood as for water. Since aortic pressure, which is not influenced by viscosity, is the only important parameter from the systemic circulation, only a deviation in characteristic impedance Z_c of the coronary circulation could be of importance. This impedance is a function of the Womersley number (a ratio of the instationary inertia

forces and the viscous forces) and was found to be only approximately 10% lower than the theoretical Z_c of the in-vivo coronary artery. This is considered an acceptable deviation.

The clamp-resistances in the coronary circulation are assumed to be linear (Segers et al., 1999): the external clamps in the model are considered to function as linear resistances; a slight non-linear behaviour might be present.

For a more convenient application of clinical techniques such as thermodilution (Pijls et al., 2002), a more physiological coronary ostium could be implemented. A second coronary circulation could be added in parallel with the current one to allow for the investigation of collateral flow phenomena such as coronary steal.

2.4.5 Extended applications

The main objective of developing the *in-vitro* model was to create a tool to validate novel diagnostic techniques. Recently, the model was used in a study on the correlation between absolute flow, thermodilution-derived mean transit time, index of myocardial resistance (Fearon et al., 2003) and true myocardial resistance (Aarnoudse et al., 2004b), and proved to be very suitable for that purpose.

2.5 Conclusions

The *in-vitro* model of the coronary circulation produces physiologically representative pressure and flow signals. The main modelling conditions are met: coronary flow is primarily driven by aortic pressure, left ventricular contraction influences coronary arterial flow and coronary blood flow is regulated by arteriolar resistance changes only. As the model indeed closely resembles the coronary circulation, it is possible to evaluate diagnostic procedures and techniques.

2.6 Acknowledgements

This work was supported by the Dutch Technology Foundation STW, project EPG 5454, and by Radi Medical Systems, Uppsala, Sweden. The authors are grateful to Paola Buratinello, Geralda van Tilborg, Ewout van der Laan and Mark van Turnhout for their contribution to this research.

Chapter 3

From bedside to bench: a physiologically representative *in-vitro* model to evaluate catheter-based intracoronary diagnostic techniques

For better understanding and evaluation of clinical diagnostic techniques, we recently developed a physiologically representative in-vitro model of the coronary circulation. The applicability of such a model is not only supported by its ability to produce physiological pressure and flow signals, but also depends on its ability to reproduce the results of well-validated catheter-based diagnostic techniques as used in the human catheterization laboratory. Therefore the aim of the present study was to test this model, extended with a collateral circulation, by predicting the outcome of clinical diagnostic indexes for the two main compartments of the coronary circulation: fractional flow reserve (FFR), characterizing epicardial stenosis severity, and index of microcirculatory resistance (IMR), quantifying hyperemic minimal resistance to blood flow of the myocardial vascular bed. In determining this latter index, collateral flow plays an important role. Over a wide range of stenosis severity and microvascular resistance, the in-vitro model accurately reproduced FFR and IMR in accordance with clinical observations. Moreover, FFR calculated from sensor-tipped guide wire based coronary pressure measurement and IMR calculated from pressure and temperature, equaled the corresponding indexes directly measured by flow. Hence the model's reciprocal usefulness for research and development of coronary diagnostic techniques is confirmed.

The contents of this chapter are based on M.C.F. Geven, W.H. Aarnoudse, M.C.M. Rutten, U. Siebert, N.H.J. Pijls, and F.N. van de Vosse. From bedside to bench: a physiologic *in-vitro* model to evaluate catheter-based intracoronary diagnostic techniques. *Physiological Measurement*, to be submitted.

3.1 Introduction

Clinical diagnostic techniques for assessment of the coronary circulation are mainly developed and tested in animal models and clinical environment. An *in-vitro* model of the coronary circulation with physiologically representative pressure and flow signals, both under resting and hyperemic conditions (maximum myocardial flow), would be a valuable supplement. Such a model can provide well-controlled evaluation circumstances, the possibility to simulate functional pathology such as an epicardial stenosis or microvascular disorder, and the methodology to assess such pathologic conditions. Characteristically, coronary flow predominantly occurs in diastole, while it is primarily driven by aortic pressure. An explanation of this phenomenon is found in the influence of left ventricular contraction to the subendocardial myocardium, resulting in a decrease in microcirculatory volume and an increase in the resistance to flow during the systolic part of the cardiac cycle. Up to now, mathematical descriptions of the coronary circulation (Bruinsma et al., 1988; Downey and Kirk, 1975; Krams et al., 1989c; Zinemanas et al., 1994) had not been translated into an experimental setup generating physiologically representative pressure and flow signals as obtained in the human coronary circulation. Recently, we developed an *in-vitro* model with pressure and flow patterns characteristic for the *in-vivo* coronary circulation both at baseline and hyperemia (chapter 2, Geven et al. (2004)). In the present study, the model was extended to consider the effect of collateral circulation (connecting the aorta and the myocardium, bypassing the coronary arteries), important in clinical physiological measurements in humans with stenotic coronary arteries.

The aim of this study was to show the value of the extended model in evaluation of clinical diagnostic techniques. Two well-validated clinical indices for the quantification of disease in the two main compartments of the coronary circulation are assessed. The first index is the fractional flow reserve (FFR), which is widely used and accepted as the gold standard to assess the hemodynamic significance of epicardial coronary stenoses (Pijls et al., 1993; De Bruyne et al., 2000; Kern, 2000; Pijls et al., 2000; Bech et al., 2001; Wilson, 2001; De Bruyne et al., 1996). The second index is the index of microcirculatory resistance (IMR). This newer and technically more complex measurement has been used to assess the microcirculation of the heart (Aarnoudse et al., 2004a,b; Fearon et al., 2003, 2004). In the calculation of this latter index, inclusion of collateral flow is of critical importance (Aarnoudse et al., 2004a,b; Fearon et al., 2004). Note that the *in-vivo* coronary circulation as well as the *in-vitro* model is a non-linear dynamic system. The calculation of the indices IMR and FFR are based on mean values of coronary pressure and flow: hence in this study a linear approach in evaluation of indices characterizing the coronary circulation is used.

Confirming bedside observations correctly by our extended bench model (including collateral circulation) was considered an excellent reciprocal test of the model's usefulness and validity in the development and evaluation of new bedside techniques for assessment of the coronary circulation.

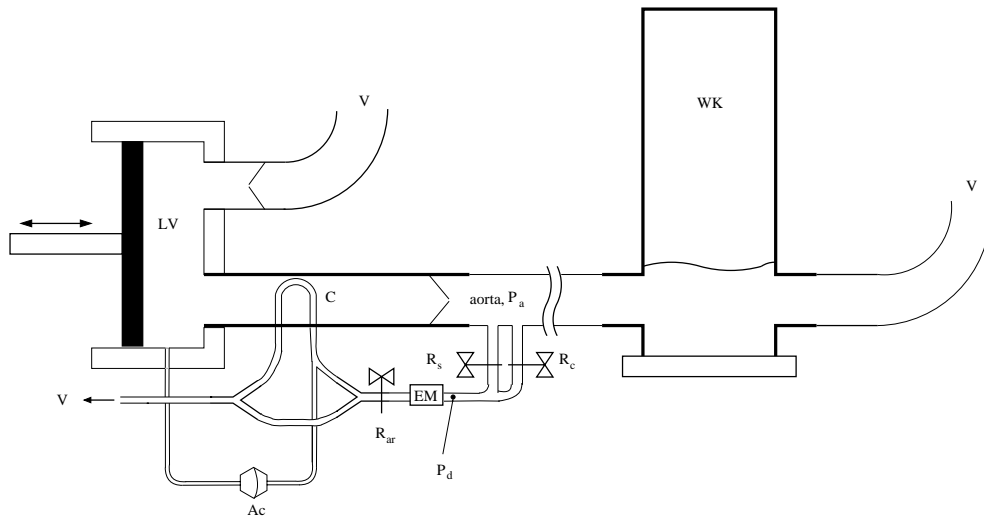


Figure 3.1: In-vitro model of the circulation used in this study; LV, left ventricle; V, venous outlet; Ac, accumulator; C, collapsible tube; R_{ar} , arteriolar resistance clamp; EM, myocardial electromagnetic flow sensor; R_s , epicardial coronary stenosis clamp; R_c , collateral clamp; P_a , pressure sensor in the aorta; P_d , distal coronary pressure sensor; WK, windkessel.

3.2 Materials and methods

3.2.1 In-vitro experimental model

The original in-vitro experimental model consists of a piston pump, a left ventricular chamber and two valves, representing the left ventricle of the heart, a systemic and a coronary circulation (figure 3.1). The systemic circulation contains a polyurethane tube (with the dimensions and mechanical properties of the aorta), and a system of compliances and resistances, creating physiological aortic pressure and flow patterns. The polyurethane coronary artery branches off the aorta directly distal to the aortic valve and bifurcates into a subendocardial and a subepicardial myocardial tube. The subendocardial branch is led through the left ventricular chamber and collapses during systole due to high left ventricular pressure. This allows for modeling the variable resistance and volume behavior of the endocardial part of the in-vivo myocardium. The arteriolar resistance clamp can be adjusted to create baseline and hyperemic flow conditions. We have previously shown that these physiologically representative elements provide physiological aortic and coronary pressure and flow patterns (Geven et al., 2004). Representative pressure and flow patterns both at rest and hyperemia, with predominant diastolic flow, were presented in chapter 2 (figure 2.4). In the present study, the model was extended to consider the effect of collateral circulation, important in clinical physiological measurements as FFR and IMR in humans with stenotic coronary arteries. A second tube branching off the aorta

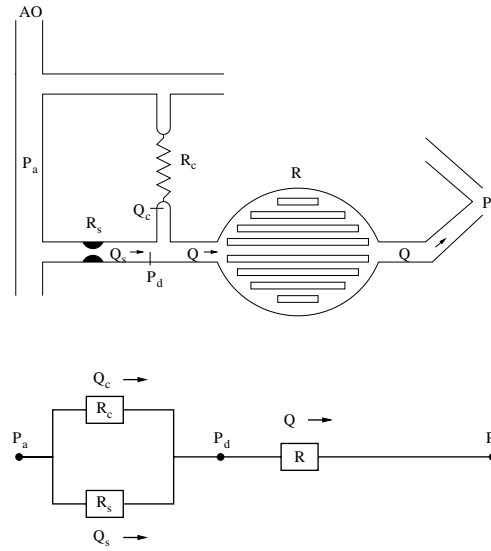


Figure 3.2: Lumped model of the average resistances in the coronary circulation, consisting of coronary stenosis (R_s), collateral (R_c) and myocardial (R) resistances. Coronary resistance is assumed zero when a stenosis is absent. Collateral resistance determines the collateral contribution to myocardial flow. Input pressure is arterial pressure P_a , distal coronary pressure P_d is measured distal of the stenosis in the coronary artery. The P_d measurement site can also be used to determine coronary wedge pressure P_w , during occlusion of the coronary artery ($R_s = \infty$), and central venous pressure P_v , when both coronary and collateral branches are occluded and myocardial flow is zero.

adjacent to the coronary artery functions as a collateral vessel: it connects the aorta to the distal coronary artery. The collateral resistance, and hence contribution to myocardial flow, can be controlled by a clamp (figure 3.1).

3.2.2 Background of the clinical indices FFR and IMR

Myocardial fractional flow reserve (FFR_{myo}) is a widely applied clinical parameter for assessing the influence of a coronary artery stenosis on maximum achievable mean myocardial blood flow (Bech et al., 2001; De Bruyne et al., 1996, 2000; Kern, 2000; Pijls et al., 2000, 1993; Wilson, 2001). It is defined as the ratio of mean hyperemic myocardial flow in the presence of a stenotic coronary artery (Q_{max}) to maximum mean flow in the hypothetical situation that no stenosis were present (Q_{max}^N) (Pijls et al., 1993):

$$FFR_{myo,Q} = \frac{Q_{max}}{Q_{max}^N} \quad (3.1)$$

To represent this ratio by coronary pressure measurements, we expressed the coronary circulation as a combination of serial and parallel resistances (figure 3.2). Myocardial flow in the presence of a stenosis in the supplying coronary artery (Q) is given by the mean pressure difference over the myocardium (distal coronary pressure P_d minus central venous pressure P_v) divided by myocardial resistance (R):

$$Q = \frac{P_d - P_v}{R} \quad (3.2)$$

In the hyperemic situation, myocardial resistance R is assumed to be minimal and constant. If no stenosis is present, P_d equals P_a and Q_{max}^N can be written as:

$$Q_{max}^N = \frac{P_a - P_v}{R} \quad (3.3)$$

As FFR_{myo} is defined as Q_{max}/Q_{max}^N (3.1), it follows from (3.2) and (3.3):

$$FFR_{myo} = \frac{P_d - P_v}{P_a - P_v} \quad (3.4)$$

In case of a normal coronary artery (absence of stenosis) collateral flow can be assumed to be zero and myocardial flow equals coronary flow. With an increasing degree of stenosis, however, collaterals will be recruited (in a variable degree across patients) and total myocardial flow Q is the sum of blood flow through the coronary artery (Q_s) plus collateral flow (Q_c).

$$Q = Q_s + Q_c = \frac{P_a - P_d}{R_s} + \frac{P_a - P_d}{R_c} \quad (3.5)$$

Now, the relative contributions of coronary artery flow and collateral flow to total myocardial flow can be expressed as their respective FFR ratios and coronary FFR_{cor} and collateral FFR_{col} can be defined by analogy with FFR_{myo} by dividing by Q^N

$$\begin{aligned} \frac{Q}{Q^N} &= \frac{Q_s}{Q^N} + \frac{Q_c}{Q^N} \\ \frac{Q_s}{Q^N} &= \frac{(P_a - P_d)R}{(P_a - P_v)R_s} \\ \frac{Q_c}{Q^N} &= \frac{(P_a - P_d)R}{(P_a - P_v)R_c} \end{aligned} \quad (3.6)$$

and

$$FFR_{myo,Q} = FFR_{cor,Q} + FFR_{col,Q} \quad (3.7)$$

During occlusion of the coronary artery Q_c equals Q and the distal coronary pressure is defined as coronary wedge pressure P_w .

$$\frac{P_a - P_w}{R_c} = \frac{P_w - P_v}{R} \quad (3.8)$$

Substituting (3.4) and (3.8) in (3.6) leads to FFR_{cor} and FFR_{col} determined by pressure

$$FFR_{cor} = \frac{P_d - P_w}{P_a - P_w} \quad (3.9)$$

$$FFR_{col} = \frac{(P_w - P_v)(P_a - P_d)}{(P_a - P_v)(P_a - P_w)} \quad (3.10)$$

The resistance of the second compartment of the coronary circulation, the myocardial microvasculature (R), is eliminated in all equations above. Hence, R cannot be analyzed merely by pressure measurements. To be able to evaluate myocardial resistance using guidewire-based technique, the index of microcirculatory resistance (IMR) was developed and validated in animal and human studies (Fearon et al., 2003; Aarnoudse et al., 2004a,b; Fearon et al., 2004).

By rearranging (3.2), myocardial resistance equals myocardial perfusion pressure divided by myocardial blood flow (figure 3.2):

$$R = \frac{P_d - P_v}{Q} \quad (3.11)$$

Since myocardial flow cannot be measured directly during catheterization, in the clinical definition of IMR, blood flow is replaced with the inverse mean transit time T_{mn} , obtained from the thermodilution curve following injection of a bolus of saline into the coronary artery at room temperature (De Bruyne et al., 2001b; Pijls et al., 2002) ($Q \sim 1/T_{mn}$).

$$R \sim (P_d - P_v)T_{mn} \quad (3.12)$$

or

$$IMR_{app} = (P_d - P_v)T_{mn} \quad (3.13)$$

Inverse T_{mn} , however, represents coronary rather than myocardial blood flow, and therefore, (3.12) and (3.13) only represent microvascular resistance if no collateral flow is present. Henceforth, the expression apparent index of microvascular resistance (IMR_{app}) is used. As previously described (Aarnoudse et al., 2004b), in the *in-vitro* validation study of IMR no collaterals were present. However, due to collateral contribution to myocardial flow in case of coronary stenosis in humans, using T_{mn} in the presence of an epicardial stenosis will underestimate myocardial flow, and thus, overestimate myocardial resistance. Therefore, as repeatedly shown in earlier studies, the index IMR should be corrected for general use in stenotic coronary arteries with collateral flow by including coronary wedge pressure P_w as follows (Aarnoudse et al., 2004a,b; Fearon et al., 2004):

$$IMR = IMR_{app} \frac{Q_{cor}}{Q_{myo}} = P_a T_{mn} \frac{(P_d - P_w)}{P_a - P_w} = P_a T_{mn} FFR_{cor} \quad (3.14)$$

When P_w equals zero, the original definition (3.13) is obtained.

3.2.3 FFR and IMR measurement in this study

Pressures are measured in the aorta by a pressure gauge (P10EZ-1, Becton Dickinson), and in the distal coronary artery by a 0.014" floppy pressure wire (PressureWire-4, Radi Medical Systems, Uppsala, Sweden), used with an amplifier and signal processor with modified software (Radi Analyzer). Electromagnetic flow meters (Transflow 1401, Skalar) are used to measure myocardial and reference aortic flow rates. The distal coronary PressureWire, connected to the Analyzer, was also used as a thermistor to determine the thermodilution mean transit time T_{mn} from the injection of a bolus of cold saline, as described earlier (De Bruyne et al., 2001b; Pijls et al., 2002).

All FFR measurements were performed at hyperemic flow conditions, with a normal maximum myocardial flow (i.e. normal microvasculature and no epicardial stenosis) of approximately 250 ml/min. For the assessment of FFR, four levels of collateral resistance were used, characterized by a maximal contribution of collateral flow to myocardial flow at coronary occlusion of approximately 0, 20, 40 and 60% of normal myocardial flow. These numbers are derived from the maximum collateral contribution in the human coronary circulation (Vanoverschelde et al., 1993). At each level of collateral resistance, epicardial stenosis severity was increased by adjustment of the epicardial clamp in 7 - 10 steps from no stenosis to full occlusion. Each series was repeated threefold. After occlusion the vessel was fully opened again and reachievement of baseline conditions was verified. At all steps P_a , P_d and Q were measured. In the presence of collateral flow, coronary wedge pressure P_w was defined as P_d at total occlusion, in accordance with its clinical definition. Central venous pressure P_v was approximately 6 mmHg. From the pressure and flow measurements FFR_{myo} (calculated by pressure), $FFR_{myo,Q}$ (calculated by flow), FFR_{cor} , FFR_{col} , and the myocardial resistance R were calculated. The value of Q_{max}^N (to be used in the computation of $FFR_{myo,Q}$), and P_w (in FFR_{cor} and FFR_{col}) were corrected for changes of P_a from its initial value in the absence of a stenosis as described before (Pijls et al., 1993, 2002).

For the assessment of IMR, seven measurement series at seven levels of collateral resistance (collateral contribution varying in percentages of maximum myocardial flow without collaterals, from 0% (total occlusion) to 100% (no stenosis)) were obtained. In each series adjusting the clamp, in 6 steps, increased epicardial resistance. Per step, average Q , P_d and P_a were recorded. P_w was measured by the distal pressure sensor during total occlusion of the coronary artery tube. For each degree of stenosis at each level of collateral resistance, thermodilution curves were obtained by injection of a bolus of cold saline. T_{mn} was calculated automatically and completely in congruence with the technique used at the bedside and validated in animals and humans previously (De Bruyne et al., 2001b; Pijls et al., 2002). From the measured pressures, flows, and mean transit times, IMR_{app} , IMR , and FFR_{myo} were calculated. The range of variations in IMR and IMR_{app} were compared to that of true myocardial resistance R by normalizing them to their respective values at the measurement series' maximum FFR_{myo} .

3.2.4 Statistical analysis

We used linear regression techniques to analyze the relationships between (1) $FFR_{myo,Q}$ and FFR_{myo} , and in addition Spearman's rank correlation, for (2) IMR and FFR_{myo} , and (3) IMR_{app} and FFR_{myo} . For the analysis of $FFR_{myo,Q}$ and FFR_{myo} linear regression was performed for all 12 measurement series of variation of epicardial stenosis (three series per collateral level) separately, and the coefficients found for the slope and intercept of the linear relation were represented as mean \pm standard deviation.

For the analysis of IMR and IMR_{app} versus FFR_{myo} , all collateral levels were pooled. In a sensitivity analysis, we evaluated quadratic rather than linear functions in the regression analysis. Explained variance (R^2) was used to determine the goodness of fit of our regression models. P-values less than 0.05 were considered statistically significant.

3.3 Results

Myocardial fractional flow reserve based on pressure measurements (FFR_{myo} , equation (3.4)) in the in-vitro coronary circulation strongly correlated with the flow-derived $FFR_{myo,Q}$. This correlation exists for all levels of collateral resistance and was independent of the level of collateral flow (figure 3.3). Linear regression of all twelve series of stenosis variation at the four levels of collateral flow separately produced estimates for the slope (1.13 ± 0.07) and intercept (-0.15 ± 0.06) of the linear relation between FFR_{myo} and $FFR_{myo,Q}$. For all analyses, R^2 was 0.99.

The relative contribution of collateral and coronary flow to myocardial flow was expressed by FFR_{col} and FFR_{cor} (figure 3.4). If no collateral flow was present, FFR_{myo} equaled FFR_{cor} for the entire flow range (figure 3.4, a). For increasing maximum collateral flow, the slope of FFR_{cor} increased. In other words, the contribution of coronary flow to myocardial flow decreased faster with stenosis severity at higher maximum collateral flow as expected. Minimum myocardial flow was always achieved when it was equal to collateral flow ($FFR_{cor} = 0$, $P_d = P_w$, $FFR_{myo} = FFR_{col} = P_w/P_a$). As a matter of fact, further increase of epicardial stenosis severity did not lower distal coronary pressure.

When myocardial resistance was characterized by IMR_{app} (without taking collateral influence into account, equation (3.13)), it increased with decreasing FFR_{myo} (i.e. increasing stenosis severity), fully in congruence with observations in humans (Aarnoudse et al., 2004a) (figure 3.5, Spearman's rank coefficient $R_S = -0.59$, $p < 0.001$, significant linear ($p < 0.003$), nonsignificant quadratic ($p = 0.63$) correlation). The apparent increase becomes stronger with increasing collateral contribution. The value of IMR_{app} is increasing asymptotic towards $FFR_{myo} = P_w/P_a$, where further increase of epicardial resistance does not lead to a decrease in myocardial flow, due to collateral contribution. In contrast, the true IMR (3.14) remained unchanged, independent of the level of collaterals and the epicardial stenosis severity ($R_S = -0.18$, $p = 0.24$, no significant linear ($p = 0.21$) or quadratic ($p = 0.98$) correlation). These results are fitting well with previous observations in animals and men (Aarnoudse

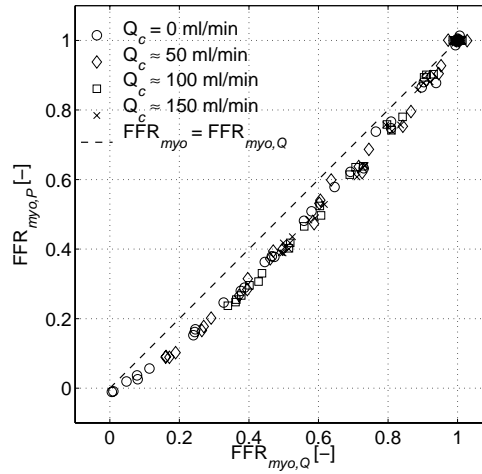


Figure 3.3: FFR_{myo} vs. $FFR_{myo,Q}$ for all series and all collateral levels. The course of FFR_{myo} was not influenced by the maximum collateral flow. Linear regression of all series separately produced estimates for slope (1.13 ± 0.07) and intercept (-0.14 ± 0.06) of the linear relation between FFR_{myo} and $FFR_{myo,Q}$. R^2 was 0.99 for all analyses.

et al., 2004a; Fearon et al., 2004).

When the variation in IMR and IMR_{app} was compared to that in the real myocardial resistance directly calculated from pressures and volumetric flow according to (3.11), the increase in IMR_{app} was up to eight times higher than any variation in true R (figure 3.6). In contrast, IMR remained equal to R . The variation in normalized IMR increases with decreasing FFR_{myo} . All data were normalized to their value at the series' maximum FFR_{myo} .

3.4 Discussion

Our present study demonstrates that our in-vitro model of the coronary circulation, extended by collaterals, is a useful tool to study two important clinical diagnostic techniques in which also the collateral circulation plays an important role.

All data obtained were in perfect congruence with the previous validation studies in animals and humans (Aarnoudse et al., 2004a; De Bruyne et al., 1996, 2000; Fearon et al., 2004; Pijls et al., 1993). Furthermore, the role of collaterals in assessing clinically used physiological parameters and potential biases by not taking them into account, could be better understood.

Our results show that FFR_{myo} as assessed by pressure measurements correlates well with $FFR_{myo,Q}$ as measured directly by flow measurements as was shown previously in animals, thus underlining the suitability of the model to simulate clinical diagnostic techniques. Furthermore, the *in-vitro* evaluation of IMR fitted well with the

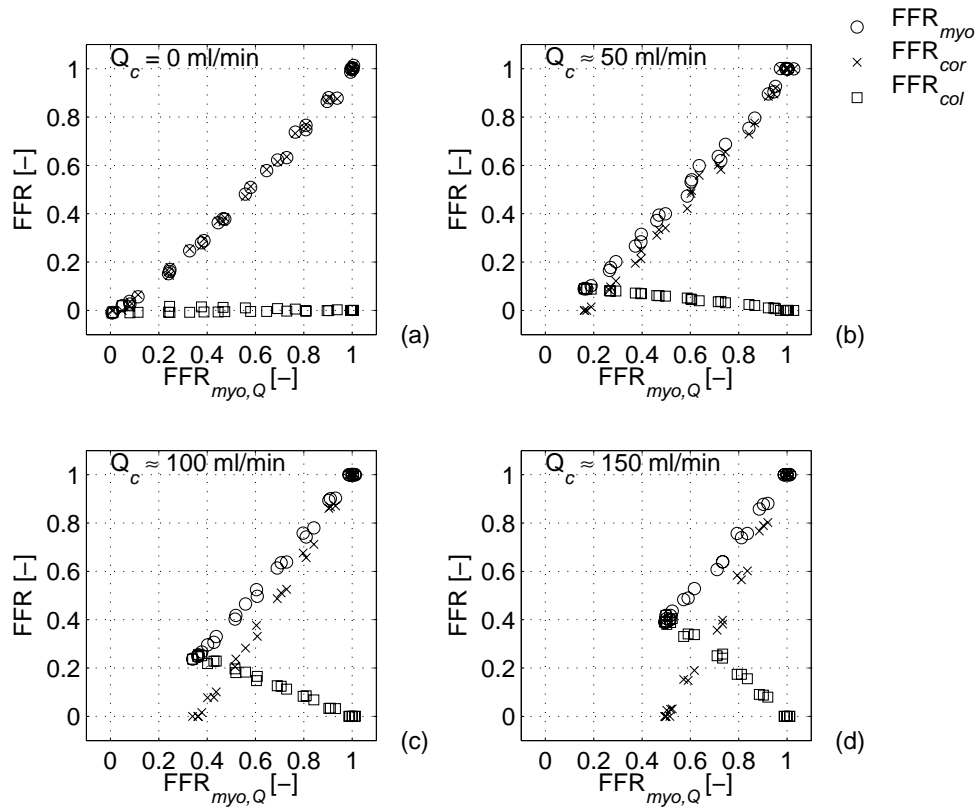


Figure 3.4: Fractional flow reserve determined by pressure (FFR_{myo} , FFR_{cor} and FFR_{col}) compared to $FFR_{myo,Q}$ as directly measured by flow measurement, for different levels of collateral flow ((a) to (d), from 0 to 150 ml/min in steps of 50 ml/min) and different stenosis severity (characterized by $FFR_{myo,Q}$). The relative contributions of coronary and collateral flow to myocardial flow are represented by FFR_{cor} and FFR_{col} , respectively. The maximum collateral flow (determined by the collateral resistance) determines the course of FFR_{cor} and FFR_{col} and the minimum value of FFR_{myo} . In all four situations FFR_{myo} equals the sum of FFR_{cor} and FFR_{col} .

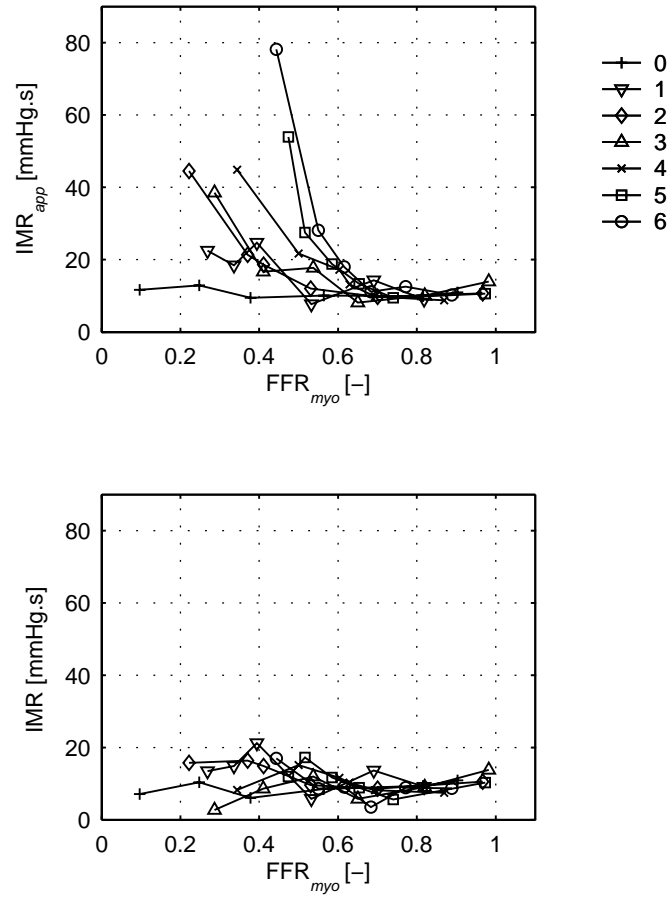


Figure 3.5: Apparent (IMR_{app} , top) and true index of microcirculatory resistance (IMR , bottom), for seven levels of maximum collateral flow, ranging from 0 to 60% of normal myocardial flow. IMR_{app} was significantly dependent on FFR_{myo} , whereas IMR was completely independent.

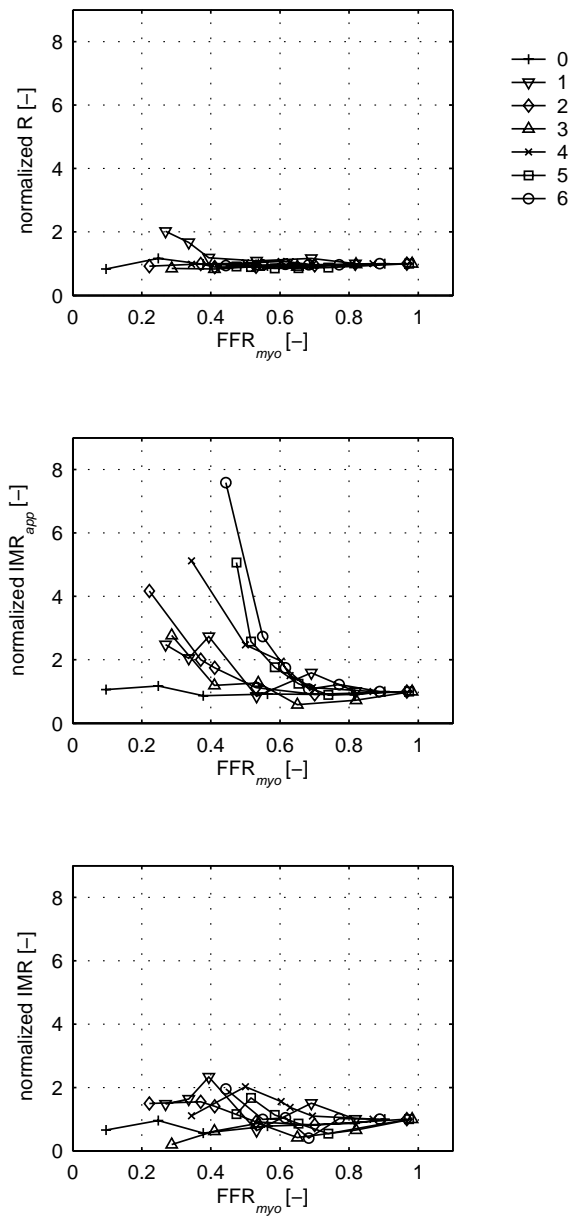


Figure 3.6: True myocardial resistance R , IMR and IMR_{app} , all normalized to the maximum of FFR_{myo} in the measurement series, for seven levels of maximum collateral flow, from 0 to 60% of normal myocardial flow. The slight changes in true myocardial resistance are up to eight times smaller than those in IMR_{app} .

predicted model, as described in our earlier *in-vitro* study on IMR without influence of collateral flow (Aarnoudse et al., 2004b). When appropriately adjusted for collateral contribution to myocardial flow in this bench model, this index was found to be independent of stenosis severity, as earlier observed in animals (Fearon et al., 2004) and the catheterization laboratory (Aarnoudse et al., 2004a).

The relative contribution of coronary and collateral flow was reflected by FFR_{cor} and FFR_{col} summed up to FFR_{myo} (figure 3.4) over a wide range of collateral flow and epicardial stenosis severity. The relation between FFR_{myo} and $FFR_{myo,Q}$ was not influenced by the source (coronary or collateral) of the flow (figure 3.4), and hence its theoretical value for quantification of the influence of the stenosis on the myocardial flow reserve was confirmed, in accordance with the results of the previous animal study (Pijls et al., 1993).

Because of the uneven distribution of the data over the entire range of FFR (less points in lower FFR range because of a higher minimum value in the presence of higher collateral flow), the deviations from unity in slope (1.13 ± 0.07) and intercept (-0.15 ± 0.06) were larger when the average of all series was taken, than when only the non-collateral situation was evaluated (three series, slope = 1.04 ± 0.002 , intercept = -0.07 ± 0.006). These values are comparable to the results of Segers et al. (1999). They found a slight underestimation of $FFR_{myo,Q}$ by FFR_{myo} of 0.06 ± 0.07 , and similar variations in myocardial resistance. However, in their study a model without a physiological flow pattern was used, and collaterals were not included.

The levels of collateral flow during occlusion of the coronary vessel were set at 20, 40 and 60% of maximum myocardial flow without stenosis. In most humans with coronary artery stenosis, maximum achievable collateral flow is in the range of 10-30% of normal maximum myocardial flow. However, sometimes, it can reach values up to 60% of normal maximum flow (Vanoverschelde et al., 1993). In our study, we also studied the higher levels of collateral flow to test the suitability of our model in predicting correct FFR_{myo} and IMR over a wide range.

The independence of stenosis severity of the appropriately defined IMR confirmed the results of similar studies in animal models and patients (Aarnoudse et al., 2004a; Fearon et al., 2004). In earlier studies (Chamuleau et al., 2003; Marzilli et al., 2000; Sambuceti et al., 2001) the microcirculatory resistance has been assessed using methods based on evaluation of coronary flow as a representative for myocardial flow. From this approximation, microvascular resistance was found to increase with epicardial stenosis severity. This study confirms that this may be contributed to the underestimation of myocardial flow by the neglect of collateral contribution, as shown previously (Aarnoudse et al., 2004a; Fearon et al., 2004).

The slight change in myocardial resistance (and underestimation of FFR_{myo}) does not influence the outcome of the IMR evaluation: the increase in IMR_{app} is far larger than the variation in myocardial resistance, as can be seen in figure 3.6. However, it may be the reason for the slight trend of a correlation between IMR and FFR_{myo} as indicated by Spearman's rank coefficient $R_S = -0.18$. The results of the regression analysis confirm Spearman's rank analysis: for both situations only a linear correlation between IMR_{app} and $FFR_{myo,Q}$ was present and no higher order term was statistically significant.

The increasing variability of IMR with decreasing FFR_{myo} may be explained by the methodology to measure low flow rates by mean transit times. Then T_{mn} is larger and the physical influence of the injection of saline on flow increases, resulting in a larger variation between measurements.

3.5 Limitations

Our study has several limitations. The slight underestimation of FFR_{myo} could be related to the non-linear pressure-dependent behavior of the average myocardial resistance. Unlike in humans, R in this *in-vitro* model (the ratio between $P_d - P_v$ and Q) decreases with myocardial flow, because P_d is reduced with respect to Q and FFR_{myo} will be slightly underestimated compared to $\text{FFR}_{\text{myo},Q}$. This is a limitation inherent to the design of the model and the material used.

Furthermore, our evaluation of several levels of stenosis severity showed that the maximum myocardial flow increased with decreasing collateral resistance (up to approximately 300 ml/min at 60%). Hence, the minimal levels of $\text{FFR}_{\text{myo},Q}$ were not exactly equal to 0.20, 0.40 and 0.60, respectively, but slightly higher. This did not directly influence the results, but additionally indicated non-linearity in the resistances in the model.

3.6 Conclusion

The usefulness and validity of our model, which mimicks the physiology of the coronary circulation and takes into account collateral flow, was supported by evaluating two clinical invasive coronary techniques, FFR and IMR, for characterization of epicardial stenosis severity and microvascular resistance, respectively. The observations in our model with respect to both indexes correlated excellently with corresponding expert clinical observation. Therefore, we believe that the model used in this study can be proposed for further bench studies of intracoronary diagnostic techniques.

3.7 Acknowledgements

This study was supported by the Dutch Technology Foundation (STW) project EPG.5454, and by Radi Medical Systems, Uppsala, Sweden. The authors would like to thank Vincent Bohté, Petra van den Berg, Arjen van der Horst, Petra Nijman, Gijs Snieders and Marian van der Veen for their contribution to the evaluation of the *in-vitro* set-up.

Chapter 4

Continuous infusion thermodilution for assessment of coronary disease: theoretical background and *in-vitro* validation

Direct volumetric assessment of coronary flow during catheterization has not been available so far. Coronary thermodilution is a method to obtain a derivative of flow: the mean transit time of a bolus of cold saline injected into the coronary artery. In the current study a (for coronary flow assessment) new method is evaluated, based on continuous infusion of saline into a selective artery. From the temperature of the blood, the saline, and the mixture downstream to the infusion site, combined with the known infusion rate, volumetric flow can be calculated. Aim of the current study is to optimize the measurement method in an in-vitro model of the coronary circulation. The influence of several parameters is assessed: catheter design, infusion rate, and location of infusion and temperature measurement. Full mixing of the saline and blood is found to be the main prerequisite for accurate determination of the flow. With the use of an appropriate catheter design (infusion mainly through distally located sideholes), a high enough infusion rate (25 ml/min), and measurement of the mixing temperature between 5 and 8 mm distal from the tip of the infusion catheter, the flow could be assessed with 95% limits of agreement of $107\% \pm 8\%$, or an absolute accuracy of 7 ± 4 ml/min, over the entire physiological flow range of 50 - 250 ml/min. Hence absolute coronary flow rate can be directly, reliably measured by the continuous infusion method when full mixing is present, under the conditions mentioned above.

The contents of this chapter are based on M.C.F. Geven, M. van 't Veer, M.C.M. Rutten, A. van der Horst, W.H. Aarnoudse, N.H.J. Pijls and F.N. van de Vosse. Continuous infusion thermodilution for assessment of coronary disease: theoretical background and in-vitro validation. *Medical Engineering and Physics*, to be submitted.

4.1 Introduction

In the assessment of the coronary circulation intracoronary pressure and blood flow are the parameters characterizing the functional significance of disease. Intracoronary pressure is widely used to quantify the severity of an epicardial stenosis (De Bruyne et al., 1996; Kern, 2000). To interrogate the condition of the myocardial microvasculature also quantification of coronary or myocardial flow is needed. However, techniques for direct absolute flow measurement are still not available for common clinical practice. Methods for indirect measurement aim for the determination of coronary flow reserve (CFR), the ratio between resting flow and maximum achievable hyperemic flow (Gould et al., 1990) by substitutes of coronary flow, such as velocity or transit times. In the present chapter, the theoretical background for absolute coronary flow measurement and its *in-vitro* validation will be described.

Generally, direct and indirect flow measurement methods can be divided into two groups: non-invasive and invasive methods (Vassalli and Hess, 1998). Non-invasive measurements include positron emission tomography (PET), in which radiopharmaceutical blood flow tracers are used to determine regional myocardial blood flow (Schwaiger and Muzik, 1991; Schelbert et al., 1982), and magnetic resonance imaging (MRI), especially applicable to determine flow velocity in larger vessels (Rebergen et al., 1993; Sakuma et al., 1996; Ibrahim et al., 2002). In the catheterization laboratory an invasive assessment can be carried out by using a ultrasound Doppler flowmeter, mounted on a guidewire (White, 1993). With an ultrasonic velocimetry probe, phasic and mean flow velocity can be measured during baseline and hyperemic conditions. To accurately determine CFR, the sensing direction should be stable, as well as the coronary diameter, and the relation between flow velocity and flow rate should be linear, which is often not the case (Gould et al., 1990; Vassalli and Hess, 1998). Another invasive method uses the injection of an indicator into the blood, and monitoring of the transit time of this indicator in the blood flow (Meier and Zierler, 1954). The conventional, clinically applied indicator dilution method is thermodilution, where the indicator is a bolus of cold saline, briskly injected into the coronary ostium. The mean transit time of the bolus is inversely correlated to the local coronary flow and from the ratio of the transit times at baseline and hyperemia CFR can be determined. Although the validity of this method was shown in several *in-vivo* and *in-vitro* studies, still no absolute flow rate can be measured unless the exact vascular volume would be known (Barbato et al., 2004; De Bruyne et al., 2001b; Pijls et al., 2002).

To overcome these drawbacks and derive real blood flow during catheterisation the thermodilution method by continuous infusion of saline is investigated in this study. Theoretically, absolute blood flow is measured from the mixing temperature of a known infusion rate at known temperature, and the constant temperature blood. More than 30 years ago Ganz et al. (1971) proposed continuous infusion, but only for the measurement of coronary sinus flow due to technical limitations at that time. Recently, we applied the method in animal and patient studies (Pijls et al., 2007; Aarnoudse et al., 2007). During catheterization, the instrumentation was performed as depicted in figure 4.1. The sensor-tipped pressure-temperature guidewire was

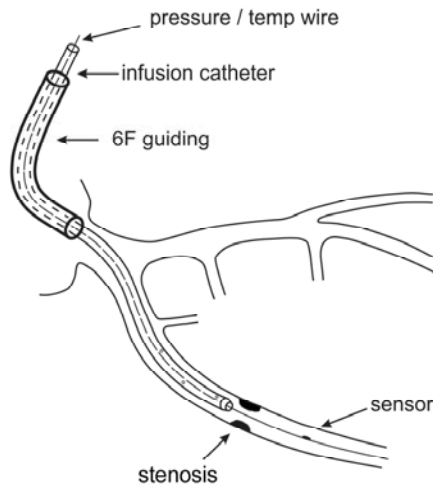


Figure 4.1: Set-up of the instrumentation in the coronary artery, with guiding catheter, infusion catheter and guidewire. The temperature sensor is located at the guidewire, 3 cm from the tip. The wire can be pulled back inside the infusion catheter to register the temperature of the infusate.

positioned through the guiding catheter into the coronary artery. Thereafter, the infusion catheter was advanced over the wire, situating its tip inside the selected artery, with the temperature sensor a few centimeters distal to the infusion site (at the tip). Distal temperature of the mixture of saline and blood, as well as the infusate temperature inside the infusion catheter were measured. Strong correlations between real flow rate and flow derived from mixing temperatures were obtained. The main prerequisite for applicability of the continuous infusion method for measurement of absolute coronary blood flow was found to be full mixing of the infusate and blood and accurate measurement of the mixing temperature. For that purpose, the design and characteristics of the infusion catheter were important.

In the current study we provide a more detailed theoretical background, and take the method to the bench to investigate its fundamental characteristics more closely under well-controlled circumstances in a physiologically representative model of the coronary circulation. The model allows for measurement and control of all relevant parameters such as fluid temperature and flow rate.

The aim of the study is to investigate the boundary conditions for optimal mixing and accurate application of the method (with respect to the design of the infusion catheter and the location of infusion and measurement sites) and to compare the flow rates derived by this method with real flow. Hence, we aim to contribute to better understanding and optimisation of flow measurement by continuous infusion for clinical purposes by catheter and methodological design.

4.2 (Theoretical) background

4.2.1 Measurement principle

The temperature distribution in the vessel during infusion can be described using the heat equation, expressing the conservation of energy within the system. The general form is given by

$$\rho c_p \left[\frac{\partial T}{\partial t} + (\vec{u} \cdot \nabla) T \right] = k \nabla^2 T \quad (4.1)$$

where ρ is density, c_p is specific heat, T is temperature, t is time, u is velocity, and k is thermal conductivity. The first term on the left hand side describes the local temperature variations in time. In the continuous infusion experiments the heat transfer due to mixing is assumed to be stationary, hence $\frac{\partial T}{\partial t} = 0$. The diffusion of heat is assumed to be small compared to convective heat transfer due to the fluid flow: $(\vec{u} \cdot \nabla) T \gg k \nabla^2 T$. Now the simplified heat equation becomes:

$$\rho c_p (\vec{u} \cdot \nabla) T = 0 \quad (4.2)$$

In this general form, only one fluid is considered. In the measurement situation cold fluid (subscript i) is added to the blood (subscript b):

$$\rho_b c_{p,b} (\vec{u}_b \cdot \nabla) T + \rho_i c_{p,i} (\vec{u}_i \cdot \nabla) T = 0 \quad (4.3)$$

When optimal mixing is assumed, integration over the vessel surface (to achieve volumetric flow Q) and in the direction of the flow (to derive temperature differences from temperature gradients) is allowed and gives:

$$\rho_b c_{p,b} Q_b (T_b - T) + \rho_i c_{p,i} Q_i (T_i - T) = 0 \quad (4.4)$$

Rearranging (4.4) the expression for Q_b can be found

$$Q_b = \frac{\rho_i c_{p,i} (T - T_i)}{\rho_b c_{p,b} (T_b - T)} Q_i = \frac{\rho_i c_{p,i}}{\rho_b c_{p,b}} \left[\frac{T_b - T_i}{T_b - T} - 1 \right] Q_i \quad (4.5)$$

In (4.5) Q_b is the blood flow during infusion of cold saline: hence the blood flow is assumed not to be affected by the infusion. However, if the aortic pressure is not increased by the infusion and the myocardial resistance remains constant, the total flow during the myocardium will not increase (figure 4.2). Hence the measured flow is decreased by Q_i and the original blood flow can be found using:

$$Q_{b,orig} = Q_b + Q_i = \frac{\rho_i c_{p,i}}{\rho_b c_{p,b}} \left[\frac{T_b - T_i}{T_b - T} - 1 \right] Q_i + Q_i \quad (4.6)$$

In the clinical situation the myocardial resistance is assumed to be constant and minimal during hyperemia, T_i and T are measured relative to the blood temperature,

Table 4.1: Values for temperature, density and specific heat as used in the clinical situation. Saline concentration is 9 g l^{-1} . In the current study water was used as a flow medium, as well as for the infusion.

	T [$^{\circ}\text{C}$]	ρ [kg m^{-3}]	c_p [$\text{kJ kg}^{-1} \text{K}^{-1}$]
blood	37	1050	3.60
saline	33	1001	4.17
water	37	994	4.18
water	33	995	4.18

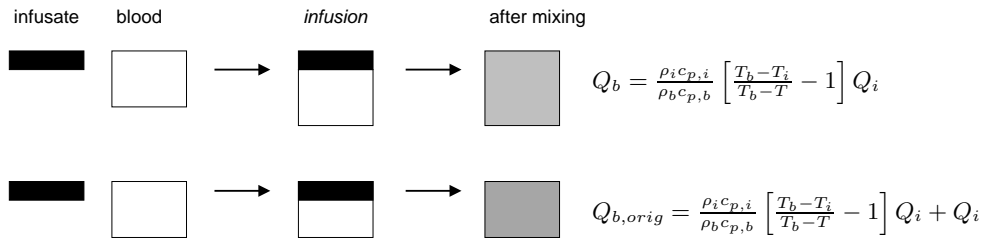


Figure 4.2: Two limit situations for calculation of blood flow by continuous infusion at constant perfusion pressure: varying myocardial resistance (top) and constant myocardial resistance (bottom).

and the densities and specific heats for blood and saline from table 4.1 are used. Hence the expression for calculation of the blood flow becomes:

$$Q_{b,orig} = 1.09 \left[\frac{T_i}{T} - 1 \right] Q_i + Q_i \quad (4.7)$$

In the current study water is used as a flow medium and infusate, and from table 4.1 the fraction in equation 4.7 is 1.002. Some of the boundary conditions required to be met for accurate calculation of coronary flow from the measurement of infusate and mixing temperature are already mentioned above. The first, principal condition requires for the infusate and the blood to be fully mixed: a non-homogeneous mixture will lead to a possibly fluctuating too high or low mixing temperature measured and to a corresponding over- or underestimation of the flow rate. The design of the infusion catheter can influence the mixing process: the presence of sideholes, and their size and position determine the inflow velocity and direction. Sideholes positioned closely together and the endhole tapered around the wire, are expected to enhance mixing due to the "spraying" effect during infusion. Another factor is the nature of the blood flow at the injection site. The occurrence of secondary flows, flow disturbances due to geometrical irregularities and possible turbulent spots, induced by the infusion, will enhance and maintain mixing. Favourable locations for measurement are found near the coronary ostium (entrance flow), in strong curves and in vessel parts with non-smooth surfaces. A second important assumption is that the mixing temperature is only determined by the two inflow fluids, blood and infusate. This results in the mixing temperature

to be constant in the vessel distal to the mixing area. However, due to the slight temperature difference between the mixture and the vessel wall heat transfer between the fluid and the wall occurs. The fluid will be heated gradually with increasing distance from the infusion site. Both the mixing circumstances as well as the heat transfer to the surroundings will be investigated in the current study. Third, in the calculation of blood flow from fluid temperatures an assumption for the possible change in myocardial resistance should be made: hence the influence of the infusion to total myocardial flow should be determined (figure 4.2).

4.3 Methods

4.3.1 *In-vitro* model of the coronary circulation

As described in chapter 2, the *in-vitro* experimental model consisted of a piston pump, a left ventricular chamber and two valves, representing the left ventricle of the heart, a systemic and a coronary circulation. The systemic circulation contained a polyurethane tube (with the dimensions and mechanical properties of the aorta), and a system of compliances and resistances, creating physiological aortic pressure and flow patterns. The polyurethane coronary artery branched off the aorta directly distal to the aortic valve and bifurcates into a subendocardial and a subepicardial myocardial tube. The subendocardial branch was led through the left ventricular chamber and collapses during systole due to high left ventricular pressure. This allowed for modelling the variable resistance and volume behaviour of the endocardial part of the *in-vivo* myocardium. The arteriolar resistance clamp could be adjusted to create baseline and hyperemic flow conditions. We have previously shown that these elements provide physiological aortic and coronary pressure and flow patterns (chapter 2, Geven et al. (2004)). Representative pressure and flow patterns both at rest and hyperemia, with predominant diastolic flow, are shown in figure 2.4. The model was filled with water and kept at a constant fluid temperature of $37.00 \pm 0.02^\circ\text{C}$ by an external thermal bath and circulator (F34-HL, Julabo). The infusate was water as well (at room temperature), and was injected at a constant, adjustable flow rate by an infusion pump (Angiomat 6000, Liebel-Flarsheim). For all measurements, the model was tuned to hyperemic coronary flow of approximately 250 ml/min. A coronary stenosis was created by a clamp directly proximal to the myocardial model, allowing for variation of coronary flow between 0 and 250 ml/min. Aortic pressure was measured directly distal to the aortic valve using a pressure transducer (P10EZ-1, Becton Dickinson) and bridge amplifier (Picas-CA2CF, Peekel Instruments). For direct aortic and coronary flow measurement ultrasound flow probes were applied (4PSB, Transonic); distal coronary pressure and temperature were registered by a pressure-temperature sensor-tipped guidewire (PressureWire-5, Radi Medical Systems). The sensor is located at 3 cm from the wire tip; all temperatures were measured relative to the model fluid temperature T_b .

Table 4.2: Geometrical properties of the two infusion catheters used in this study.

	model A	model B
nr of sideholes	3	4
sideholes distributed over	30 mm	5 mm
outer \varnothing	1 mm	1.17 mm
inner \varnothing	0.53 mm	0.97 mm

4.3.2 Infusion catheters

To show the importance of good mixing, the use of two different over-the-wire infusion catheters was evaluated: the first one was a general model frequently used in the cathlab (model A), with three sideholes equally distributed over the distal 3 cm of the catheter, the second a specifically designed catheter (model B), in which four sideholes were laser-punched over a length of 0.5 cm, from 0.5 to 1.0 cm from the tip. The distal end of catheter B was tapered to minimize infusion through the end-hole. Geometrical properties of the catheters can be found in table 4.2. Care was taken to locate the tip of the infusion catheter to have all sideholes positioned inside the coronary artery, but close to the coronary ostium. Mixing is facilitated by non-fully developed entrance flow and secondary flows due to the curvature and irregular shape of the connection.

4.3.3 Procedures

Infusion rate

All experiments were carried out at two infusion rates (as in the animal and human studies): a low rate of 15 ml/min, and a higher rate of 25 ml/min.

Guidewire pullback

To investigate the mixing behaviour of the infusate with the heated model water, the influence of warming of the mixture via the vessel wall, and the optimal location for measurement of the infusate temperature T_i , a pullback protocol was carried out. The local temperature during infusion was measured by step-wise manual pullback of the guidewire, from a sensor position 10 cm distal of the tip of the infusion catheter to 4 cm inside the infusion catheter at intervals of 1 cm. Pullback temperature curves were made for both catheters, at baseline and hyperemic coronary flow rates of 50 and 250 ml/min, respectively, and with infusion rates of 15 and 25 ml/min.

Flow measurement at fixed position

Coronary flow was derived by continuous infusion and correlated to the real flow measured by the ultrasound flow probe. The coronary flow rate was set from 50 to 250 ml/min in steps of 50 ml/min by the distal coronary clamp. From the pullback curves sensor positions for measurement of mixing temperature T and

infusion temperature T_i were derived (between 5 and 6 cm from the tip of the infusion catheter, and 1 cm inside, respectively). The position of the infusion catheter was fixed during the procedure. Aortic pressure P_a , temperature and pressure at the guidewire sensor and coronary flow were monitored. Initially the guidewire sensor was positioned at the distal position, and initial values for all parameters were determined. Infusion was started and the mixing temperature T was registered, subsequently the guidewire was pulled back inside the catheter for measurement of T_i . After stopping the infusion all final parameters were compared to their initial values. The data were analysed by a Bland-Altman method, visualising the accuracy of the estimation of the real flow (Bland and Altman, 1986).

Position of infusion catheter

The position of the infusion catheter was initially chosen proximal in the coronary artery, to possibly encounter the positive effect of the secondary flow in the ostium curvature. This influence was qualified by performing measurements at three positions of the tip of the infusion catheter: the proximal position (0 cm), +3 cm, and +6 cm. In all situations the distance between the tip and the wire sensor was 6 cm for the measurement of T , T_i was registered 1 cm inside the catheter. Coronary flow was 50 or 250 ml/min, infusion rate 25 ml/min.

4.4 Results

4.4.1 Guidewire pullback

All temperature registrations during the pullback curves show variations in temperature between 3 and 10 cm from the catheter tip (figure 4.3). Between 0 and 3 cm from the tip the instationary variations in temperature were larger than further downstream for both catheters.

To evaluate the course of the temperature difference as a function of the distance, all temperatures were normalised to the mean temperature between 3 and 10 cm (figure 4.4). The shape of the curves was similar for both catheters and the distance could be divided into three characteristic zones, (a) < 5 cm: the temperature was unsteady (model A) or decreasing (model B) towards the tip, (b) 5 - 8 cm: a steady or decreasing temperature was present with increasing distance distal from the tip, (c) > 8 cm: a gradual rise in temperature was seen with both catheters.

Inside the catheter (between 0 and -4 cm), the temperature profile was different for the two catheters (figure 4.3, inside). For catheter A a gradual decrease in temperature and increase in pressure was found with each position further inside the catheter. The temperature inside catheter B was changing less gradually.

4.4.2 Flow measurement at fixed position

In the calculation of the blood flow the myocardial resistance was assumed to be constant before and during infusion. This was confirmed by the registration of the

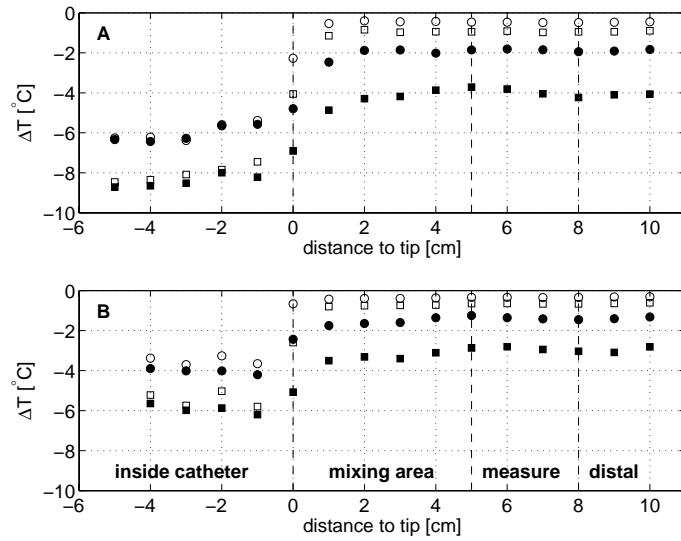


Figure 4.3: Temperature measured during guidewire pullback at two infusion rates: $\square = 25 \text{ ml/min}$, $\circ = 15 \text{ ml/min}$. Open symbols denote coronary flow of 250 ml/min , filled symbols 50 ml/min . Two infusion catheters were used: top: model A, bottom: model B (catheter specifications are summarized in table 4.2). The distance is measured relative to the tip of the infusion catheter.

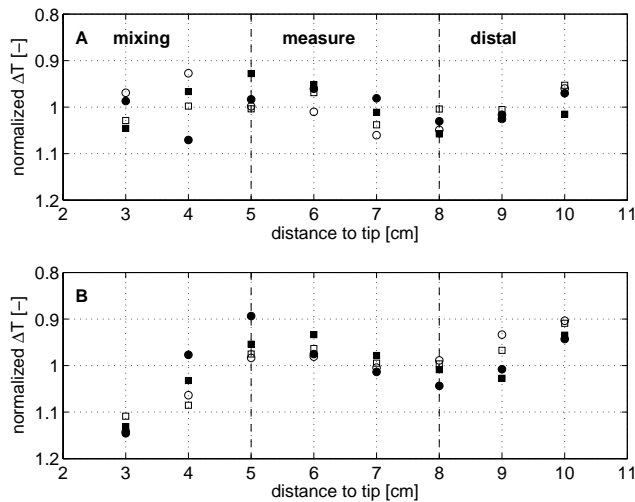


Figure 4.4: Detail (normalized) of figure 4.3 outside the catheter: ΔT normalized to the mean ΔT over 3 - 10 cm, distal to the infusion site for both catheters. Open symbols denote coronary flow of 250 ml/min , filled symbols 50 ml/min , infusion rates $\square = 25 \text{ ml/min}$, $\circ = 15 \text{ ml/min}$.

real coronary flow: the relative difference in flow between before and during infusion was $0.8\% \pm 1.1\%$ for all fixed position measurements. Hence the original blood flow was calculated by (4.6).

At a coronary flow of 50 ml/min, for both infusion rates and catheters the flow rate was accurately determined (figure 4.5). At an infusion rate of 15 ml/min, for both catheters increasing flow rate was increasingly underestimated, hence the mixing temperature was too low. At the higher infusion rate of 25 ml/min, the flow rate was reliably calculated by the continuous infusion method with catheter B, whereas the ratio between calculated and real flow deviates from unity for $Q_{cor} > 200$ ml/min for catheter A. Hence, for consistent flow estimation catheter B had to be used at the high infusion rate of 25 ml/min.

From the Bland-Altman representation the accuracy of the method could be determined, provided that no relation between the absolute value and the difference between the real and calculated flow were present. In the Bland-Altman plots for catheter A and B at low infusion rate (figure 4.6, left), and catheter A at high infusion rate (figure 4.6, top, right), such a relation is visible: the absolute flow rate is progressively underestimated with increasing flow rate. This indicates that the accuracy of the measurement is strongly related to the absolute value, and not only linearly related to amplitude, and a general estimation for the accuracy cannot be given. Catheter B used in combination with a high infusion rate resulted in 95% limits of agreement for the method over the entire range of $107\% \pm 8\%$ of the flow, or a mean absolute difference between calculated and direct measured flow over the entire range of 7 ± 4 ml/min.

4.4.3 Position of infusion catheter

The influence of the position of the infusion site was determined by measurements at 3 infusion sites at increasing distance from the coronary ostium, for a coronary blood flow of 50 and 250 ml/min and an infusion rate of 25 ml/min. For both catheters the accuracy for 50 ml/min does not vary much with infusion position (figure 4.7), for 250 ml/min at the most proximal position (1, indicated by +) the flow was calculated most accurately, although for the catheter A also at position 3 a better estimate was obtained than for catheter B.

4.5 Discussion

In the current study an *in-vitro* model was used to investigate the most critical boundary condition for clinical application of continuous infusion flow measurement: the mixing of the blood and infusate. The mixing is influenced by infusate and blood flow conditions and the geometry of the vessel and catheter. Hence the influence of infusion catheter design, position of the temperature sensor, location of the infusion site, and the infusion flow rate on the accuracy of the determination of the flow were investigated.

From the wire pullback a varying temperature with the distance to the catheter

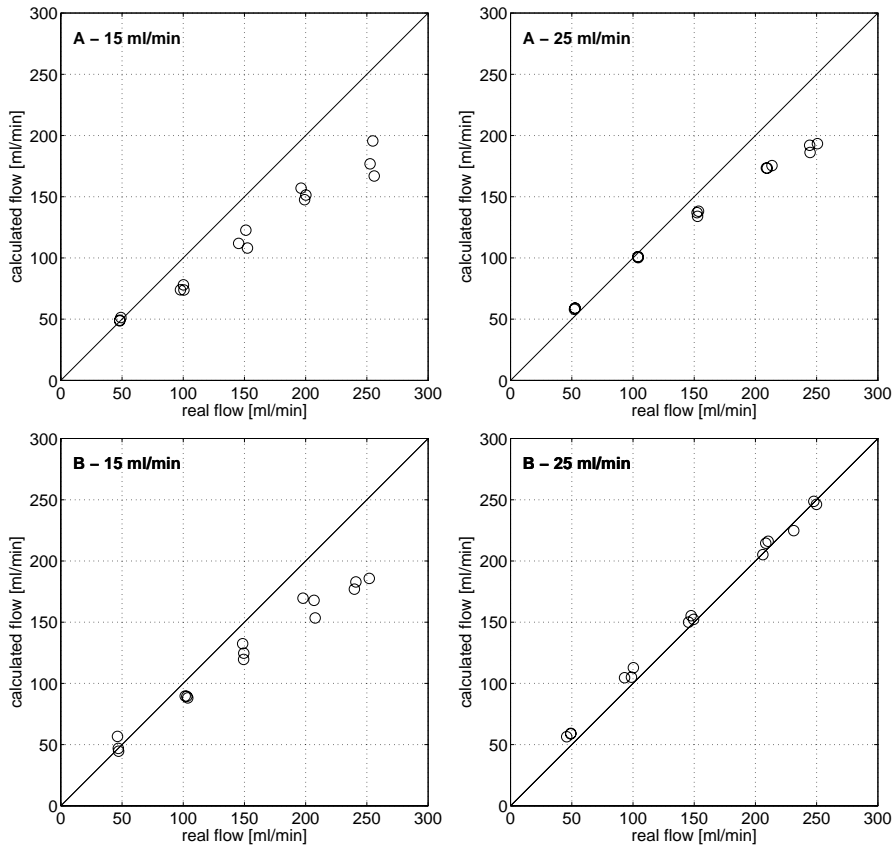


Figure 4.5: Coronary flow rate calculated from continuous infusion vs. real measured flow, for the two catheters (A and B) and two infusion rates (15 and 25 ml/min). Infusate temperature T_i was measured at 1 cm inside the infusion catheter; mixing temperature T in the appropriate measurement zone at 6 cm distal to the tip.

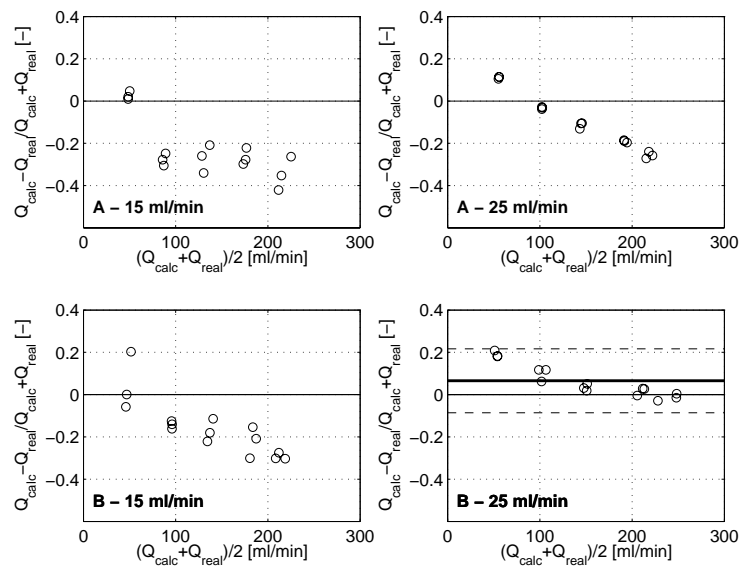


Figure 4.6: Bland-Altman representation of the data in figure 4.5 comparing the calculated flow to the direct measured flow. The 95% limits of agreement for the use of catheter B at an infusion rate of 25 ml/min are $107 \pm 8\%$. The mean absolute difference between calculated and direct measured flow for all measurements with catheter B at an infusion rate of 25 ml/min is 7 ± 4 ml/min.

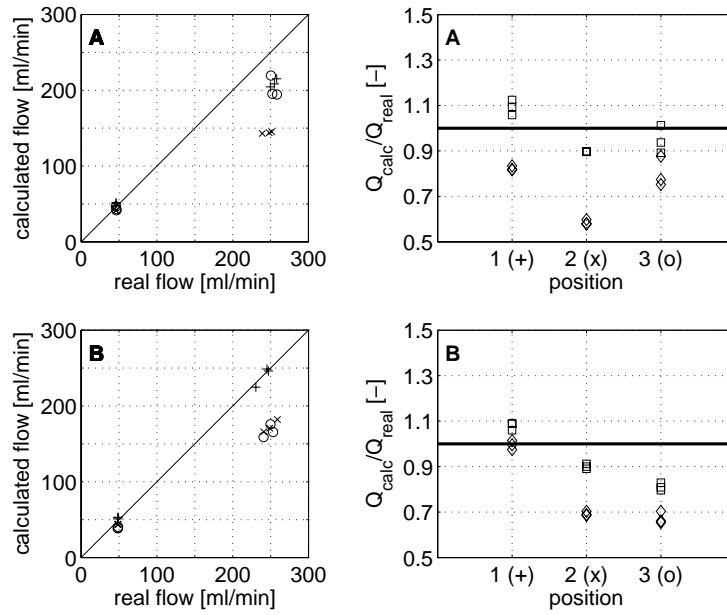


Figure 4.7: The tip of the infusion catheter was positioned at three distances: most proximal, as in the other experiments (position 1, +), and at 3 cm (position 2, x), and 6 cm (position 3, o) further distal. Left: calculated flow for each position. Right: relative accuracy of calculated to real flow ($\square = 50$ ml/min, $\diamond = 250$ ml/min) for each position. T_i and T were measured at 1 cm inside and 6 cm distal to the tip of the infusion catheter, respectively.

tip was found: this indicates incomplete mixing. The pattern of the variations was similar for both infusion rates and both flow rates used. The first few centimeters distal to the tip may be defined as mixing chamber, from 5 to 8 cm the temperature was relatively stable or slightly decreasing, and after 8 cm the temperature difference between the mixture and inflow blood decreased. The latter effect may be due to heat loss through the wall, however, no clear reason for the characteristic 8 cm for this effect to occur is available. An alternative explanation for the effect on the entire range of 3 to 10 cm may be found in incomplete mixing and the presence of swirl of the cold infusate in the vessel. The occurrence of that effect in a coronary artery would be unfavourable, because of the large variety in curvature of the vessels. In that case the reliability of the method is negatively influenced, because no guarantee for complete mixing can be given.

Inside the catheter the infusate temperature T_i is determined during the procedure. For catheter A the temperature should be measured directly proximal to the sideholes, there T_i could be reliably determined over 3 cm. Inside catheter B the temperature variations were larger. However, the variations in T_i were not of significant influence in the calculations, because of the limited relative importance of a small absolute variation in T_i to the ratio of T and T_i .

From the fixed position data the mixing was seen to become worse with increasing coronary flow. This can be explained by the decreasing ratio of infusion flow velocity and blood flow velocity. For the catheter B the measurement was accurate over the entire range (figure 4.5), but when the catheter tip was only slightly less close to the ostium, mixing was immediately worse and the flow underestimated (figure 4.7). Hence the occurrence of secondary flows or flow disturbances are of great importance. These effects may be induced by choosing a high infusion rate. The better mixing properties of catheter B may be explained by the position of the sideholes over a small distance (table 4.2), and the tapering of the distal end of the catheter. The influence of the infusion velocity on the flow may be damped out between the sideholes of catheter A.

The calculation method for the blood flow was dependent on the myocardial resistance and aortic pressure (figure 4.2). As expected, in the *in-vitro* model the assumption of a constant myocardial resistance was found justified, the total myocardial resistance remained constant before, during and after infusion. In hyperemic flow conditions the *in-vivo* resistance is expected to be constant as well, since in the animal experiments also no significant increase in direct measured flow was seen during infusion.

Limitations of this study can be found in the coronary flow pattern which may be less complex in the model than in an *in-vivo* coronary artery. On one hand the wall of the model tube is smooth, without irregularities that can possibly induce more complex flow patterns. On the other hand, water is used as a medium, while the flow was not scaled, so the relatively high Reynolds number could indicate an increased probability for flow instabilities to occur, enhancing the mixing process. The difference in viscosity between water and blood may additionally affect the mixing process. Also the heat transfer to the wall may be different between the water in the model tube and the blood in the vessel. However, when the sensor position is chosen

close to the end of the mixing zone, no significant influence is expected.

4.6 Clinical implications

Because clinically applicable catheters and infusion equipment were used, the optimization of the methodology and catheter design performed in this study can be directly used in the catheterization laboratory. Optimal mixing between the saline and the blood was indicated to be the main prerequisite for successful measurement of coronary flow. The nature of coronary flow is expected to be even more favourable towards optimal mixing than the *in-vitro* flow, due to the complex geometry and the beating of the heart. The use of the derived methodology in further studies in humans is recommended, to optimize the protocols for specific *in-vivo* application. This study contributes to the feasibility of continuous infusion flow measurement in selective coronary arteries, providing the first methodology to perform such absolute flow measurement.

4.7 Conclusions

Absolute coronary flow rate can be directly measured reliably over the entire physiologic range of 50 to 250 ml/min by the continuous infusion method, under the condition that a suitable infusion catheter is used at a high infusion rate of 25 ml/min and positioned in an area with a complex flow pattern. The measurement location should be chosen appropriately, slightly distal to the mixing zone.

4.8 Acknowledgements

This study was supported by the Dutch Technology Foundation (STW) project EPG.5454, and by Radi Medical Systems, Uppsala, Sweden. The authors would like to thank Boston Scientific, Natick (MA), USA, and Occam International, Eindhoven, The Netherlands, for the design and production of the infusion catheters.

Chapter 5

PressureWire thermoconvection flow measurement: background and experimental evaluation

An easily applicable method for simultaneous assessment of coronary pressure and flow during catheterization could provide an important contribution to clinical decision making. A clinically available sensor-tipped guidewire may be used for flow assessment by applying the principle of hot-film anemometry. The guidewire sensor is heated above ambient temperature and convectively cooled by the flow. The electrical power needed to maintain the temperature difference then is a measure for the local flow. In the current study the feasibility of flow measurement by using this thermoconvection method is investigated in in-vitro models: controlled flow in a glass tube and coronary flow in a coronary circulation model. From theoretical models the heat transfer in stationary flow is described using boundary layer theory on the viscous and temperature boundary layers along the sensor. Hence an approximate theoretical relation between electrical power and flow is derived. In instationary flow, deviations from theory are expected due to dynamically complex boundary layers and heat capacitance effects of the sensor material. The validity of using the stationary calibration relation in case of steady flow, as well as the deviations from theory in instationary flow are investigated. In steady, unsteady sinusoidal and coronary flow, the accuracy of estimation of mean flow using the stationary calibration curve was found to be well and comparable for all situations. The pattern of phasic flow could be clearly recognized in all measurements, but further research including 3D numerical simulations and flow velocity calibration is needed to determine the direct transfer function between estimated and real flow.

The contents of this chapter are based on M.C.F. Geven, A. van der Horst, M.C.M. Rutten, W.H. Aarnoudse, N.H.J. Pijls and F.N. van de Vosse. Blood flow measurement in coronary arteries by a novel thermoconvection method: background and experimental evaluation. *Annals of Biomedical Engineering*, to be submitted.

5.1 Introduction

For the quantification of the functional significance of coronary disease, direct determination of instantaneous pressure and flow would be desirable during catheterization. Currently, guidewire-tipped pressure sensors are commercially available and widely used for the quantification of epicardial stenosis severity using the principle of fractional flow reserve (FFR). To directly determine the resistance to flow, local pressure and flow should ideally be determined using a single wire (De Bruyne et al., 1996; Meuwissen et al., 2002). Such a wire combining pressure and flow velocity assessment is available (Siebes et al., 2004), but no methodology for assessment of absolute flow rate invasively had even been developed in a separate device. Recently, we introduced and evaluated the method of continuous infusion flow measurement using the commercially available pressure-temperature sensor-tipped PressureWire (Aarnoudse, 2006), as described in the previous chapter. With this methodology assessment of direct, volumetric coronary flow and simultaneous coronary pressure became available. However, clinical application of continuous infusion involves the use of additional equipment (infusion catheter, infusion pump) and additional, time-consuming steps to the protocol during catheterization. Also, only mean coronary flow is measured, while assessment of the phasic pattern has also been indicated to be valuable in the clinical setting (Kern, 1992; Kern et al., 1994; Iwakura et al., 1999). In this study a novel approach to flow assessment using the PressureWire, based on the principle of hot-film anemometry, is investigated.

In the 1970's, efforts were made to measure blood flow velocity by hot-film probes (Seed and Wood, 1970a,b, 1972; Clark, 1974; Nerem et al., 1976; Paulsen, 1980a,b). On the surface of these probes a film was mounted, kept at a constant temperature a few degrees above blood temperature. The probe (typically L-shaped with a diameter of 1 mm), was punched through the vessel wall. The blood flowing past the probe convectively cooled the sensor. Hence with higher blood flow the amount of heat transferred to the fluid increased, leading to a larger electrical power needed to maintain the film temperature. The electrical power could be related to the blood flow using calibration methods based on physical models describing the heat transfer between the film and the blood (Bellhouse and Rasmussen, 1968; Pedley, 1972a,b, 1976). The main drawback of the method at that time was the necessity to insert the probe through the wall, and, although the principle is still widely used by fluid dynamicists (Bruun, 1996), the technique was abandoned for further clinical research.

In the current study, we discuss this thermoconvection flow measurement principle by using the sensor of a commercially available pressure-sensor-tipped guidewire as a hot-film flow sensor. This will allow for local coronary blood flow assessment simultaneous with pressure measurement, by merely positioning the wire sensor at the desired measurement location during standard catheterization procedures. In this study the theoretical background and feasibility of this novel method for mean and phasic coronary flow measurement will be validated in *in-vitro* models.

5.2 Materials and methods

5.2.1 Analytical description: general hot-film models

From boundary layer theory on the thermal and viscous boundary layers developing along the heated wire positioned in the blood stream, relations between the heat transfer q from the sensor to the fluid, the shear rate $\dot{\gamma}$ on the sensor surface, and the flow Q can be derived in case of stationary flow and heat transfer (appendix A). Assuming steady flow, forced heat transfer exceeding free convective heat transfer and a small thermal boundary layer thickness compared to the thickness of the viscous boundary layer, the relation between heat transfer and shear rate at the sensor is

$$q \sim \dot{\gamma}^{\frac{1}{3}} \quad (5.1)$$

In laminar, fully developed steady flow along the axis of a cylinder, the shear rate is linearly related to the main stream velocity U , and flow rate Q

$$\dot{\gamma} \sim U \sim Q \quad (5.2)$$

Hence first order approximation of the relation between the heat transfer and the flow is

$$q \sim Q^{\frac{1}{3}} \quad (5.3)$$

The source of the heat transfer from the sensor is the electrical power supplied to the resistance to keep it at constant temperature. Hence by measuring the voltage over the resistance, the electrical power can be determined, representing the convective heat transfer dependent of the flow

$$q \sim P \quad (5.4)$$

$$P \sim Q^{\frac{1}{3}} \quad (5.5)$$

Deviations from the steady boundary layer theory are expected when the measurement principle is applied in coronary flow. On one hand the viscous and thermal boundary layers and hence the relations between heat transfer, shear rate, and flow vary in time in instationary flow. On the other hand capacitive effects of the sensor material may come into play, storage and release of heat in the sensor material will affect the instantaneous heat transfer from the sensor itself. Analytical models for hot-film heat transfer in instationary flow were derived by Pedley (1972a,b, 1976), the capacitive effects were modelled by Bellhouse and Rasmussen (1968) (appendix A). Despite the fact that these analyses are only valid for a simplified partially heated flat plate configuration, they lead to complex mathematical descriptions and hence only general insight in the determinant parameters may be derived.

In our case, a much more complex configuration is used and hence, and because of the already expected deviations from the relations between heat transfer and flow



Figure 5.1: PressureWire sensor.

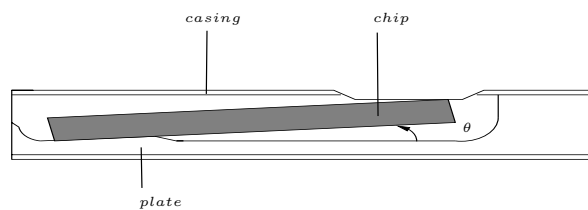


Figure 5.2: Schematic representation of the PressureWire sensor: the chip is glued on the plate and the casing is placed around it. The outer diameter is 0.355 mm.

from derived above, a general form of calibration curves for heat transfer to stationary flow is commonly used

$$P = P_0 + P_1 \left[\frac{Q}{Q_0} \right]^n \quad (5.6)$$

In this expression the absolute measured electrical power P is given. P_0 is the absolute power at zero flow (the heat loss due to diffusion), because the theory describes convective heat transfer. P_1 and n are constants, depending on the overheat of the sensor to the blood, the geometry of the probe, and the thermal properties of the blood (Clark, 1974). Q_0 is the scaling parameter for flow, $Q_0 = \pi r \nu$ (based on the dependency on Re^n , see appendix A), r is the diameter of the vessel, and ν the dynamic viscosity. P_0 and P_1 both depend on the overheat ΔT .

5.2.2 PressureWire®

The sensor of the Radi PressureWire used in this study is conventionally used as a pressure-temperature sensor and incorporated in a 0.014" guidewire with a working length of 175 cm. The sensor is located at 3 cm from the tip, and consists of two temperature-dependent resistances on a chip connected with three cables inside the wire. The chip is glued onto a plate at a small angle θ . A metal casing is placed around the plate, leaving the chip exposed to the fluid. The chip can be regarded

as the bottom of a small cavity, partly covered by silicone to protect the electrical connections. One of the resistances is the pressure sensor (strain gauge), mounted on a deformable membrane. The other resistance is a similar gauge, situated next to the membrane and used for compensation of the pressure sensor for ambient temperature changes.

In the current study, the latter resistance is incorporated in a feedback controlled Wheatstone bridge, as is common in constant temperature anemometry (figure 5.3). Using this electronic circuit, the resistance is regulated to any overheat/resistance value chosen, by feedback control of the bridge voltage and hence the power dissipated by the sensor (the heat transferred to the fluid).

5.2.3 Specific problems in PW application

For application of the PressureWire sensor in thermoconvection flow measurement, the relation between the electrical power dissipated in the heat transfer and the flow should be determined. The calibration curves found in stationary flow are to be compared to those from instationary flow of varying amplitude and frequency. Hence the feasibility for mean and phasic coronary flow measurement is assessed.

For this application specific points of attention can be addressed (besides the validity of boundary layer theory in instationary flow and heat transfer). First a trade off between the overheat and signal-to-noise ratio (SNR) should be made. From a physiological point of view the overheat should be limited to only a few degrees to minimize the danger of damaging the blood cells, while a higher overheat is expected to increase the SNR. Also, a higher overheat will probably reduce the sensitivity to small ambient temperature fluctuations on one hand, but increase the diffusive (flow-independent) part P_0 on the other hand. Secondly, the non-Newtonian and even discontinuous nature of blood at the length scale of the boundary layer thickness may complicate the relation between heat transfer and flow. Thirdly, the complex geometry of the PressureWire, with the resistance placed at the bottom of a cavity, may lead to complex flow patterns and capacitive effects of the sensor material, deviating the calibration curve from the theoretical relation.

5.2.4 Measurement set-up

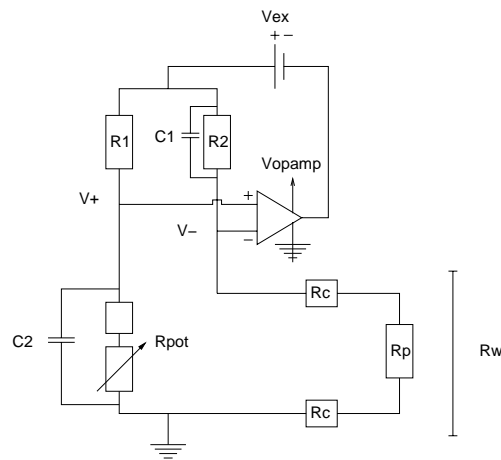
For the *in-vitro* evaluation the PressureWire incorporated in a Wheatstone bridge was used in two set-ups. For steady and instationary dynamic characterization a piston-controlled tube flow was created, for evaluation in coronary flow the model of the coronary circulation previously developed (see chapter 2, (Geven et al., 2004)) was used.

Electronic circuit

The Wheatstone bridge used to set and maintain the constant resistance of the PressureWire (R_w) is depicted in figure 5.3. R_w equals the sum of the resistance of the cables connecting the PressureWire sensor with the connector end (R_c),

Table 5.1: Values of the components of the electrical circuit

Component	value	unity
R_a	$2.0 - 3.7 \cdot 10^3$	[Ω]
R_p	$2.0 - 3.7 \cdot 10^3$	[Ω]
R_c	$4.0 \cdot 10^1$	[Ω]
C_1	$1.0 \cdot 10^{-7}$	[F]
C_2	$1.0 \cdot 10^{-7}$	[F]
R_1	$2.6967 \cdot 10^3$	[Ω]
R_2	$2.6870 \cdot 10^3$	[Ω]
R_{pot}	$3.0320 - 3.1365 \cdot 10^3$	[Ω]

**Figure 5.3:** Schematic representation of the electrical circuit used to set the overheat by R_w

and the resistance itself (R_p). The circuit consists of a Wheatstone bridge, with a feedback operational amplifier (LM324AN, National Semiconductor, Santa Clara, CA), in which R_p and R_c are incorporated. The other components of the bridge are two fixed resistors (R_1 , R_2), a potentiometer (R_{pot}), two capacitors (C_1 , C_2) and two power supplies (ES 030-5, Delta Electronica B.V., Zierikzee, The Netherlands): V_{op-amp} and V_{ex} . The values of all the components are listed in the table in figure 5.3. The two capacitors are incorporated to slightly slow down the feedback of the op-amp, to stabilize the bridge. By manually adjusting the value of R_{pot} the value of R_w for which the bridge is balanced is set and the power through the bridge is accordingly controlled by the operational amplifier. The voltage over the PressureWire is measured by a digital multimeter (DMM 199, Keithley Instruments Inc, Cleveland, Ohio).

Straight tube piston flow

A glass tube with an inner diameter of 3 mm (similar to that of a coronary artery) was placed in a water bath (F34-HL, Julabo Labortechnik GmbH, Seelbach, Germany). The water temperature of the water bath could be set at a specific temperature at a resolution of $\pm 0.01^\circ\text{C}$. Controlled flow through the tube was created using a piston pump, driven by a computer-controlled linear motor (ETB32, Parker). At the distal end of the tube the flow was registered by an ultrasonic flowmeter (4PSB, Transonic Systems Inc, Ithaca, NY). The PressureWire was introduced into the glass tube, and incorporated into the circuit described in the previous section. To avoid variation of the cable resistance R_c due to temperature changes, the PressureWire was almost entirely submerged in the thermal bath. The signals from the flow meter and multimeter were simultaneously recorded via an acquisition board (PCI-6024, National Instruments, Austin, TX) to a computer at a sampling frequency of 50 Hz.

Coronary circulation model

In addition to the controlled tube flow, also the coronary circulation model described in chapter 2 was used for evaluation at coronary flow circumstances. The model was kept at a constant temperature of 37°C by circulation via the water bath (F34-HL, Julabo Labortechnik GmbH, Seelbach, Germany). The flow measurement and data acquisition were identical to those in the tube model.

5.2.5 Characterization of the relation between flow and electrical power

For characterization of the relation between the electrical power dissipated in the sensor and the reference flow, first the non-linear (power-law), stationary calibration curve has been derived. Using this curve, the electrical power measured in instationary flow was linearized. Or, in other words, converted to an estimated calculated flow. Then, the accuracy of mean flow estimation in instationary flow was assessed and compared to the stationary accuracy. Furthermore, for dynamic characterization towards the assessment of phasic coronary flow, simplified single-harmonic flow patterns were used. The characteristic features of coronary flow (with respect to mean, amplitude, and frequency of the flow signal), were separately analyzed by varying the mean, amplitude, and frequency of the single-harmonic flow in a straight glass tube.

For the steady and dynamic characterization, several parameters have been varied. In all experiments, the range of interest was chosen to be the physiological coronary range, mean flow from 0 to 250 ml/min.

Overheat variation

First, the optimal overheat temperature for the characterization was determined varying the sensor temperature at an ambient temperature of 37°C . Because we

were interested in both mean and phasic determination of the flow, a simplification of coronary flow was used, a sine-wave variation with amplitude equal to the mean value of the flow and a frequency of 1 Hz.

$$Q = \bar{Q} + \bar{Q} \cos(2\pi ft) \quad (5.7)$$

Geometrical boundary conditions

Geometrical boundary conditions were varied, considering the influence of the relation between shear rate and flow. Hence the sensor was rotated axially in the vessel while the sensor is positioned near the vessel wall, and, in addition to the 3 mm tube, a tube with a diameter of 4 mm was used.

Furthermore, the influence of small changes in ambient temperature was examined and, to show the inter-wire reproducibility, power-flow relations were also determined for different wires. For these measurements sine wave flow patterns with amplitude equal to offset (5.7) were used.

Stationary calibration

To determine the stationary relation between electrical power and flow, the calibration curve was fitted to the power law model (5.6).

Dynamic characterization

For dynamic characterization, instationary flow with varying mean, amplitude, and frequency was used

$$Q = \bar{Q} + \hat{Q} \cos(2\pi ft) \quad (5.8)$$

Hence, not only the deviation of the mean electrical power to the stationary situation can be determined for all situations, quantifying the accuracy of the measurement of mean coronary flow, but also the amplitude and phase response. Hereto the instationary power signal may be converted to the estimated flow using the steady calibration curve. From a linearized signal the amplitude response may be determined relative to the real flow. By depicting the signals in time, the phase difference between the reference and estimated flow was shown.

Analysis of coronary flow

After the characterization in standardized, sinusoidal flow patterns, in both the tube and the coronary circulation models also the determination of a coronary flow pattern was assessed.

5.2.6 Data analysis

The results of variation in overheat, sensor orientation, tube diameter, ambient temperature, were assessed by evaluation of the average values of electrical power

and flow in time.

For obtaining the stationary calibration curve, the data of electrical power P and steady reference flow Q_{ref} were fitted to the power law model defined in equation (5.6), using the Levenberg-Marquardt algorithm. Subsequently, the estimated flow Q_e for each measured value of electrical power was determined using the calibration curve. The accuracy of flow estimation was determined using a Bland-Altman representation of the difference between estimated and reference flow. All accuracies were expressed in mean and standard deviation of the absolute difference between the two.

The instationary electrical power responses for all data of sinusoidal flow with varying amplitude \hat{Q} , mean \bar{Q} , and frequency f were first calculated to estimated flow using the stationary calibration curve. The pattern of estimated flow was initially compared to the original sinusoidal flow by normalizing with respect to amplitude and time. From this comparison the general deviations in shape of the signal, referred to as instationary effects, were determined, as well as the amplitude modulation and the general phase difference between estimated and reference flow.

Characteristic parameters for the analysis of the dynamic response are the ratio of frequency f and mean flow \bar{Q} (resembling the Strouhal number), and the amplitude-offset ratio \hat{Q}/\bar{Q} (see also appendix A). Because the mean flow is present in both parameters, the effects of variation in \hat{Q}/\bar{Q} , f , and \bar{Q} were separated.

The accuracy of the determination of mean flow was compared for variations in f and \hat{Q}/\bar{Q} by assessment of the Bland-Altman representations. Furthermore, the amplitude of the estimated flow was determined by

$$\hat{Q}_e = \frac{1}{2}(Q_{e,max} - Q_{e,min}) \quad (5.9)$$

and the variation of the amplitude response \hat{Q}_e/\hat{Q}_{ref} with f , \bar{Q} and \hat{Q}/\bar{Q} was examined.

The summarized results of instationary effects (or appearance of higher harmonics), amplitude modulation, phase difference, and estimation of mean flow could be compared to the estimated coronary flow pattern and to findings from earlier studies.

Finally, the accuracy of estimation of mean flow in the coronary circulation model was determined.

5.3 Results

5.3.1 Overheat variation

For every overheat used (between 5 and 35°C), the dynamic behaviour of the reference sinusoidal flow applied according to equation (5.7) was closely followed by the power signal (figure 5.4), although with a lag of the electrical power of approximately 0.2 s. For the overheat of 35°C the lag was slightly smaller than for 5°C, and for decreasing flow smaller than for increasing flow.

The mean electrical powers relative to the value at zero flow ($P - P_0$) for all overheats are depicted in figure 5.5. Increasing the sensor temperature resulted in

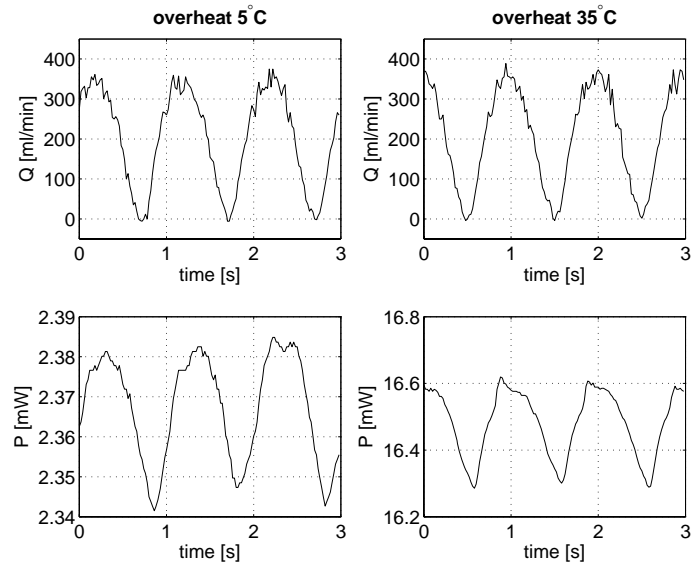


Figure 5.4: The electrical power and recorded flow for a sensor overheats of 5°C (left) and 35°C (right).

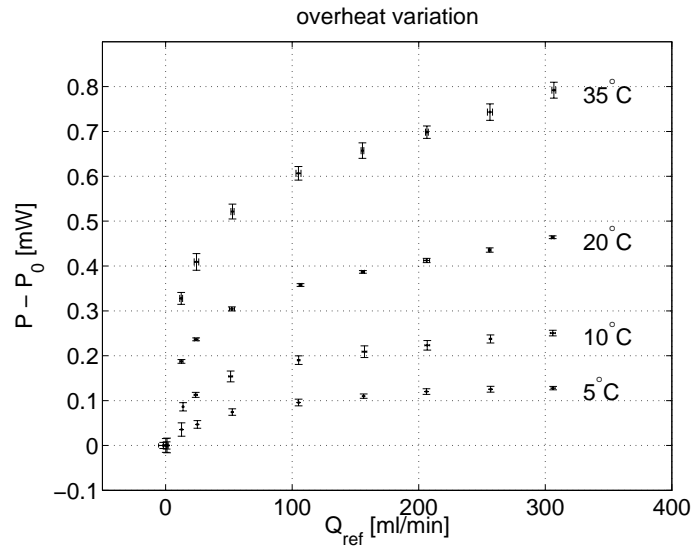


Figure 5.5: The mean measured electrical power versus the mean flow (sinusoidal, equation (5.7)) for different ΔT .

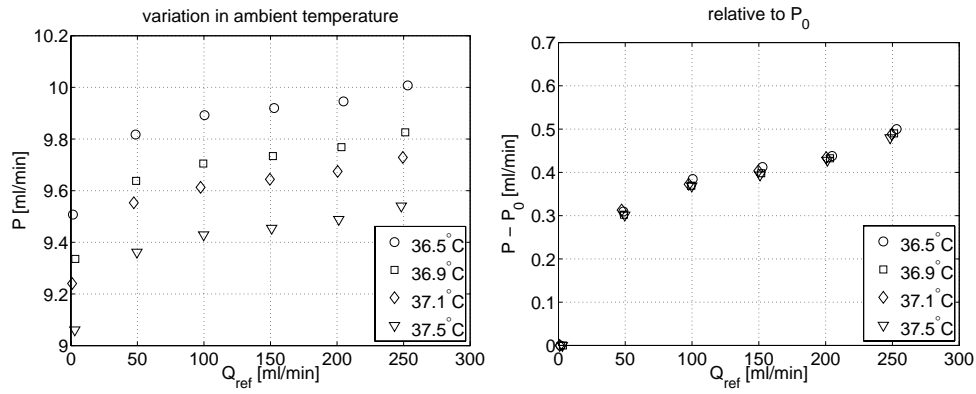


Figure 5.6: The mean power - mean flow relationship at an ambient temperature of: 36.5, 36.9, 37.1, 37.5°C. Left: The absolute electric power. Right: The electrical power relative to P_0 .

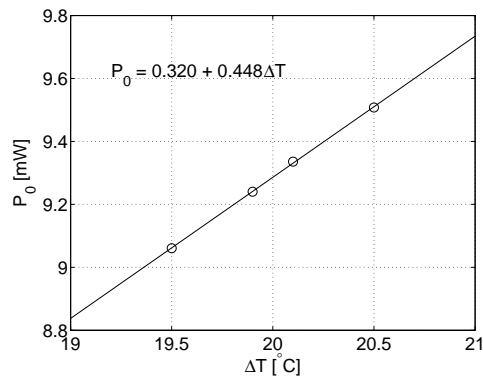


Figure 5.7: Values for P_0 from figure 5.6 versus the overhear, together with a linear regression fit ($R^2 = 0.9997$).

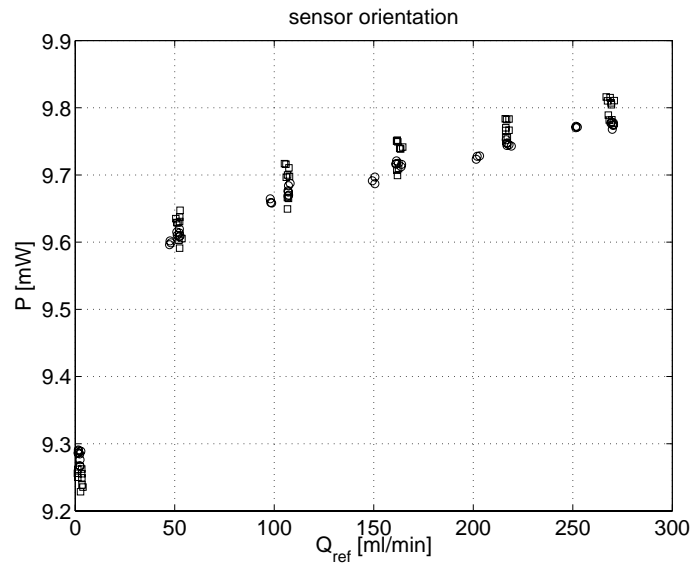


Figure 5.8: Variation in sensor orientation: mean electrical power vs. reference flow for the cavity facing the vessel wall (□), and the centre (○).

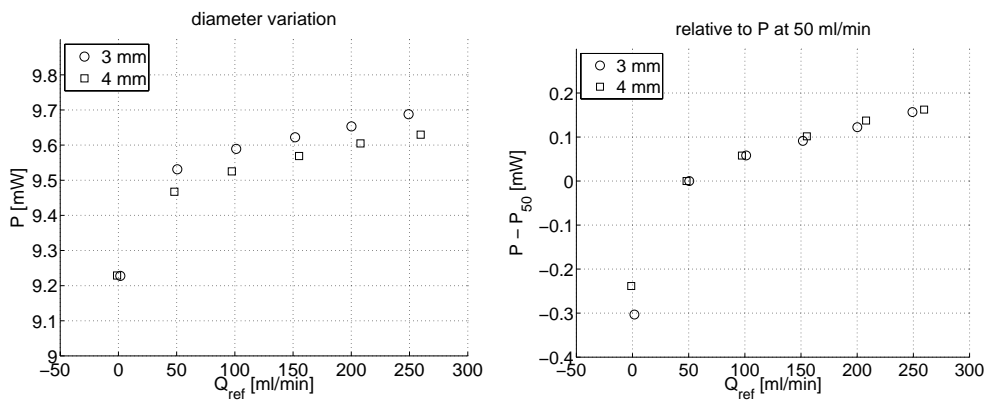


Figure 5.9: Mean electrical power vs. mean flow in 3 (□) and 4 (○) mm straight glass tube (left), and the same data relative to the electrical power at 50 ml/min.

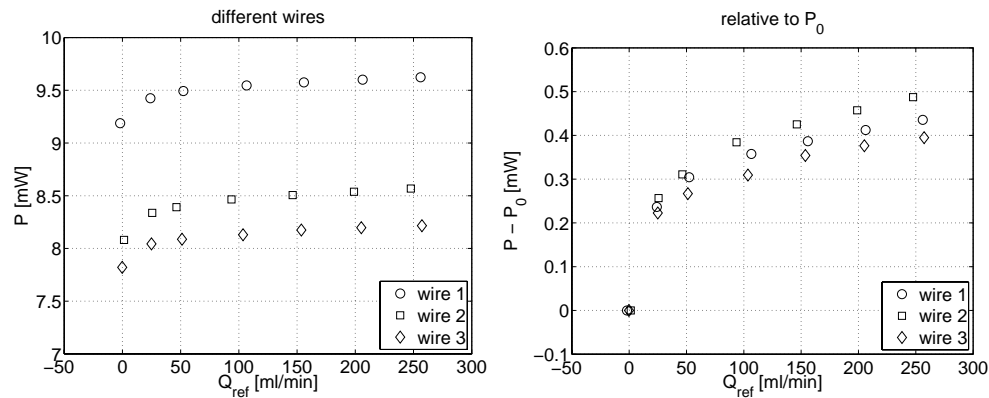


Figure 5.10: Power - flow relation for three different wires. Wire 1 (\circ) was used in all other experiments. Left: absolute power. Right: power relative to the value at zero flow.

a higher sensitivity to flow. The errorbars indicate the standard deviation of the 5 measurements. These errorbars indicate that, although the sensitivity is better for an overheat of 35°C , the reproducibility of the measurements favours an overheat of 20°C . Keeping in mind that this method has to be applicable to blood instead of water an overheat of 20°C is also more favourable than 35°C . Because of the good sensitivity to mean flow together with the excellent reproducibility, the overheat of 20°C was used in all further experiments.

5.3.2 Small changes in ambient temperature

Since the overheat is given by the difference between sensor and ambient temperature, and the heat transfer is related to the overheat, a sensitivity to small changes in ambient temperature is present (figure 5.6, left). Temperature changes as little as 0.2°C have a large effect on the absolute heat loss from the sensor. However, P_0 was found to be the main determinant of the deviations in heat transfer. When the electric power was corrected for P_0 (figure 5.6, right), the convective heat loss from the sensor, represented by the shape of the power-flow relation, was not very sensitive to small ambient temperature deviations. An ambient temperature difference of up to 1.0°C had a very limited effect on the shape of the curve, whereas the temperature sensitivity of P_0 was found to be $0.448 \text{ mW}/^{\circ}\text{C}$ (5.7), comparable to the difference between the power measured at zero flow and $250 \text{ ml}/\text{min}$.

When measuring *in-vivo*, obtaining the power at zero flow might not be possible. Hence, while the mean convective behaviour is not very sensitive to ambient temperature changes, to be able to calculate the mean flow the ambient temperature has to be measured for appropriate estimation of P_0 .

5.3.3 Geometrical boundary conditions

Wire orientation

The approximate position of the wire inside the glass tube was decentralized, towards the bottom of the tube. In figure 5.8 the mean electrical power versus the reference flow is depicted for 3 series of 3 measurements at two orientations: with the cavity facing the wall (\square), or facing the centre of the tube (\circ). While the reproducibility of the measurements was less for the data obtained when the cavity was facing the wall, the mean electrical power response was comparable for both situations. The comparable response may be explained by a limited difference in shear rate on both sides of the wire, or by the entire wire acting as a hot-film, and not only the resistance itself.

Vessel diameter

The theoretical relation between the electrical power and flow was derived using boundary layer theory and initially relates shear rate in the viscous boundary layer to heat transfer (5.1). In vessels of varying diameter, the local shear rate will decrease with increasing diameter when Poiseuille flow is assumed and the flow rate is constant. The mean electrical power for flow in a vessel of 4 mm diameter was indeed smaller than in the vessel of 3 mm when plotted relative to P_0 (figure 5.9, right). However, when the electrical power data was represented relative to the power at 50 ml/min, the convective heat transfer coincided for both diameters. The difference in P_0 in the right panel was 0.065 mW, according to the results from the previous section corresponding to a temperature difference of 0.15°C. Possibly, the temperature of the fluid during flow was slightly different from the value at zero flow, or the temperature was the same and the explanation of the difference in the convective heat transfer is indeed found in different local flow velocity and shear rate.

5.3.4 Different wires

For each of the wires, a reproducible relation between mean electrical power and reference flow could be obtained (figure 5.10). Between the wires, the absolute resistance value and resistance-temperature relation varied. Hence the absolute value for P_0 (the diffusion dominated heat transfer) is variable as well (figure 5.10, left). When the electrical power was taken relative to P_0 , also the shape of the curve was found to be different between the wires. An explanation to this phenomenon may be found in the slightly variable position of the heated resistance relative to the cavity opening. Hence, calibration of each wire should be performed separately.

5.3.5 Steady flow: stationary flow and heat transfer

In all experiments described in the current and following sections, wire 1 was used at an overheat of 20°C .

Table 5.2: Summary of the effects of parameter variation. In section 5.4 these results are compared to the effects expected from literature as described in appendix A.

parameter	higher harmonics	amplitude modulation	phase lag	estimated mean flow
$\hat{Q}/\bar{Q} \uparrow$	↑↑	↓	-	-
$\bar{Q} \uparrow$	↑↑	↓↓	-	-
$f \uparrow$	↑↑	↑↑	↑↑	-

The relation between applied flow and electrical power was determined between 0 and 200 ml/min. The theoretical relation between electrical power and flow from equation (5.6) could be very accurately fitted to the electrical power measured under steady flow conditions (figure 5.11, $P_0 = 9.228$ mW, $P_1 = 0.0805$ mW, $Q_0 = 0.198$ ml/min, $n = 0.245$, $R^2 = 1.00$). The value for n is reasonably close to the value $1/3$ obtained from the partially heated flat plate approximation. The estimated flow Q_e calculated from the power values using the calibration curve (figure 5.12, left), the mean absolute difference between the values for reference and calculated flow was 14 ± 8 ml/min. (figure 5.12, right).

5.3.6 Unsteady flow

Amplitude-offset variation

The ratio of flow amplitude and mean flow or offset (\hat{Q}/\bar{Q}) was chosen 0.25, 0.50, 0.75 and 1.00. The frequency of oscillation was 1 Hz. For all measurements Q_e was estimated from the electrical power data using the stationary calibration curve obtained in the previous section. For the minimum (0.25) and maximum (1.00) ratio, Q_e normalized to its amplitude \hat{Q}_e was plotted for a mean flow of 50, 150, and 250 ml/min (figure 5.13). When the shape of the curve for Q_e was compared to that of the reference flow Q_{ref} , larger deviations were seen with increasing offset (for both amplitude-offset ratios). These deviations were stronger at the high amplitude-offset ratio (right panel). Generally, the phase of the estimated flow lagged behind the reference flow; at the ratio of 1.00 the phase difference increased with increasing mean flow. For all situations, in decreasing flow the course of Q_e was smoother than in increasing flow.

The average values for estimated flow varied with an accuracy comparable to that of the estimated flow data for stationary flow (figure 5.15, left). When the mean Q_e was averaged per ratio of amplitude and offset, only a small decrease in Q_e relative to Q_{ref} could be noted (figure 5.15, right). At the mean flow of 250 ml/min the average value of electrical power for the large-amplitude flow was higher, possibly related to the occurrence of flow instabilities.

The amplitude of the estimated flow (\hat{Q}_e , equation (5.9)) was compared to the amplitude of the reference flow (\hat{Q}) for all combinations of offset and amplitude-offset ratio. The amplitude was increasingly underestimated for all ratios with increasing offset (figure 5.17, left). Assessing the same data per offset (figure 5.17,

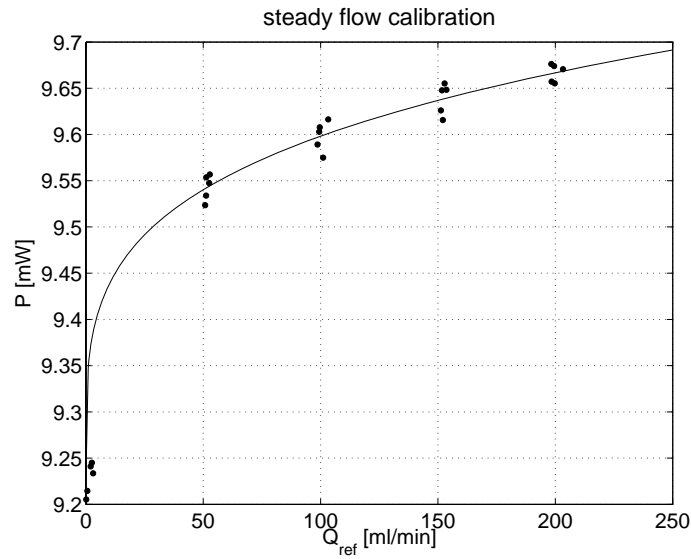


Figure 5.11: Electrical power vs. reference flow, stationary conditions. The overheat was 20° C (ambient temperature 37° C).

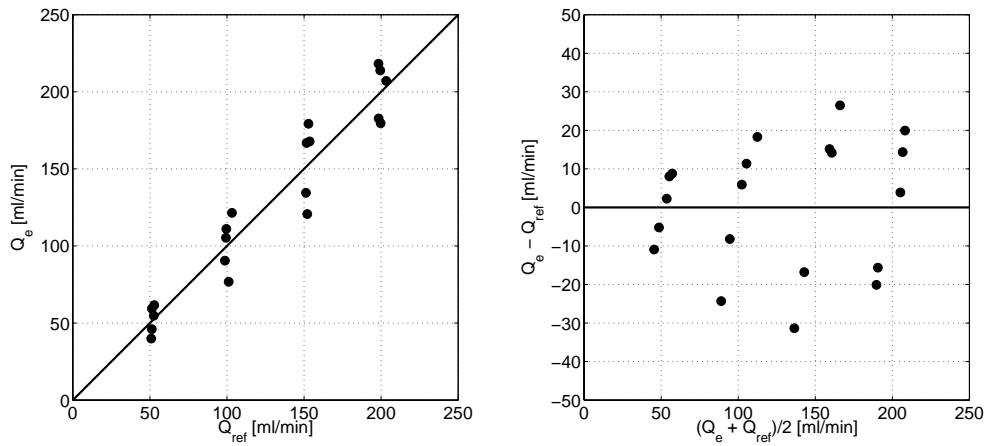


Figure 5.12: Estimated flow (derived using the fitted calibration curve) vs. reference flow (left), together with the Bland-Altman representation of the absolute difference between the mean and estimated flow (right).

right), the damping was also slightly increasing with the ratio.

Frequency variation

Similar to the amplitude variation, the frequency was varied between 0.5 and 4.0 Hz at an amplitude-offset ratio of 1.00. The time-dependent Q_e was compared to Q_{ref} , normalized to amplitude and time. For the left and right panels of figure 5.14, the mean flow was 50 and 150 ml/min, respectively. Deviations in curve shape were smaller for the lower flow, slightly increasing with frequency. The phase lag also increased with frequency, stronger in increasing flow than in decreasing flow.

The mean flow was increasingly overestimated with increasing frequency (figure 5.16), again even more strongly expressed at the mean flow of 250 ml/min.

Assessing the amplitude response (figure 5.18), a slight increase with the mean flow was present for all frequencies (left). With larger frequency, the damping of the amplitude was stronger (right).

The effects found with the parameter variation are summarized in table 5.2.

5.3.7 Coronary flow

Next to the sinusoidal flows for dynamic characterization, the sensor response to coronary flow patterns was assessed in the glass tube model. Coronary flow was varied between 50 and 250 ml/min, the estimated flow was derived from the stationary calibration curve derived in section 5.3.5. The estimated flow followed the reference flow (figure 5.19, left). The amplitude was underestimated larger for the smaller systolic flow peak (i.e. 0.2-0.5 s) than for the larger diastolic flow part (0.5-1.0 s). Also the phase lag of the estimated flow was present in the entire pattern. From the Bland-Altman representation of the mean estimated and reference flow (figure 5.19, right), a progressive underestimation of the mean flow by the estimated flow was found.

In the *in-vitro* coronary model, coronary flow was created in the flexible, silicone, curved coronary tube. When the calibration curve was used corrected to the offset power P_0 at zero flow (9.223 mW), the measured average power values were entirely outside the predicted range (figure 5.20, left, solid line).

However, when electrical power data for non-zero flow were fitted to the shape of the curve $P_1 [Q/Q_0]^n$, an R^2 of the fit of 0.91 was found (figure 5.20, left, dashed line). The fitted value for P_0 was 9.644 mW. The accuracy of the estimated flow using the newly fitted calibration curve (dashed line in figure 5.20) was generally less than in the glass tube, without structural over- or underestimation.

A situation similar to that of the diameter variation (section 5.3.3) existed. If the value for the newly fitted P_0 represented the constant temperature during non-zero flow, different from the temperature at zero flow, the temperature difference may be derived from the difference between the two values for P_0 using its temperature-dependency determined in section 5.3.2. The difference would be 0.93°C. Or the flow velocity and resulting shear rate on the wire were much higher in the location of measurement in the curved tube, and no temperature difference was present.

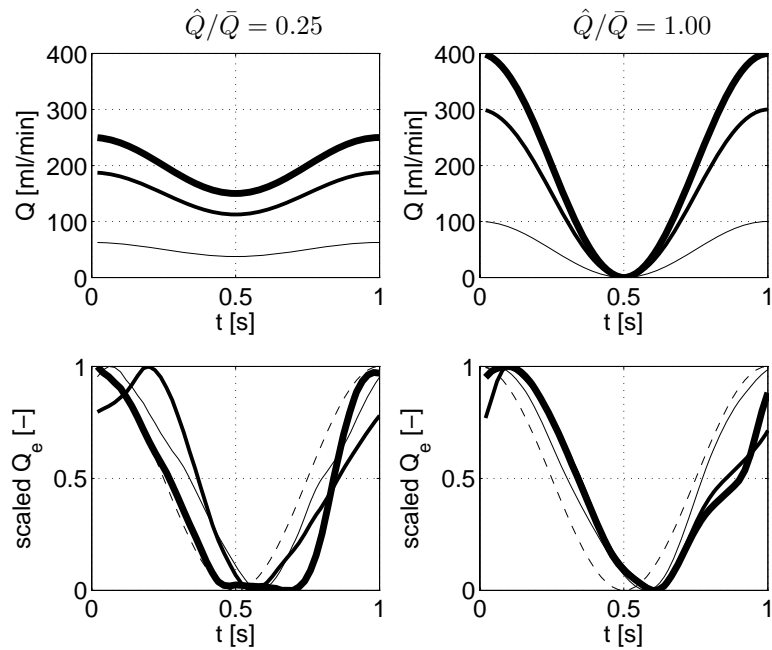


Figure 5.13: Variation in amplitude-offset ratio (\hat{Q}/\bar{Q}) of sinusoidal flow ($f = 1 \text{ Hz}$). Top panels: flow, bottom panels: flow estimated from electrical power using the stationary calibration curve, normalized to the amplitude of the estimated flow signal. Left: $\hat{Q}/\bar{Q} = 0.25$, right: $\hat{Q}/\bar{Q} = 1.00$. Thin, medium and thick lines are $\bar{Q} = 50$, 150 , and 200 ml/min , respectively. The dashed line is the normalized reference flow.

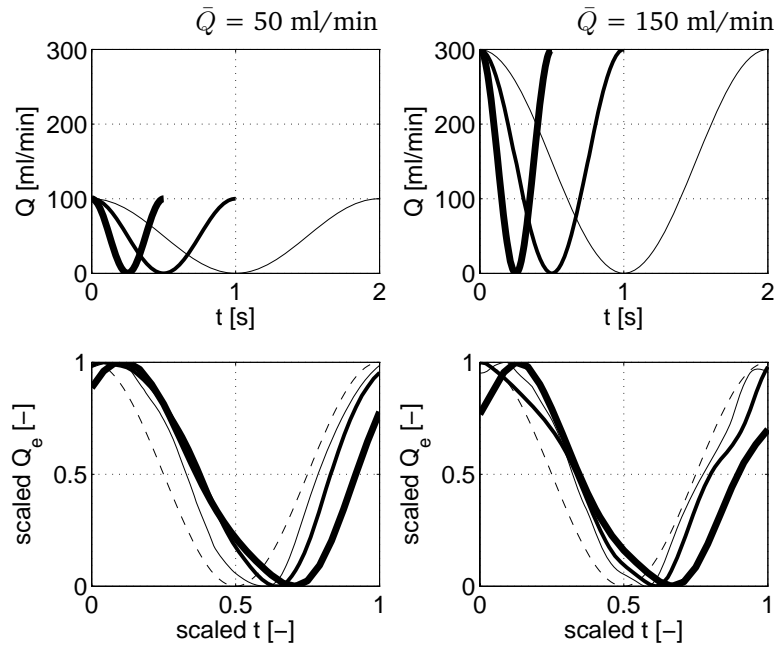


Figure 5.14: Variation in frequency of sinusoidal flow ($\hat{Q}/\bar{Q} = 1.00$). Top panels: reference flow, bottom panels: flow estimated from electrical power using the stationary calibration curve, normalized to the amplitude of the estimated flow signal and one period. Left: $\bar{Q} = 50$ ml/min, right: $\bar{Q} = 150$ ml/min. Thin, medium and thick lines are $f = 0.5$, 1.0 , and 2.0 Hz, respectively. The dashed line is the normalized reference flow.

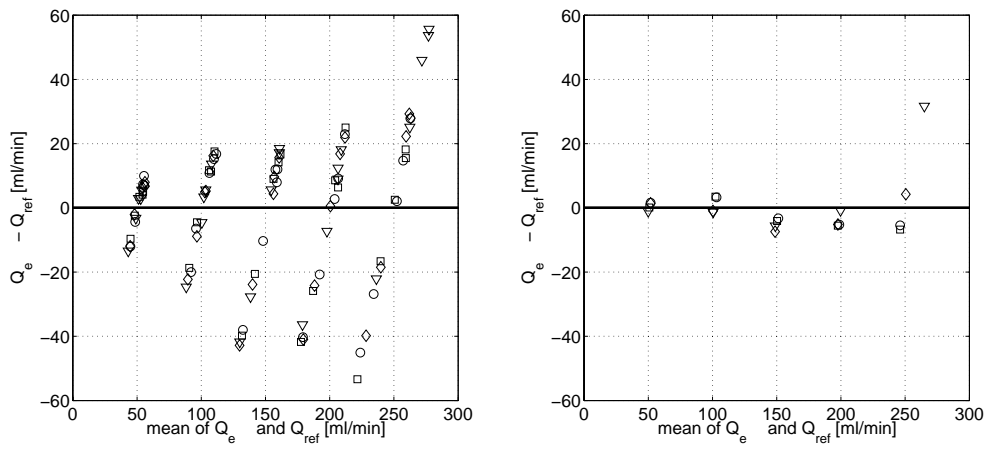


Figure 5.15: Variation in amplitude-offset ratio (\hat{Q}/\bar{Q}) of sinusoidal flow ($\circ = 0.25$, $\square = 0.50$, $\diamond = 0.75$, $\nabla = 1.00$). Frequency was 1 Hz. Left: difference between reference flow and flow calculated using the stationary calibration curve from steady flow, all measurements. Right: data average per ratio.

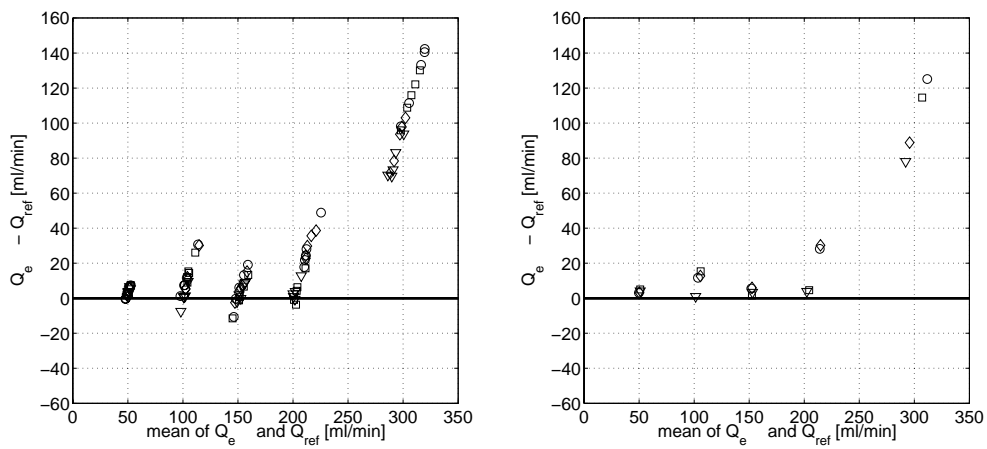


Figure 5.16: Variation in frequency of sinusoidal flow ($\circ = 0.5$ Hz, $\square = 1.0$ Hz, $\diamond = 2.0$ Hz, $\nabla = 4.0$ Hz). Amplitude-offset ratio was 1.00. Left: difference between reference flow and flow calculated using the stationary calibration curve from steady flow, all measurements. Right: data average per frequency.

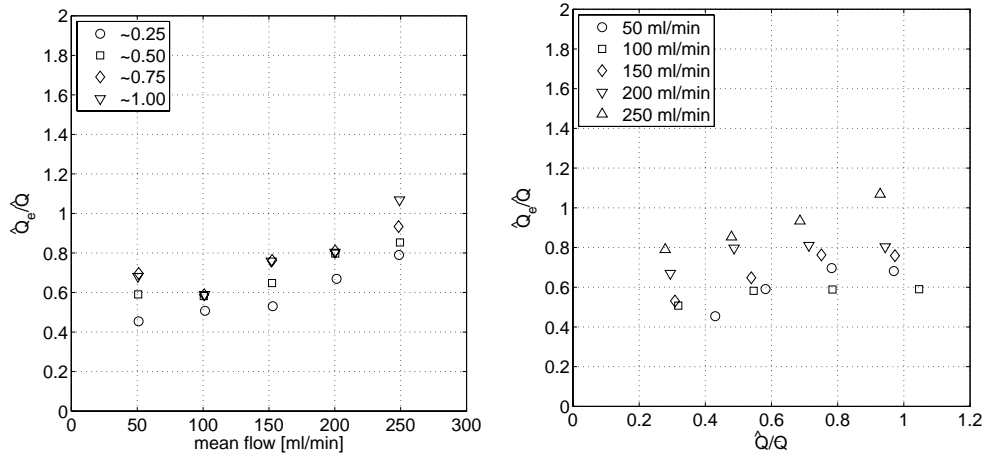


Figure 5.17: Amplitude response for the variation in offset and amplitude, $f = 1 \text{ Hz}$. Left and right panels are two representations of the same data. Left: the response per ratio \hat{Q}/\bar{Q} vs. the offset \bar{Q} , right: response per \bar{Q} versus \hat{Q}/\bar{Q} .

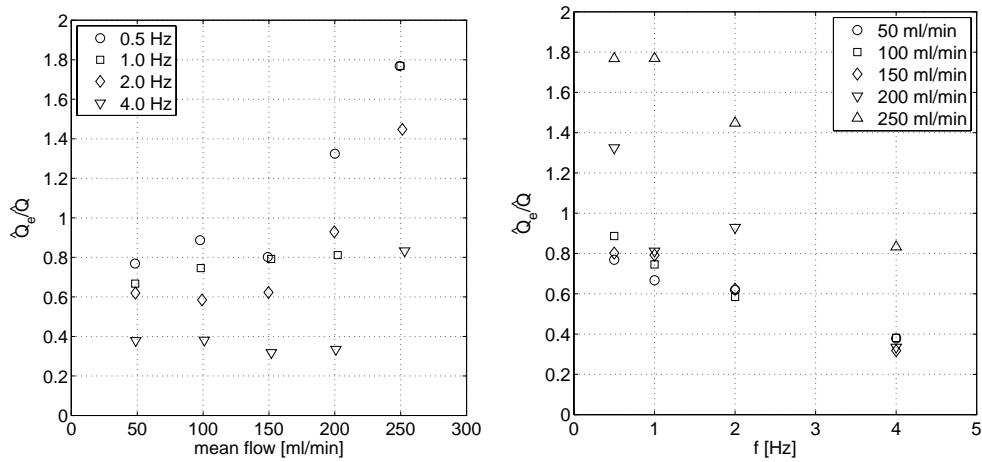


Figure 5.18: Amplitude response for the variation in frequency, $\hat{Q}/\bar{Q} = 1$. Left and right panels are two representations of the same data. Left: the response per frequency f vs. offset \bar{Q} , right: response per \bar{Q} versus f .

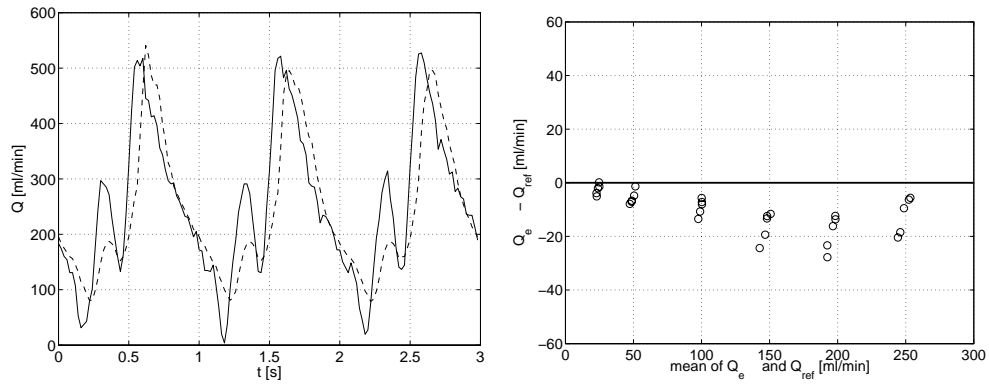


Figure 5.19: Coronary flow applied in the glass tube model. Flow was estimated from the electrical power using the calibration curve from figure 5.11. Left: estimated (dashed) and reference flow (solid) for hyperemic mean flow of 250 ml/min. Right: Bland-Altman representation of estimated and reference mean flow.

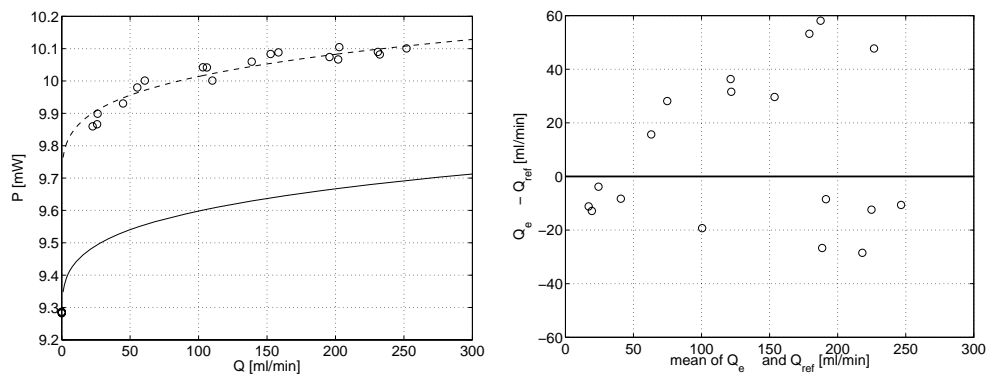


Figure 5.20: Flow in the model of the coronary circulation.

5.4 Discussion

In steady flow, calibration of the electrical power to the reference flow was found to be well possible in multiple wires, reproducible, and according to theory. In instationary flow, the determination of the mean flow was comparably accurate for all parameter variations. In all measurements, at the flow of 250 ml/min flow instabilities were suspected to cause the structural overestimation of the flow by the estimated value, increasing with amplitude and frequency. At this high flow $Re_D \approx 1300$, and hence instabilities may be expected. The estimated flow response over time was characterized with respect to variations of \hat{Q}/\bar{Q} , \bar{Q} , and f . Similar response to characteristic components could directly be detected in the coronary flow signal.

The theoretical relation between electrical power and flow could be very accurately fitted for the stationary flow data. The value for n of 0.245 was close to the theoretical value of $1/3$, suggesting that the assumptions explained in appendix A were appropriate. In previous calibration studies different L-shaped probes were used. The theoretical value for n was $1/2$ there, because of a different relation between shear rate and flow for a free stream velocity over a flat plate, and experimentally determined values were between 0.46 and 0.51 (Clark, 1974).

For the assessment of the estimation of instationary flow using the stationary calibration curve, the first parameter, the amplitude-offset ratio \hat{Q}/\bar{Q} , was chosen to be a representative parameter for the problem. Increasing ratio indicates larger deviation from steady conditions. A second parameter of importance is defined to be similar to the Strouhal number, reflecting the time taken for the boundary layer to respond to variations in velocity U , compared to the characteristic time $(1/f)$: f/U . A proper length scale to obtain a dimensionless group is not obvious as boundary layer thickness, tube radius, as well as radius of the wire are believed to be involved. Detailed three-dimensional numerical analysis of the entire domain may provide an indication of the appropriate length scale. With increasing f/U , deviation from steady conditions is also expected to be larger. Because in the current study we were not only interested in dynamic characterization, but also in the determination of mean flow, we assessed the influence of changes in \bar{Q} and f separately. Flow, and not flow velocity was prescribed in the tube flow. In fully developed stationary tube flow, flow rate is proportional to flow velocity and hence Q is used and not U . Deviations from theory were described in terms of deviations from the sinusoidal shape of the flow, amplitude modulation between reference and estimated flow, and phase difference.

With respect to the amplitude modulation, the increase in amplitude underestimation with increasing mean flow and decreasing frequency was in accordance with larger deviations from steady response for increasing Str as explained in appendix A. Since the boundary layer development depends on the instantaneous flow (Seed and Wood, 1972), within each period the accuracy of Q_e was expected to vary with Q_{ref} . Q_e should be more accurate at peak flow, which was clearly represented by the comparison of the estimated coronary flow signal. This effect was also found in previous analytical and *in-vitro* studies (Pedley, 1972a; Seed and Wood, 1970b). In the amplitude modulation, the underestimation was not found to decrease with

decreasing amplitude as predicted by theory from appendix A, but to remain at the same level or even increase slightly.

Generally, the phase of the estimated flow lagged behind the reference flow, as expected from literature (appendix A). The phase difference increased with frequency, while the difference was non-uniform over the flow pattern: stronger in decelerating than accelerating flow. The sensor response in increasing flow is more local than in decreasing flow as heat is entering the system solely through the resistance; in decreasing flow heat is transferred along the sensor body as well. Part of the phase lag could be explained by the developing boundary layer, together with the capacitive effect of the backing material, as shown by Bellhouse and Rasmussen (1968).

Instationary effects, or the appearance of higher harmonics, influencing the deviations from the sinusoidal shape of the response were found to increase with increasing amplitude-offset ratio and increasing frequency and mean flow. From the analysis of Sr and \dot{Q}/\bar{Q} in appendix A, only the latter effect was unexpected. Besides the boundary layer development and capacitive effect mentioned earlier, also the occurrence of secondary flows and the situation of the resistance at the bottom of a small cavity in the wire could play a role in the deviation from sinusoidal flow shape. Eddies may form and be washed out inside the cavity during the flow cycle.

In the estimated coronary flow, the effects described above were similarly recognized. Especially the amplitude underestimation was less at higher, systolic flow, and the general phase lag was comparable.

Shear rate, flow velocity or flow rate?

From the variation of wire orientation, little influence on the mean heat transfer was found. Hence, either the shear rate does not differ substantially between the two sides of the wire, the resistance and its environment material may be lumped to a larger thermoconvection sensor, or the relation between the viscous and thermal boundary layers is inappropriately described by the flat plate approximation. The latter explanation may be supported by the findings from the variation in diameter and the use of the coronary circulation model. There, similar convective heat transfer response was found in all situations after correction for apparent deviations in temperature between the absence and presence of flow. To investigate this hypothesis on one hand, the reference temperature should be registered directly upstream of the sensor during all registrations. Correction for small ambient temperature changes by merely adapting the value for P_0 was found to be legitimate: the temperature-dependency of the shape of the calibration curve is much smaller than that of P_0 .

On the other hand, if the ambient temperature did not change between absence and presence of flow, the variations in convective response may originate from a different local flow velocity and resulting shear rate on the wire. The average flow velocity would indeed be lower in a 4 mm tube than in a 3 mm tube, and the larger shear rate or flow velocity in the coronary model could be a result of the curvature of the silicone tube.

Besides temperature registration, calibration in two-dimensional flow at known

velocity would be helpful for clarification in this matter. Submersion of the probe in a cylindrical fluid container mounted on a turntable has been suggested by Seed and Wood (1969), but the sensor mounted on the guidewire may not easily be aligned accurately with the flow in such a configuration.

Application in blood

The optimized overheat of 20°C may induce problems in *in-vivo* application, concerning damage to blood cells and fibrin deposition on the probe (Seed and Wood, 1972). First of all, using more sophisticated electronic circuitry and signal processing methods, a much lower overheat may also result in sufficient sensitivity and signal-to-noise ratio. Furthermore, the thickness of the thermal boundary layer is theoretically less than that of the cell-depleted layer along the wire, reducing the risk of blood damage (Seed and Wood, 1970b). And besides all, because the resistance is so small, the absolute power dissipated is very limited. Anyway, compensation for deviation in ambient temperature from the value during calibration is of major importance towards clinical application of thermoconvection flow measurement. The appropriate value for P_0 should be estimated from a reference temperature. A possibility for reference temperature assessment may be found in using a second temperature-dependent resistance mounted on the sensor. According to Seed and Wood (1972), also the value for P_0 at the same temperature may differ between blood and water: this effect could be quantified by *in-vitro* evaluation of P_0 in blood and water. The similar shape of the calibration curve was also found in previous studies (Seed and Wood, 1972; Clark, 1974).

5.5 Conclusions

Mean flow could be reliably estimated from the electrical power signal in steady and unsteady flow conditions. Although the relation between shear rate on the sensor, local flow velocity at the measurement location, and volumetric flow has not become clear, a consistent relation between estimated and reference flow was apparently present.

The phasic pattern of sinusoidal and coronary flow could clearly be recognized in all measurement series. However, information on merely the magnitude and phase response of the first harmonic of the linearized estimated flow will not be sufficient to reconstruct the exact original flow pattern from the electrical power signal. Especially more insight in the characteristic length scales for the heat transfer, as well as the separate influence of flow-related (complex flow pattern inside the cavity), and capacitance-related (of the sensor material) effects is required.

Chapter 6

PressureWire thermoconvection flow measurement: animal validation

Direct flow assessment in the coronary arteries would be helpful for quantification of functional severity of disease. Flow may be measured by the thermoconvection principle: a guidewire sensor introduced into a coronary artery is heated above blood temperature and varying blood flow varies the cooling of the sensor. The electrical power needed to maintain the constant sensor temperature is a measure for the local blood flow. Aim of this study is to investigate thermoconvection flow assessment in an animal model. Three Yorkshire swine were instrumented with an epicardial volumetric flow meter and occluder to create an artificial stenosis at the proximal LAD. A sensor-tipped guidewire (PressureWire, Radi Medical Systems, Uppsala, Sweden) was introduced into the LAD by regular catheterization technique. The sensor of the guidewire was connected to an electronic circuit to keep the sensor heated to 20°C above blood temperature. The electrical power needed to maintain the temperature difference was monitored and compared to the reference flow. 47 measurements were performed at varying flow rates (0 - 90 ml/min). The electrical power signal strongly correlated with the coronary blood flow; mean flow could be derived at an absolute accuracy of 11 ± 11 ml/min ($R^2 = 0.84, 0.58, \text{ and } 0.94$ for the three swine, respectively). Using the principle of thermoconvection, a sensor-tipped wire can be used directly for assessment of coronary blood flow.

The contents of this chapter are based on M.C.F. Geven, Y.-D. Ho, W.F. Fearon, T.C. Nguyen, A. Itoh, A. van der Horst, W. Aarnoudse, M. van 't Veer, M.C.M. Rutten, N.H.J. Pijls, F.N. van de Vosse. Blood flow measurement in coronary arteries by a novel thermoconvection method: animal validation. *Circulation*, **submitted**.

6.1 Introduction

For the assessment of coronary flow in conscious humans, so far only technically complex methods or indirect parameters of flow are available (Kern et al., 2006). However, for the understanding of coronary physiology and pathology, measurement of mean and phasic coronary blood flow in selective coronary arteries would be useful (Kern, 1992; Kern et al., 1994; Iwakura et al., 1999). Measuring the absolute value of coronary artery flow combined with local pressure measurement also allows absolute myocardial and collateral resistance to be calculated quantitatively (Gould et al., 1990; Pijls et al., 1993; Fearon et al., 2003). Currently intracoronary pressure measurement is widely used, but a methodology for simultaneous absolute flow measurement would be a valuable tool in the clinical research of the coronary circulation and follow-up of patients with complex myocardial disease.

In the 1970's, efforts were made to measure blood flow velocity by hot-film probes (Seed and Wood, 1970a,b; Clark, 1974; Nerem et al., 1976). The measurement principle was based on the convective cooling of a slightly heated sensor by the blood flow. With higher blood flow the amount of heat transferred to the fluid increased, and hence the electrical power dissipated in the probe can be related to the blood flow. The main drawbacks of the method at that time were the large dimensions of the probe (typically 1 mm), and the necessity to insert it through the vessel wall.

In the current study, we aim for clinical application of this thermoconvection measurement principle for instantaneous coronary blood flow measurement in a selective coronary artery, using the sensor of a commercially available 0.014" pressure-sensor-tipped guidewire as a hot-film flow sensor. This will allow for local coronary blood flow assessment similar to pressure measurement, by merely positioning the wire sensor at the desired measurement location during standard catheterization procedures. In this study the theoretical background and feasibility of this novel method for thermoconvection coronary flow measurement will be validated in an animal model.

6.2 Methods

6.2.1 Physical background of thermoconvection flow measurement

All measurement devices require calibration to a known standard before clinical application. For appropriate calibration of the thermoconvection sensor, the relation between the power needed to maintain the constant sensor temperature and the local blood flow has to be known. Using physical models for the temperature and flow velocity distribution in the vessel at the presence of a heated sensor, a power-law relation between electrical power and flow is used:

$$P = P_0 + P_1 \left[\frac{Q}{Q_0} \right]^n \quad (6.1)$$

where P is the measured electrical power, P_0 is the electrical power when the flow is zero, Q is the blood flow, and P_1 , Q_0 and n are constants, depending on the overheat of the sensor to the blood, the geometry of the probe, and the thermodynamic properties of the blood (Clark, 1974). To determine the relation between the measured electrical power and the blood flow for a specific sensor, the calibration parameters P_0 , P_1 , Q_0 , and n are determined beforehand during the manufacturing process by fitting equation (6.1) to measured data of electrical power and reference flow over the entire physiological flow range. Each of the three sensors used in this study was pre-calibrated in steady water flow of 37°C in a glass tube with an internal diameter of 3 mm. Different overheat temperatures were tested, optimal signal-to-noise ratio and resolution were obtained at a sensor overheat of 20°C. It should be noted that only a very small part of the wire ($35 \times 35 \mu\text{m}$) was actually heated up to 57°C. Because preliminary tests in canine blood showed no thrombus formation or contamination of the sensor at this overheat, 20°C was also used in the current study.

6.2.2 Application to the pressure guidewire

A commercially available 0.014" pressure-sensor-tipped guidewire (PressureWire, Radi Medical Systems) was used in this study, with adapted measurement electronics to keep an electrical, temperature dependent resistance present at the sensor surface at constant, chosen overheat. The electrical power was derived from monitoring the voltage over the sensor resistance. The physical characteristics of the wire are completely identical to the regular PressureWire and the wire can be handled in the same manner as during pressure measurement. No additional intervention or action besides switching on the overheat is needed during the catheterization procedure.

6.2.3 Animal preparation

Three Yorkshire swine were studied. The study was approved by Stanford's Institutional Animal Care and Use Committee. The swine were premedicated with intramuscular telazol (6 mg/kg), anesthesia was maintained with 2% isoflurane, and supplemental oxygen was given via endotracheal intubation. An arterial sheath was surgically placed in the right femoral artery. Coronary angiography was performed via a 6F catheter. A left lateral thoracotomy was performed using standard surgical techniques, the pericardium fully opened and the heart suspended in a pericardial cradle. The proximal left anterior descending coronary artery (LAD) was carefully skeletonized using sharp and blunt dissection. An ultrasonic (US) flow probe (Transonic Systems Inc, Ithaca, NY) was placed around the proximal LAD for quantitative coronary flow measurement; a vascular occluder (In Vivo Metric, Healdsburg, CA) was placed distal to the flow probe, with care taken to ensure that there were no branch vessels between the two.

6.2.4 Measurements in the LAD

The coronary sensor-tipped guidewire was advanced into the LAD. The sensor, located 3 cm from the tip, was positioned directly proximal to the flow probe. The sensor was kept at a constant overheat above ambient blood temperature using an attached custom-made electronic circuit. The electrical power needed to maintain the overheat of 20°C was derived from the predetermined sensor resistance and the voltage over the sensor registered by a digital multimeter (DMM model 2000, Keithley Instruments Inc, Cleveland, Ohio). The electrical power signal was recorded simultaneously with the reference flow during 10 second periods at a sampling frequency of 50 Hz by a data acquisition computer system. Such a 10 second steady state period will be referred to as one measurement. Intracoronary papaverine was used to induce coronary hyperemia; together with the artificial stenosis of any chosen severity by the epicardial occluder, this allowed for assessment of the entire physiological flow range.

At first, thermoconvection measurement was performed at baseline flow. Next, maximum hyperemia was induced by intracoronary administration of 20 mg papaverine. Measurements were performed at peak hyperemia and at regular intervals during the flow decrease to baseline. Subsequently, stenosis severity was increased in gradual steps to obtain electrical power and flow data at regular intervals from baseline levels to zero flow. Multiple measurements were obtained per stenosis severity to assess the reproducibility of the measurement method by the accuracy of the determination of flow.

6.2.5 Data analysis

The mean values for electrical power P and reference flow Q_{ref} during the 10 second measurement periods were compared to the *in-vitro* derived relationship between electrical power and flow in equation (6.1). Since the overheat and ambient temperature slightly deviated from the *in-vitro* conditions, the offset power P_0 was different between the *in-vitro* and *in-vivo* data. This was compensated for by using the calibration curve relative to P_0 . The quality of the shifted calibration curve for the relation between P and Q_{ref} was reflected by R^2 .

Subsequently thermoconvection flow Q_{tc} was calculated from P and the calibration curve, and the accuracy for the new flow measurement method was assessed from Bland-Altman representations of the data. The mean and standard deviation of the absolute difference between Q_{ref} and Q_{tc} were determined.

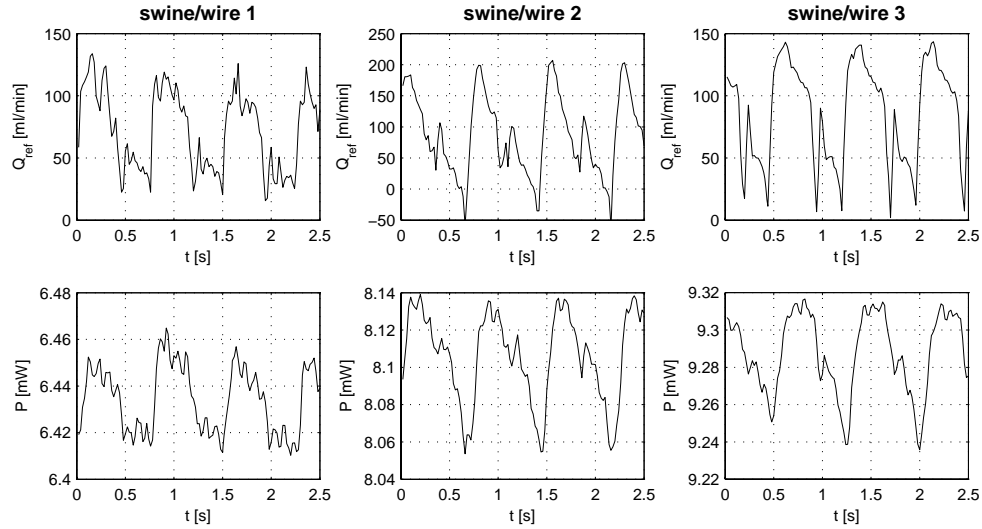
6.3 Results

6.3.1 Procedural results and hemodynamic characteristics

Three swine (body weight 35, 37 and 38 kg) were successfully instrumented with the epicardial flow meter and vascular occluder. Cardiac catheterization was uncomplicated in all swine, and coronary angiography established a good instrumentation. Guided by the angiogram, the sensor was positioned while care

Table 6.1: Characteristic data for all of the three swine. Diameter was determined at the guidewire sensor location.

Swine	weight [kg]	Q_{rest} [ml/min]	Q_{max} [ml/min]	\varnothing_{LAD} [mm]	number of measurements
1	35	21	76	2.8	16
2	37	37	88	3.3	19
3	38	28	82	3.0	12

**Figure 6.1:** Raw data for reference flow (top) and measured power (bottom) of one measurement from each swine/wire combination.

was taken not to place the intracoronary sensor in direct contact with the vessel wall to ensure direct exposure of the sensor to the blood flow. Weight, resting flow, maximum hyperemic flow, and vessel diameter at the location of measurement for all swine are presented in table 6.1. The data were acquired following the protocol described above, resulting in 16, 19, and 12 measurements for the three swine/wires, respectively, a total of 47 measurements.

6.3.2 Raw data: time-based registration of electrical power and reference flow

In all measurement series, the coronary flow pattern could be directly and clearly recognized from the measured electrical power P , without any signal processing of the raw data (figure 6.1). Hence, besides the determination of the mean flow from the electrical power signal, the phasic nature of coronary flow may also be assessed using the thermoconvection method.

6.3.3 Thermoconvection derived flow versus reference flow

For each of the experiments the mean electrical power P and mean reference flow Q_{ref} were found to coincide well with the shape of the *in-vitro* calibration curve (figure 6.2). The shape of the *in-vitro* calibration curve was fitted to the *in-vivo* data to derive an appropriate value for P_0 . The value of R^2 for the shift of P_0 was 0.84, 0.58, and 0.94 for the three swine/wires, respectively. Next, Q_{tc} was calculated from P (figure 6.3, top). For swine/wire 1, 2, and 3 the absolute difference between calculated and real flow was 13 ± 15 , 12 ± 9 , and 6 ± 6 ml/min, respectively (figure 6.3, bottom). Gathering the data from all 47 measurements, the difference between Q_{ref} and Q_{tc} was found to be 11 ± 11 ml/min (figure 6.4).

6.4 Discussion

In this study we investigated the *in-vivo* feasibility of coronary flow measurement by using the PressureWire as a hot-film anemometer. The mean flow calculated by this thermoconvection method corresponded well with absolute flow, measured by the perivascular flow probe. All measurements could be carried out quickly, easily, and without any manipulation besides positioning the wire at the location of measurement. Furthermore, the phasic nature of the coronary flow pattern was always clearly present in the measured electrical power.

For all three swine the measured data corresponded with the calibration curve for the wire used after correction for the deviation in P_0 , indicating the appropriateness of pre-calibration in water flow. The resulting accuracy for calculation of the flow differed slightly between the wires (13 ± 15 , 12 ± 9 , and 6 ± 6 ml/min, for wire 1, 2, and 3, respectively), the overall absolute difference between the real and calculated flow was 11 ± 11 ml/min.

6.4.1 Limitations

Not correcting for changes in ambient temperature may be considered a main limitation of this study. Due to this, the value for P_0 in the calibration curve had to be fitted to the measured data before the flow could be calculated. In particular, the open-chest model may have had a cooling effect on the vessel. However, the blood flowing past the sensor was expected to be at core body temperature, because only the vessel itself was exposed and the chest was almost closed during the measurements. The shift in P_0 could be performed appropriately, indicating that the temperature during the procedure had been fairly constant. However, for accurate calculation of coronary flow in a novel measurement setting, constantly monitoring the ambient temperature at a high resolution by an additional temperature-sensitive resistance on the sensor is necessary to directly adapt the value for P_0 . Monitoring the temperature at a high enough temporal resolution will also increase the accuracy of the measurements.

Furthermore, improvement to the accuracy of the measurements may also be found in modification of the electronic circuit used to maintain the constant

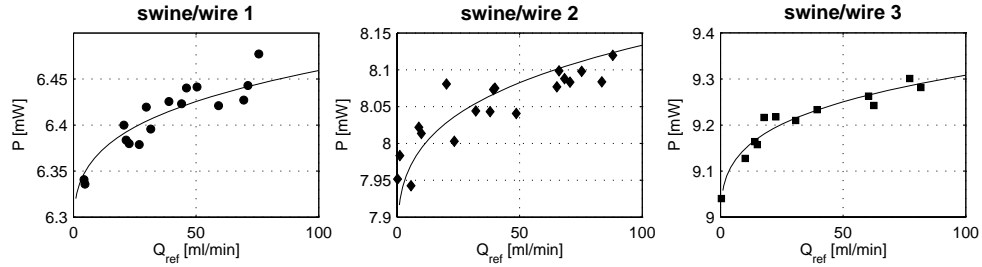


Figure 6.2: Measured power versus reference flow by the ultrasound probe, together with the calibration curve previously obtained in-vitro .

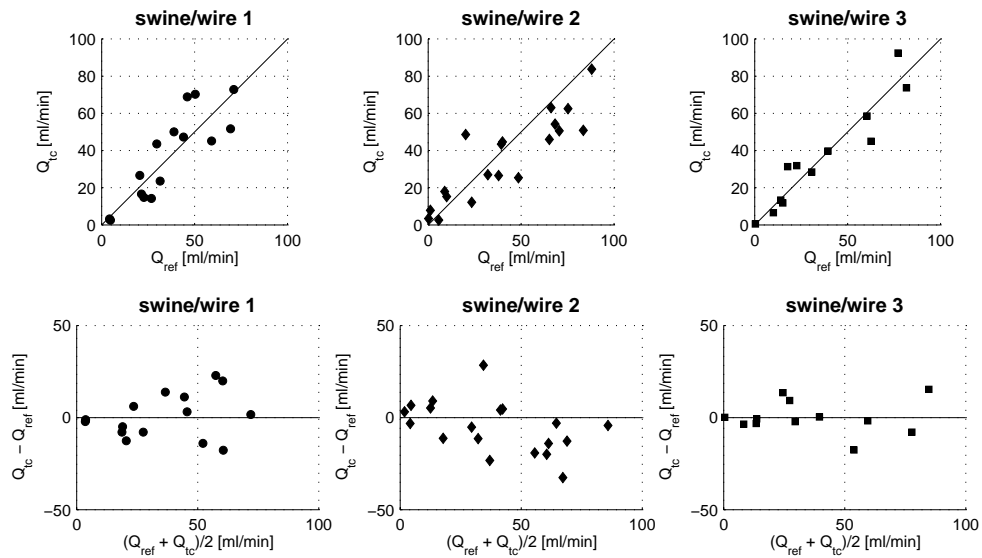


Figure 6.3: Top: using the calibration curve depicted in figure 6.2, the measured electrical power data were calculated to thermoconvection flow and depicted versus the reference flow. Bottom: the difference between the thermoconvection and reference flow in a Bland-Altman representation.

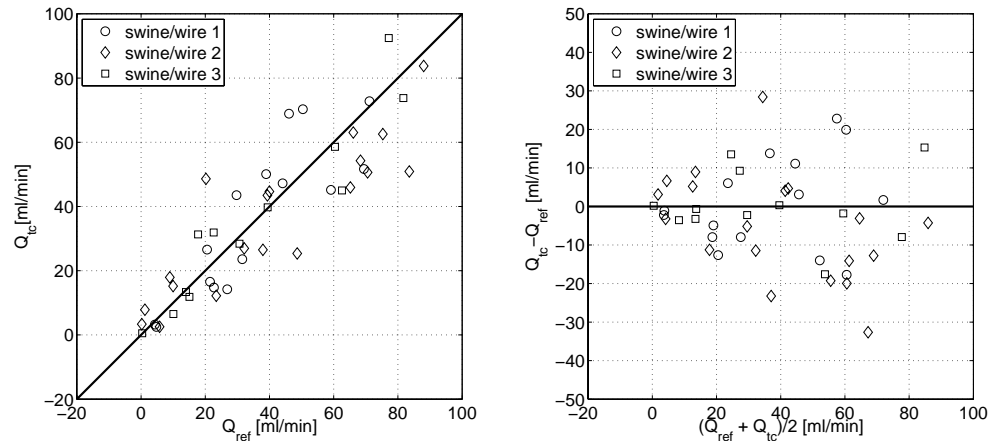


Figure 6.4: Thermoconvection flow vs. reference flow for all three swine/wires, a total of 47 measurements (left), together with the Bland-Altman representation of the absolute difference between the thermoconvection and reference flow (right). The mean absolute difference between reference and thermoconvection flow for all measurements was 11 ± 11 ml/min.

temperature. In the current study a very basic circuit design was used, which may be expanded and optimized to improve the signal-to-noise ratio and stability of the signal.

The 20°C overheat used in the current study (a sensor temperature of approximately 57°C) was based on *in-vitro* experience and was not found to cause any visible damage to whole blood. However, a lower overheat would be favourable. Pilot measurements in the current study indicated sufficient sensitivity to flow at such a temperature, but did not result in a consistent relation between power and flow. Hence increased stability, accuracy and signal-to-noise ratio by registering the reference temperature and/or adapting the sensor or circuit design as indicated above, may enable the use of a lower overheat temperature.

The maximum achievable flow in these animal models was low compared to normal values in humans, in whom maximum hyperemic flow is typically in the order of magnitude of 250 ml/min in the large epicardial vessels. The *in-vitro* calibration covered the entire human flow range, however, the *in-vivo* sensor response should also be evaluated in the higher flow region.

Also, the diameter of the vessels in the *in-vivo* as well as *in-vitro* experiments was approximately 3 mm. The shape of the calibration curve is expected to change with the diameter of the vessel, because of the differences in the temperature and flow velocity distribution in the vessel. Calibration in multiple tubes with diameters covering the range of diameters found in epicardial arteries enables use of the specific curve for the specific diameter of the target location. Obviously, such a procedure should be further investigated in *in-vitro* and *in-vivo* models.

6.4.2 Clinical implications

Not unfrequently patients come to the catheterization laboratory because of chest pain and have no significant epicardial stenosis. By being able to measure pressure and flow, one could determine the myocardial resistance to identify its potential role in the chest pain. Another important group of patients who could benefit from measurement of absolute flow are patients undergoing experimental therapy (e.g. stem cell implantation) to regenerate the myocardium. Measurement of the absolute myocardial resistance before and after treatment might be informative. Finally, patients suffering from acute myocardial infarction often have different degrees of microvascular damage, despite similar normal epicardial flow after primary PCI. Being able to measure myocardial resistance accurately could identify high risk patients who might benefit from adjunctive intervention.

6.5 Conclusions

We showed the feasibility of *in-vivo* mean and phasic coronary flow measurement by using a clinically available pressure guidewire as a hot-film anemometer. The phasic coronary flow pattern was clearly visible in the electrical power measurements, and derivation of mean flow was fairly accurate. As the methodology used can be easily applied with minimal additional steps during coronary pressure measurements in humans, mean and phasic flow recording in conscious man may be possible at cardiac catheterization.

6.6 Acknowledgements

This work was supported by the Dutch Technology Foundation STW, project EPG.5454, by grant 1 K23 HL072808-01A1 (WFF) from the National Institutes of Health, Heart Lung and Blood Institute, Bethesda, MD, and by Radi Medical Systems. The authors would like to express their gratitude to Jennifer Lyons, Alfredo Green, Yuri Suzuki, and Fumi Ikeno of Stanford's Animal Facility for their assistance during the experiments, and to Huub Oomes and Monique Kilsdonk for their support in the logistics of this study.

Chapter 7

General discussion and conclusions

The main aim of the work described in this thesis was to develop methodologies for simultaneous assessment of coronary pressure and flow, for characterization of the functional significance of coronary circulation disease. For the evaluation of such methods, a physiologically representative *in-vitro* model of the coronary circulation was designed and evaluated. The model was used in the development of two methods for coronary flow assessment using the PressureWire, based on the principles of continuous infusion thermodilution and thermoconvection. This chapter discusses the development of the model and the two measurement techniques, the main results and clinical implications. The clinical evaluation studies completing this project were carried out and described by Aarnoudse (2006).

7.1 Modelling of the coronary circulation

As is explained in chapter 2, the design of the *in-vitro* model of the coronary circulation was based on the use of physiologically representative functional elements for the relevant components of the circulation, both regarding their geometry and function. Three main modelling conditions were defined, (a) coronary flow was mainly driven by aortic pressure, (b) ventricular contraction determined the phasic systolic/diastolic coronary artery flow pattern, and (c) the autoregulation between baseline and hyperemic flow conditions was determined by arteriolar resistance only. All three conditions were met. Hereto, first a systemic circulation was used to obtain a physiological aortic pressure (a). Next, the myocardial vascular bed was divided into a subendocardial and subepicardial branch. A collapsible tube, led through the left ventricle and collapsed by the ventricular pressure, represented the variable resistance and volume behaviour of the endocardial part of the myocardium (b). Finally, adjustable resistances were used to tune the total myocardial resistance (c).

The evaluation of the model was carried out twofold. In chapter 2 the pressure and flow signals were found to closely correspond to patterns and values obtained in conscious humans. In chapter 3, the model was extended by a collateral branch, and two well-validated catheter-based diagnostic techniques as used in the human catheterization laboratory were assessed in the well-controlled *in-vitro* situation. The indices fractional flow reserve (FFR), characterizing epicardial stenosis severity, and index of microcirculatory resistance (IMR), quantifying hyperemic minimal resistance to blood flow of the myocardial vascular bed were assessed over a wide range of stenosis severities and microvascular resistances. The *in-vitro* model accurately reproduced FFR and IMR in accordance with clinical observations. Moreover, FFR calculated from sensor-tipped guidewire based coronary pressure measurement and IMR calculated from pressure and temperature, equaled the corresponding indexes directly measured by flow assessment using electromagnetic or ultrasonic flow sensors. Hence the model's reciprocal usefulness for research and development of coronary diagnostic techniques was confirmed.

In the chapters 4 and 5, the model was applied for the *in-vitro* evaluation of the newly introduced coronary flow assessment based on continuous infusion thermodilution and thermoconvection, respectively. For these applications, the fluid temperature of the model was controlled externally. Although the temperature control was found to be very reliable and accurate when the model itself was generating circulation, the constant temperature could be questioned when flow was interrupted (chapter 5). Furthermore, the spatial pattern of flow in the coronary artery could differ between the model and *in-vivo* conditions. The movement of the heart and curvature of the epicardial arteries may induce secondary flow patterns. As explained in chapters 4 and 5, these deviations from simple Poiseuille flow in a straight tube may influence the results of local continuous infusion or thermoconvection flow measurements.

7.2 Continuous infusion coronary flow measurement

Continuous infusion coronary flow measurement was derived from conventional thermodilution (Aarnoudse, 2006), replacing the bolus injection with continuous infusion in a selective coronary artery. From the temperature of the blood, the saline, and the mixture downstream to the infusion site, combined with the known infusion rate, volumetric mean flow could be calculated. The principle of measurement was evaluated in the *in-vitro* coronary model in chapter 4, assessing the boundary conditions for accurate flow measurement by variation of infusion catheter design, infusion rate, and location of infusion and temperature measurement.

Main prerequisite for reliable flow derivation was the complete and maintained mixing of saline and flow medium, accomplished by the use of an appropriate infusion catheter, high enough infusion rate, and infusion at a location with complex enough spatial flow pattern to ensure proper mixing. Besides, the optimal location of measurement was determined. From the tip of the infusion catheter a mixing chamber of 3 to 5 cm should be taken into account, allowing the saline to mix with

the blood. Preferably no sidebranches are present in the mixing segment in *in-vivo* measurement. From 5 to 8 cm distal from the tip the mixing temperature was found to be stable; further downstream the temperature increased, possibly due to heat transfer from the wall to the fluid. As mentioned in the previous section, the flow conditions in the *in-vivo* situation may be more favourable for the accomplishment of full mixing due to the increased complexity of flow by pulsatile motion of the heart and curvature of the vessel. Full mixing was indicated by the results of animal and human continuous infusion studies that were carried out within the clinical part of the project (Pijls et al., 2007; Aarnoudse et al., 2007), supporting the idea of enhanced mixing in the *in-vivo* situation.

Using continuous infusion the mean coronary flow may be derived. However, as indicated before also the phasic nature of flow is of clinical importance. Furthermore, a clinical methodology should be as little complicated as possible, whereas for continuous infusion an extensive protocol and additional equipment have to be used. To better meet these requirements for clinical application, a second method for flow assessment described in this thesis is the thermoconvection method.

7.3 Thermoconvection coronary flow measurement

The principle of thermoconvection flow measurement is that of hot-film anemometry. One of the resistances on the sensor chip was heated to a predetermined overheat temperature and the electrical power needed to maintain the temperature difference was related to the local flow rate. Using boundary layer theory for the viscous and thermal boundary layers in steady flow velocity along a partially heated flat plate, a power law relation between flow velocity and heat transfer was derived in line with literature (appendix A). In the study presented in chapter 5 a generalized form of that relation was used as a model for calibration of the heat transfer of the heated sensor of the PressureWire to water flow in a glass tube.

In this chapter the relation between the heat transfer (electrical power needed to maintain the temperature difference) and flow rate was determined by fitting the power law relation to the data measured in steady flow. The fit in steady flow was found to be very accurate. For the heat transfer in unsteady flow deviations from stationary theory were expected due to unsteadiness of the viscous and thermal boundary layers and the heat capacitance of the sensor material. In dynamic characterization, sinusoidal flow was applied with varying offset, amplitude and frequency. The steady calibration curve was used to derive the estimated instationary flow from the electrical power. Characteristic parameters for the instationary effects deviating the estimated flow from reference flow were the ratio between the time needed for the boundary layer to develop and the cycle time (f/\bar{Q}), and the amplitude-offset ratio of the flow variation (\hat{Q}/\bar{Q}). With the increase of f/\bar{Q} phase difference and amplitude modulation were indeed increased as well, for the increase of \hat{Q}/\bar{Q} these effects were less clear. Mean flow was estimated with accuracy comparable to what was obtained in the stationary situation.

While the instationary effects may be qualified by the characteristic parameters, a

direct transfer function between estimated and reference flow could not be derived from the experiments performed in this study. For accurate assessment of the phasic nature of coronary flow such a function should be available. Also sensor response to flow reversal should be subject of further investigation: besides the insensitivity of the sensor for flow direction, also complex response is expected because of the thermal wake being convected back over the sensor and other flow and heat transfer effects.

In all experiments the flow rate was used as an input variable, and related to the electrical power via fitting of the stationary calibration curve. The form of the power law equation relating electrical power to flow was derived from the partially heated flat plate model, assuming fully developed viscous and thermal boundary layers and a small relative thickness of the thermal boundary layer. Accordingly, the heat transfer is assumed to be related to the shear rate on the probe and hence the local flow velocity. In the current study, these assumptions were initially used as a point of departure. Hence differences in convective response were expected for similar flow rate in tubes of different diameters: for equal flow the average flow velocity is lower in a larger diameter tube. However, similar convective response was found (the shape of the calibration curve could be accurately fitted to the measured data), but the value for the power at zero flow (P_0) estimated from the fitted curve was different from the measured electrical power at zero flow (diffusion dominated response). Similar results were obtained in the curved tube in the *in-vitro* model of the coronary circulation, where also P_0 deviated from the value expected from fitting the calibration curve. These at first sight unexpected results may be explained threefold. First, the value for P_0 was found to be strongly temperature dependent, and in the coronary model the temperature may differ between flow being present or absent (as indicated above). As a consequence a different response of the sensor between zero or no flow and convection dominated heat transfer can be expected. Secondly, the diffusion dominated heat transfer may not only depend on temperature, but also on the geometrical boundary conditions, obviously different in the glass tubes of different diameter and the silicone coronary tube. This also could explain a different value for P_0 in different geometrical flow configurations. Thirdly, the values for convective and diffusive heat transfer may not depend only on variable circumstances, but the entire shape of the curve would be genuinely different. This has been affined to the unknown length scale or relation between shear rate, flow velocity, and flow mentioned in the discussion of chapter 5. Analysis of these different phenomena could be performed by accurately registering the inflow temperature, sensor calibration in a known flow velocity, or analysis of local flow velocity and temperature fields in a detailed three-dimensional numerical analysis of the measurement situation.

With respect to clinical application, the sensor response in blood in genuine physiological conditions remained unknown, as well as the consequences of using the slightly heated probe in blood. Therefore an *in-vivo* study was performed, using three Yorkshire swine instrumented with an epicardial volumetric flow meter and occluder to create an artificial stenosis (chapter 6). The calibration curves obtained *in-vitro* were compared to the data of the electrical power and reference flow measured *in-vivo*, and were found to coincide well. Again, the reference temperature was

not registered and was fitted from the convective flow response. As in the *in-vitro* study, additional measurement of reference temperature was found to be necessary to provide insight in the phenomena discussed above. Accuracy of determination of mean flow was comparable to that *in-vitro*.

7.3.1 Ethical considerations for the use of the swine model

In the work described in this thesis on the development of methodology for assessment of the coronary circulation an important focus was the *in-vitro* evaluation. During the measurement design process of the thermoconvection method, important parameters in the use of the method were tuned in these models. Furthermore, the accuracy of the method was determined and found sufficient for proceeding the development process towards clinical application in humans. However, the response in blood and genuine physiological conditions remained unknown, as well as the consequences of using the slightly heated probe *in-vivo*. Therefore, an *in-vivo* evaluation in a minimal number of animals was carried out. The animals had been included in a larger study requiring similar instrumentation, and hence were not separately sacrificed for this study. The results of the study confirmed the findings of the *in-vitro* experiments, and marked an important step towards clinical application.

7.4 Thermoconvection or continuous infusion?

The accuracy of mean *in-vitro* flow measurement was comparable between thermoconvection and continuous infusion. Continuous infusion for mean flow measurement is directly clinically applicable, whereas the controversies in thermoconvection remain with respect to possibly varying temperature and assumptions on the relation between heat transfer and shear rate, flow velocity and flow rate. On the other hand, continuous infusion involves the use of additional equipment and a separate protocol, application of thermoconvection only requires positioning of the wire. Furthermore, the phasic pattern of coronary flow is clearly detected by thermoconvection, and may – after adequate further research – be available for representing the actual coronary flow over time.

7.5 Conclusions

In the work described in this thesis the novel techniques of coronary flow assessment based upon continuous infusion and thermoconvection were developed and evaluated. To facilitate the development process a physiologically representative model of the coronary circulation was designed. The model was successfully used and provided well-controlled evaluation circumstances and limitation of animal and patient studies. Continuous infusion involves a complex protocol and careful consideration of boundary conditions such as catheter design and measurement protocol, but may directly be applied in the catheterization laboratory for determination of mean flow.

Thermoconvection is a very easily applicable method, potentially valuable for clinical assessment of mean and phasic coronary flow. However, thermoconvection requires further validation studies to the potential damage to the blood, to elucidate the appropriate model for instationary heat transfer, the relation between shear rate, flow velocity and flow rate, and the temperature and geometry dependence of the electrical power at zero flow.

Appendix A

Background of hot-film anemometry

A.1 Introduction

This appendix is supplemental to chapter 5, and elaborates on the general models from literature used for hot-film application of the PressureWire in assessment of blood flow in the coronary arteries.

The velocity and temperature field in a given domain may be analyzed using the general equations of conservation of mass, momentum and energy. Using these equations for the specific problem of the convective heat transfer from a heated sensor to a fluid flowing past it, a theoretical relation between heat transfer and flow may be derived for the stationary situation. Furthermore, the influence of instationary flow to this relation may be described analytically as well. In this appendix the general form of the governing equations will be described, as well as the specific boundary layer theory leading to the heat transfer-flow relation at stationary conditions. Furthermore, earlier studies on instationary flow will be discussed to obtain insight in the effect of deviations from the general boundary layer theory.

A.2 Governing equations

A.2.1 Conservation of mass, momentum and energy

The general equations describing the velocity, pressure and temperature field are the laws of conservation of mass, momentum and energy. The conservation laws can be derived regarding a control volume $d\Omega$ (Schlichting and Gersten, 2000). Conservation of mass requires that the rate of change of mass inside the control volume $d\Omega$ is equal to the mass flux across the boundary. The momentum may be described as the product of the mass of the control volume and its velocity. The momentum equation states that mass times acceleration equals the net force on the volume. This net force consists of

body ($\rho\vec{f}$) and surface forces (pressure and friction forces). When incompressibility is assumed, the combination of the mass and momentum balance equations are the Navier-Stokes equations:

$$\nabla \cdot \vec{u} = 0 \quad (\text{A.1})$$

$$\rho \left[\frac{\partial \vec{u}}{\partial t} + (\vec{u} \cdot \nabla) \vec{u} \right] = -\nabla p + \eta \nabla^2 \vec{u} + \rho \vec{f} \quad (\text{A.2})$$

The temperature-dependent density in the (gravity only) body force term can be described using the thermal expansion coefficient β at constant pressure in the Boussinesq approximation:

$$\beta = -\frac{1}{\rho} \left(\frac{\partial \rho}{\partial T} \right)_p \quad (\text{A.3})$$

$$\rho \vec{f} = \rho_a \vec{g} (1 - \beta(T - T_a)) \quad (\text{A.4})$$

where T is temperature and T_a and $\rho_a = \rho(T = T_a)$ are temperature and density in the main flow respectively. Henceforth $\rho = \rho_a$ is assumed.

According to the first law of thermodynamics, the net enthalpy of the control volume $d\Omega$ is equal to the sum of the heat transfer and the power, represented by the viscous dissipation term Φ :

$$\rho c_p \left[\frac{\partial T}{\partial t} + (\vec{u} \cdot \nabla) T \right] = -k \nabla^2 T + \eta \Phi \quad (\text{A.5})$$

$$\begin{aligned} \Phi = 2(\mathbf{D} : \mathbf{D}) = 2 \left[\left(\frac{\partial u}{\partial x} \right)^2 + \left(\frac{\partial v}{\partial y} \right)^2 + \left(\frac{\partial w}{\partial z} \right)^2 \right] + \left[\left(\frac{\partial u}{\partial y} \right) + \left(\frac{\partial v}{\partial x} \right) \right]^2 + \\ \left[\left(\frac{\partial w}{\partial y} \right) + \left(\frac{\partial v}{\partial z} \right) \right]^2 + \left[\left(\frac{\partial u}{\partial z} \right) + \left(\frac{\partial w}{\partial x} \right) \right]^2 \end{aligned} \quad (\text{A.6})$$

k is the thermal conductivity and c_p is specific heat. The heat flux q is defined by Fourier's law of heat conduction:

$$q = -k \nabla T \quad (\text{A.7})$$

q is also assumed to be linear with the temperature difference between the PressureWire sensor and the blood, coupled by the heat transfer coefficient h

$$q = h(T_s - T_a) \quad (\text{A.8})$$

(Bejan, 1995; Oosthuizen and Naylor, 1999; Schlichting and Gersten, 2000)

A.2.2 Scaling

To estimate the relative importance of the terms in (A.1), (A.2) and (A.5) for characteristic values of the variables in coronary artery assessment with the PressureWire, scaling analysis is performed. The equations are transformed into dimensionless form using the following substitutions:

$$\vec{u}^* = \frac{\vec{u}}{U} \quad x^* = \frac{x}{L} \quad p^* = \frac{p}{\rho U^2} \quad t^* = \frac{t}{\theta} \quad \vec{f}^* = \frac{\vec{f}}{U^2/L} \quad T^* = \frac{T}{\tau} \quad \Delta T^* = \frac{T - T_a}{T_s - T_a} \quad (\text{A.9})$$

In terms of these dimensionless variables and after rearranging, the conservation equations (A.1), (A.2) and (A.5) become respectively:

$$\nabla \cdot \vec{u}^* = 0 \quad (\text{A.10})$$

$$Sr \frac{\partial \vec{u}^*}{\partial t^*} + (\vec{u}^* \cdot \nabla) \vec{u}^* + \nabla p^* - \frac{1}{Re} \nabla^2 \vec{u}^* - \frac{Gr}{Re^2} \Delta T^* = \vec{f}^* \quad (\text{A.11})$$

$$Sr \frac{\partial T^*}{\partial t^*} + (\vec{u}^* \cdot \nabla) T^* + \frac{1}{RePr} \nabla^2 T^* + \frac{Ec}{Re} \Phi^* = 0 \quad (\text{A.12})$$

The significance of each term in this set of equations is now determined by: the Strouhal number, the dimensionless frequency,

$$Sr = \frac{L}{\theta U} \quad (\text{A.13})$$

the Reynolds number, the ratio between inertia and viscous forces,

$$Re = \frac{\rho U L}{\eta} \quad (\text{A.14})$$

the Grashof number, the ratio between buoyancy and viscous convective forces,

$$Gr = \frac{g \rho^2 \beta \Delta T L^3}{\eta^2} \quad (\text{A.15})$$

the Prandtl number, the relative importance of viscous vs. thermal diffusivity,

$$Pr = \frac{\eta c_p}{k} = \frac{\nu}{\alpha} \quad (\text{A.16})$$

with thermal diffusivity α

$$\alpha = \frac{k}{\rho c_p} \quad (\text{A.17})$$

and the Eckert number,

$$Ec = \frac{U^2}{c_p \Delta T} \quad (\text{A.18})$$

Table A.1: Characteristic parameters Clark (1974); Lide (2006)

	blood	water at 37 °C		
U	0.1	0.1	[m/s]	mean blood flow velocity at rest
L	$1.5 \cdot 10^{-3}$	$1.5 \cdot 10^{-3}$	[m]	radius of coronary artery
ρ	1050	994	[kg/m ³]	density at 37°C
θ	1	1	[s]	inverse frequency of 1st harmonic
ΔT	20	20	[K]	temperature difference between sensor and fluid
c_p	$3.60 \cdot 10^3$	$4.18 \cdot 10^3$	[J/kgK]	specific heat at constant pressure
k	0.55	0.62	[W/mK]	thermal conductivity
η	$4.0 \cdot 10^{-3}$	$6.9 \cdot 10^{-4}$	[kg/ms]	dynamic viscosity
ν	$3.8 \cdot 10^{-6}$	$0.7 \cdot 10^{-6}$	[m ² /s]	kinematic viscosity
α	$1.46 \cdot 10^{-7}$	$1.50 \cdot 10^{-7}$	[m ² /s]	thermal diffusivity
β	$3.4 \cdot 10^{-4}$	$3.6 \cdot 10^{-4}$	[1/K]	thermal expansion coefficient
g	9.81	9.81	[m/s ²]	gravitational acceleration

From Clark 1974 the characteristic values for flow in the coronary arteries in table A.1 are obtained. Using these values the order of magnitude of the dimensionless groups can be calculated. The values for water as a flow medium are also derived, when applicable, values are presented as [blood, water].

$Re = [40, 214]$ indicates that convection cannot be neglected compared to diffusion in the flow field. $Sr = 1.5 \cdot 10^{-2}$ is small, therefore little instationary effects can be expected. The Peclet number $Pe = RePr = [1040, 1006]$ is large, so the heat transfer is convection-dominated. Viscous dissipation can be ignored because $Ec/Re = [3.5 \cdot 10^{-9}, 2.6 \cdot 10^{-12}]$. And finally, $Gr/Re^2 = [1 \cdot 10^{-2}, 1 \cdot 10^{-2}]$, indicating that the influence of the temperature difference on the velocity field is negligible. The process of heat transfer in such flows is described as forced convection.

Using the conclusions from the scaling analysis and assuming no external forces are applied (A.1), (A.2) and (A.5) reduce to

$$\nabla \cdot \vec{u} = 0 \quad (\text{A.19})$$

$$\rho(\vec{u} \cdot \nabla)\vec{u} = -\nabla p + \eta \nabla^2 \vec{u} \quad (\text{A.20})$$

$$\rho c_p(\vec{u} \cdot \nabla)T = -k \nabla^2 T \quad (\text{A.21})$$

In this set of equations, where the temperature dependency of η is neglected, the mass and momentum equations are decoupled from the energy equations. Hence the velocity field can be determined without taking into account the heating of the sensor. Moreover, the heat transfer can be analyzed assuming a given velocity field, which will be discussed next.

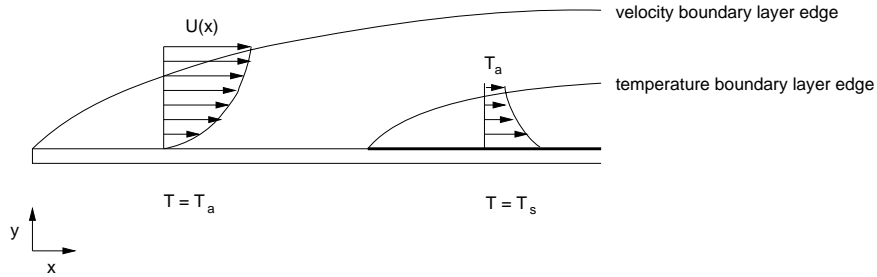


Figure A.1: Development of the velocity (or viscous) and temperature boundary layers for flow along a partially heated flat plate.

A.3 Steady flow and heat transfer

A.3.1 Boundary layer theory

In this section the general boundary layer theory leading to boundary layers such as in figure A.1 for a partially heated plate will be described.

Viscous boundary layer

To satisfy the no-slip condition (zero velocity on the wall due to viscosity of the fluid), viscosity must be incorporated for the solution of the set of equations derived in the previous section. The concept of the viscous boundary layer implies that in the bulk of the flow region inviscid flow may be assumed, but in a thin layer close to the wall viscosity plays a role.

The thickness of the viscous boundary layer can be estimated using the definition that at the interface between the boundary layer and the inviscid flow region inertial forces and friction forces in the momentum equations are of the same order of magnitude. Coordinate x is scaled with the characteristic length scale L , y with the thickness of the boundary layer δ . From the conservation of mass for incompressible fluids (A.19)

$$\frac{\partial u}{\partial x} + \frac{\partial v}{\partial y} = 0 \quad (\text{A.22})$$

it can be derived that

$$\frac{U}{L} \sim \frac{V}{\delta} \quad (\text{A.23})$$

In case of a relatively thin boundary layer terms of $O(\delta/L)$ can be neglected, therefore the momentum equation in the direction of the flow (x) in stationary flow can be written as

$$\rho(u \frac{\partial u}{\partial x} + v \frac{\partial u}{\partial y}) = -\frac{\partial p}{\partial x} + \eta \frac{\partial^2 u}{\partial y^2} \quad (\text{A.24})$$

At the interface between boundary layer and inviscid core the order of magnitude estimation gives, using (A.23)

$$\rho \frac{U^2}{L} \sim \eta \frac{U}{\delta^2} \quad (\text{A.25})$$

The expression for the boundary layer thickness then becomes

$$\delta \sim \sqrt{\frac{\eta L}{\rho U}} \quad (\text{A.26})$$

or

$$\frac{\delta}{L} \sim Re_L^{-\frac{1}{2}} \quad (\text{A.27})$$

with

$$Re_L = \frac{\rho U L}{\eta} \quad (\text{A.28})$$

Temperature boundary layer

From the scaling analysis it follows that because of the small Grashof number only forced convection occurs: the velocity field is decoupled from the temperature field and all material properties are assumed temperature-independent. In a similar way as (A.24), the energy equation for the temperature boundary layer is obtained

$$u \frac{\partial T}{\partial x} + v \frac{\partial T}{\partial y} = \alpha \frac{\partial^2 T}{\partial y^2} \quad (\text{A.29})$$

In the thermal boundary layer there is a balance between conduction from the wall into the flow and convection parallel to the wall. Since the velocity profile in the boundary layer is dependent on the viscosity, the Prandtl number ($Pr = \nu/\alpha$) is the characteristic number for the thermal boundary layer. The thicknesses of the viscous (δ) and thermal (δ_T) boundary layers are proportional to the viscosity and thermal diffusivity respectively. Therefore the Prandtl number can be seen as a measure for the ratio of these thicknesses. In the limit case of $Pr \rightarrow \infty$ the entire thermal boundary layer lies in the region where the velocity profile depends linearly on y . For intermediate Prandtl numbers (for blood $Pr = 26$) this can occur as well if the viscous boundary layer is fully developed where the temperature boundary layer starts developing. In a fully developed tube flow this implies that the shear rate $\dot{\gamma}$ is linearly related to the velocity U (and flow rate Q)

$$\dot{\gamma} \sim U \sim Q \quad (\text{A.30})$$

The equilibrium in the thermal boundary layer is evaluated from (A.29). Since the velocity profile is assumed linear in the thermal boundary layer, u^* at $y = \delta_T$ is scaled

as in (A.31), the scale for v^* on the edge of the boundary layer then follows again from the continuity equation (A.19).

$$u^* \sim \dot{\gamma} \delta_T; \quad v^* \sim \dot{\gamma} \frac{\delta_T^2}{L} \ll u^* \quad (\text{A.31})$$

The equilibrium from (A.29) becomes

$$\dot{\gamma} \frac{\delta_T}{L} \sim \frac{\alpha}{\delta_T^2} \quad (\text{A.32})$$

and the expression for δ_T is found

$$\delta_T^3 \sim \frac{\alpha L}{\dot{\gamma}} \sim Pr^{-1} \dot{\gamma}^{-1} \nu L \quad (\text{A.33})$$

or

$$\delta_T \sim Pr^{-\frac{1}{3}} \dot{\gamma}^{-\frac{1}{3}} (\nu L)^{\frac{1}{3}} \quad (\text{A.34})$$

Bejan (1995); Schlichting and Gersten (2000). An analytical solution for this partially heated flat-plate heat transfer was first obtained by L ev eque (1928) (Pedley, 1972a). Here, the simplified model described above has been chosen to emphasize the generality of the approach regarding the deviations between the flat plate model and the PressureWire configuration.

A.4 Analysis of the hot-film anemometer

The expressions for the viscous and thermal boundary layers (A.30) and (A.34) can be used to derive a first order approximation of the heat exchange in the hot-film configuration.

A.4.1 First order approximation

The definition for the heat flux q was given in section A.2.1 by (A.7) and (A.8):

$$q'' = -k \nabla T \equiv h(T_s - T_a) \quad (\text{A.35})$$

Combining the expression of the thermal boundary layer thickness (A.34) and (A.35) and assuming $\nabla T \sim \frac{(T_a - T_s)}{\delta_T}$ leads to

$$h = \frac{k}{\delta_T} \sim k Pr^{\frac{1}{3}} \dot{\gamma}^{\frac{1}{3}} (\nu L)^{-\frac{1}{3}} \quad (\text{A.36})$$

The relation between the mean heat transfer over the sensor and the sensor temperature T_s therefore becomes

$$q \sim h T_s \quad (\text{A.37})$$

where h is given by (A.36). For a sensor operated at constant temperature the relation between heat flux and shear rate would be

$$q \sim \dot{\gamma}^{\frac{1}{3}} \quad (\text{A.38})$$

Because deviations from the flat plate model are obvious and general in hot-film applications, a general dimensionless power-law model for forced-convection heat transfer is commonly used (Clark, 1974; Seed and Wood, 1970b). In this model an additional dimensionless number is used: the Nusselt number representing the dimensionless heat transfer.

$$Nu = \frac{hw}{k} \quad (\text{A.39})$$

where w is the length of the sensor normal to the stream direction. When the definition for heat transfer q being linear with the temperature difference is used

$$q = hwb\Delta T \quad (\text{A.40})$$

b is the sensor length in streamwise direction. Nu may be rewritten as

$$Nu = \frac{q}{b\Delta Tk} \quad (\text{A.41})$$

with b the sensor length in the streamwise direction. The relation between heat transfer and flow velocity (represented by the Reynolds number)

$$Nu = APr^m Re^n \quad (\text{A.42})$$

resembles A.38. The values for m and n depend on the geometry and position of the sensor: for the flat plate approximation $m = \frac{1}{3}$ and $n = \frac{1}{2}$, and when stationary flow in the annular case is assumed (as is the case in the current study), $n = \frac{1}{3}$.

A.5 Unsteady flow and heat transfer

In unsteady flow, the instantaneous relation between heat transfer and flow may deviate from the stationary situation. Influences may be separated in flow-related effects (the development of the viscous and thermal boundary layers over time) and capacitive effects (heat not only being transferred to the fluid, but also to the sensor substrate). In this section descriptions for both phenomena found in literature will be discussed.

A.5.1 Partially heated flat plate

For the partially heated flat plate model (figure A.1), the instationary behaviour of the viscous and thermal boundary layers in non-reversing sinusoidal flow has been described in complex mathematical models by Pedley (1972a; 1972b; 1976).

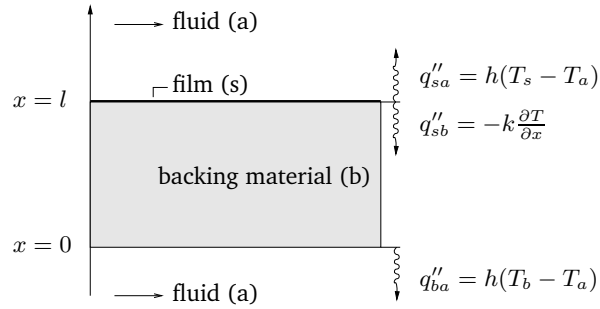


Figure A.2: 1D simplified model of the PressureWire sensor: the hot-film (resistance) is mounted on a backing material, heat is transferred from the film directly to the fluid at $x = l$, and via the backing material to the fluid at $x = 0$.

Based on a first characteristic parameter in the model, being a frequency parameter resembling the Strouhal number ($Str = fL/U$, L now being the characteristic length over which the viscous boundary layer develops), two asymptotic expansions for small and large Str were defined, allowing analysis of the problem on the entire domain. Results indicate increasing phase lag between flow and heat transfer with increasing Str , as well as a decreased amplitude response (both effects related to a relatively slowly developing boundary layer, the viscous boundary layer determines heat transfer, and requires a finite time to reach a steady state, dependent on flow velocity (Seed and Wood, 1970b) and a slightly decreased mean heat transfer, the oscillations were discussed to slightly reduce hot-film sensitivity to mean flow. A further overview of evaluation studies on non-reversing and reversing shear flow is presented by van Steenhoven and van de Beucken (1991).

A second determining parameter in the analysis was the amplitude of the oscillation of flow velocity \hat{U}/\bar{U} . For small amplitude the heat transfer was found to lag behind the local wall shear. For larger amplitude-offset ratio, the departure from the quasi-steady response (instationary effect) was larger, but the peak velocity was always determined more accurately than the minimal velocity. These results were qualitatively confirmed by the instationary calibration experiments by Seed and Wood (1970b) and Clark (1974).

A.5.2 Substrate-mounted hot-film

For incorporation of the capacitive effects of the sensor substrate, a dynamic model has been developed by Bellhouse (1968). The sensor configuration is simplified to the 1D model shown in figure A.2. The model can be schematically represented in an electrical model. From this dynamic model a description for the instationary heat transfer from the film will be derived. Both the backing material and the hot-film are in contact with the fluid flow with temperature T_a and flow velocity U . The heat transfer between the hot-film and the flow is defined as

$$q''_{sa} = h(T_s - T_a) \quad (\text{A.43})$$

the heat transfer to the backing material is

$$q''_{sb} = -k \frac{\partial T}{\partial x} \quad (\text{A.44})$$

and the heat transferred from the backing to the fluid

$$q''_{ba} = h(T_b - T_a). \quad (\text{A.45})$$

The coefficient h is assumed to be the single frequency dependent heat transfer coefficient in the model. From the electrical model the stationary total heat transfer coefficient h_{tot} for the heat transfer from the film can directly be found:

$$h_{tot,stat} = \frac{q''_{sa} + q''_{sb}}{T_s - T_a} = \frac{q''_{stat}}{T_s - T_a} = h \left(1 + \left(1 + \frac{lh}{k} \right)^{-1} \right) \quad (\text{A.46})$$

The total stationary heat transfer coefficient $h_{tot,stat}$ can be related to the flow velocity using viscous and thermal boundary layer theory as derived above (equations (A.36) and (A.38)).

For the determination of the frequency response of a dynamic system an input and output variable need to be chosen. The heat transfer q (the power needed to keep the sensor at the desired overheat temperature) is the output variable. Then any variation in temperature difference has an equal effect to a similar variation in h , since they are linearly coupled in the definition of q ($q = h\Delta T$). Hence h and T_s are kept constant, T_a is chosen to be the input variable and the transfer function is defined to relate the variations of heat flux from the hot-film to the variations of fluid temperature T_a . After normalization by $h_{tot,stat}$, an expression relating the stationary and instationary heat flux from the hot-film, the final $H(j\omega)$ is found (Bellhouse and Rasmussen, 1968)

$$H(j\omega, h) = \frac{q''_{sa} + q''_{sb}}{(q''_{sa} + q''_{sb})|_{\omega \rightarrow 0}} = \frac{1 + (\cosh(z) + \frac{hl}{k} \frac{\sinh(z)}{z})^{-1}}{(1 + (1 + \frac{hl}{k})^{-1})}. \quad (\text{A.47})$$

with

$$z = l \sqrt{\frac{\omega}{2\alpha}} (j - 1) \quad (\text{A.48})$$

and

$$\alpha = \frac{k}{\rho c_p}. \quad (\text{A.49})$$

$H(j\omega)$ is dependent of h , from (A.46) follows that h is derived from q''_{stat} . Hence in an instationary flow the transfer function varies with the flow: $H(j\omega, h)$, $h(q''_{stat})$, $q''_{stat}(U)$. The variability in T_a was taken out of $H(j\omega)$ and the transfer function and the power law model for the stationary heat transfer provide a relation between the input U and output q''_{instat} .

In the direct analysis of heat transfer in instationary flow, the h -dependency of the transfer function complicates the direct interpretation of the results. However, the results of Bellhouse and Rasmussen (1968) qualitatively demonstrate the effect of the substrate on the heat transfer: stronger phase shift and amplitude attenuation are found with decreasing cooling of the sensor.

A.6 Concluding discussion

From the analysis of unsteady boundary layers in the flat plate model, two determining parameters were found: a frequency parameter resembling the Strouhal number,

$$Sr = \frac{fL}{U} \quad (\text{A.50})$$

and the relative amplitude of the oscillation \hat{U}/\bar{U} of the flow velocity applied as

$$U(t) = \bar{U} + \hat{U} \sin(2\pi ft) \quad (\text{A.51})$$

All effects on the heat transfer - flow relation were described qualitatively: with increasing Sr , increasing phase lag, also amplitude decrease and slight decrease of mean heat transfer were found. An increase in \hat{U}/\bar{U} led to a larger departure from quasi-steady heat transfer. However, the deviations are stronger in the lower part of the flow cycle: at peak velocity the unsteady response resembles the steady response more closely.

From the analysis of the capacitive effects of the sensor substrate (or backing material), an additional phase lag in conduction, increasing errors with diminishing velocity and with increasing frequency and substrate dimensions were found.

Both analyses were performed for the partially heated flat plate model. Not only the dimensions of the sensor on the wire, but also the cavity in which the PressureWire sensor is placed may induce additional complexity in the local boundary layers of temperature and flow.

References

- W. Aarnoudse, W.F. Fearon, G. Manoharan, M. Geven, F. van de Vosse, M. Rutten, B. De Bruyne, and N.H.J. Pijls. Epicardial stenosis severity does not affect minimal microcirculatory resistance. *Circulation*, 110:2137–2142, 2004a.
- W. Aarnoudse, N.H.J. Pijls, S. Vercauteren, M. van 't Veer, P. Tonino, M.C.M. Rutten, M.C.F. Geven, B. De Bruyne, and F.N. van de Vosse. Direct volumetric blood flow measurement in coronary arteries by thermodilution: Part II: human validation. *J Am Coll Cardiol*, 49:in press, 2007.
- W. Aarnoudse, P. van den Berg, F. van de Vosse, M. Geven, M. Rutten, M. van Turnhout, W. Fearon, B. De Bruyne, and N.H.J. Pijls. Myocardial resistance assessed by guidewire-based pressure-temperature measurement: in vitro validation. *Catheter Cardiovasc Interv*, 62:56–63, 2004b.
- W.H. Aarnoudse. *Invasive assessment of the coronary microcirculation by pressure and temperature measurements*. PhD thesis, Eindhoven University of Technology, 2006.
- A.S. Abizaid, G.S. Mintz, R. Mehran, A. Abizaid, A.J. Lansky, A.D. Pichard, L.F. Satler, C. Wu, H. Pappas, K.M. Kent, and M.B. Leon. Long-term follow-up after percutaneous transluminal coronary angioplasty was not performed based on intravascular ultrasound findings: importance of lumen dimensions. *Circulation*, 100:256–261, 1999.
- T. Arts and R.S. Reneman. Interaction between intramyocardial pressure (IMP) and myocardial circulation. *J Biomech Eng*, 107:51–56, 1985.
- E. Barbato, W. Aarnoudse, W.R. Aengevaeren, G. Werner, V. Klauss, W. Bojara, I. Herzfeld, K.G. Oldroyd, N.H.J. Pijls, and B. De Bruyne. Validation of coronary flow reserve measurements by thermodilution in clinical practice. *European Heart Journal*, 25:219–223, 2004.
- G.J. Beauman and R.A. Vogel. Accuracy of individual and panel visual interpretations of coronary arteriograms: implications for clinical decisions. *J Am Coll Cardiol*, 16: 108–113, 1990.
- G.J.W. Bech, B. De Bruyne, N.H.J. Pijls, E.D. De Muinck, J.C. Hoorntje, J. Escaned, P.R. Stella, E. Boersma, J. Bartunek, J.J. Koolen, and W. Wijns. Fractional flow reserve to determine the appropriateness of angioplasty in moderate coronary stenosis: a randomized trial. *Circulation*, 103:2928–2934, 2001.
- A. Bejan. *Convection heat transfer*. John Wiley & Sons, New York, 2nd edition, 1995.

- G.A. Beller and B.L. Zaret. Contributions of nuclear cardiology to diagnosis and prognosis of patients with coronary artery disease. *Circulation*, 101:1465–1478, 2000.
- B.J. Bellhouse and C.G. Rasmussen. Low-frequency characteristics of hot-film anemometers. *DISA Information*, 6:3–10, 1968.
- J.M. Bland and D.G. Altman. Statistical methods for assessing agreement between two methods of clinical measurement. *Lancet*, 327:307–310, 1986.
- P.H.M. Bovendeerd, P. Borsje, T. Arts, and F.N. van de Vosse. Dependence of intramyocardial pressure and coronary flow on ventricular loading and contractility: a model study. *Ann Biomed Eng*, 34:1833–1845, 2006.
- T.S. Boyne, B.A. Koplan, W.J. Parsons, W.H. Smith, D.D. Watson, and G.A. Beller. Predicting adverse outcome with exercise SPECT technetium-99m sestamibi imaging in patients with suspected or known coronary artery disease. *Am J Cardiol*, 79:270–274, 1997.
- P. Bruinsma, T. Arts, J. Dankelman, and J.A.E. Spaan. Model of the coronary circulation based on pressure dependence of coronary resistance and compliance. *Basic Res Cardiol*, 83:510–524, 1988.
- H.H. Bruun. Hot-film anemometry in liquid flows. *Meas Sci Technol*, 7:1301–1312, 1996.
- S.A.J. Chamuleau, M. Siebes, K.T. Meuwissen, M. Koch, J.A.E. Spaan, and J.J. Piek. Association between coronary lesion severity and distal microvascular resistance in patients with coronary artery disease. *Am J Physiol Heart Circ Physiol*, 285:2194–2200, 2003.
- C. Clark. Thin film gauges for fluctuating velocity measurements in blood. *J Phys E Sci Instrum*, 7:548–556, 1974.
- B. De Bruyne, J. Bartunek, S.U. Sys, N.H.J. Pijls, G.R. Heyndrickx, and W. Wijns. Simultaneous coronary pressure and flow velocity measurements in humans: feasibility, reproducibility, and hemodynamic dependence of coronary flow velocity reserve, hyperemic flow versus pressure slope index, and fractional flow reserve. *Circulation*, 94:1842–1849, 1996.
- B. De Bruyne, F. Hersbach, N.H.J. Pijls, J. Bartunek, J.W. Bech, G.R. Heyndrickx, K.L. Gould, and W. Wijns. Abnormal epicardial coronary resistance in patients with diffuse atherosclerosis but "normal" coronary angiography. *Circulation*, 104:2401–2406, 2001a.
- B. De Bruyne, N.H.J. Pijls, G.R. Heyndrickx, R. Hodeige, R. Kirkeeide, and K.L. Gould. Pressure-derived fractional flow reserve to assess serial epicardial stenoses: theoretical basis and animal validation. *Circulation*, 101:1840–1847, 2000.
- B. De Bruyne, N.H.J. Pijls, L. Smith, M. Wievegg, and G.R. Heyndrickx. Coronary thermodilution to assess flow reserve: experimental validation. *Circulation*, 104:2003–2006, 2001b.
- J.M. Downey and E.S. Kirk. Inhibition of coronary blood flow by a vascular waterfall mechanism. *Circ Res*, 36:753–760, 1975.

- E. Falk, P.K. Shah, and V. Fuster. Coronary plaque disruption. *Circulation*, 92:657–671, 1995.
- W.F. Fearon, W. Aarnoudse, N.H.J. Pijls, B. De Bruyne, L.B. Balsam, D.T. Cooke, R.C. Robbins, P.J. Fitzgerald, A.C. Yeung, and P.G. Yock. Microvascular resistance is not influenced by epicardial coronary artery stenosis severity: experimental validation. *Circulation*, 109:2269–2272, 2004.
- W.F. Fearon, L.B. Balsam, H.M.O. Farouque, R.C. Robbins, P.J. Fitzgerald, P.G. Yock, and A.C. Yeung. Novel index for invasively assessing the coronary microcirculation. *Circulation*, 107:3129–3132, 2003.
- O. Frøbert, M. van 't Veer, W. Aarnoudse, U. Simonsen, and N.H.J. Pijls. Acute myocardial infarction and underlying stenosis severity. *Cathet Cardiovasc Interv*, 2007. in press.
- W. Ganz, K. Tamura, H.S. Marcus, R. Donoso, S. Yoshida, and H.J. Swan. Measurement of coronary sinus blood flow by continuous thermodilution in man. *Circulation*, 44:181–195, 1971.
- M.C.F. Geven, V.N. Bohté, W.H. Aarnoudse, P.M.J. van den Berg, M.C.M. Rutten, N.H.J. Pijls, and F.N. van de Vosse. A physiologically representative in-vitro model of the coronary circulation. *Physiol Meas*, 25:891–904, 2004.
- K.L. Gould. *Coronary artery stenosis and reversing atherosclerosis*. Arnold, London, 2nd edition, 1999.
- K.L. Gould, R.L. Kirkeeide, and M. Buchi. Coronary flow reserve as a physiologic measure of stenosis severity. *J Am Coll Cardiol*, 15:459–474, 1990.
- C.M. Grondin, I. Dyrda, A. Paternac, L. Campeau, M.G. Bourassa, and Lesperance J. Discrepancies between cine angiography and post-mortem findings in patients with coronary artery disease and recent revascularisation. *Circulation*, 49:503–708, 1974.
- T. Ibrahim, S.G. Nekolla, K. Schreiber, K. Odaka, S. Volz, J. Mehilli, M. Guthlin, W. Delius, and Schwaiger M. Assessment of coronary flow reserve: comparison between contrast-enhanced magnetic resonance imaging and positron emission tomography. *J Am Coll Cardiol*, 39:864–870, 2002.
- J.M. Isner, J. Kishel, and K.M. Kent. Accuracy of angiographic determination of left main coronary arterial narrowing. *Circulation*, 63:1056–1061, 1981.
- K. Iwakura, H. Ito, N. Nishikawa, K. Hiraoka, K. Sugimoto, Y. Higashino, T. Masuyama, M. Hori, K. Fujii, and T. Minamino. Early temporal changes in coronary flow velocity patterns in patients with acute myocardial infarction demonstrating the "no-reflow" phenomenon. *Am J Cardiol*, 84:415–419, 1999.
- M.P. Judkins. Selective coronary arteriography. I. A percutaneous transfemoral approach. *Radiology*, 89:815–824, 1967.
- M.J. Kern. Interpretation of cardiac pathophysiology from pressure waveform analysis: coronary hemodynamics. Part II: patterns of coronary flow velocity. *Cathet Cardiovasc Diagn*, 25:154–160, 1992.
- M.J. Kern. Coronary physiology revisited: practical insights from the catheterization laboratory. *Circulation*, 101:1344–1351, 2000.

- M.J. Kern, F.V. Aguirre, T.J. Donohue, R.J. Bach, E.A. Caracciolo, M.S. Flynn, T. Wolford, and J.A. Moore. Continuous coronary flow velocity monitoring during coronary interventions: velocity trend patterns associated with adverse events. *Am Heart J*, 128:426–434, 1994.
- M.J. Kern, A. Lerman, J.-W. Bech, B. De Bruyne, E. Eeckhout, W.F. Fearon, S.T. Higano, M.J. Lim, M. Meuwissen, J.J. Piek, N.H.J. Pijls, M. Siebes, and J.A.E. Spaan. Physiological assessment of coronary artery disease in the cardiac catheterization laboratory. *Circulation*, 114:1321–1341, 2006.
- R. Krams, P. Sipkema, and N. Westerhof. Varying elastance concept may explain coronary systolic flow impediment. *Am J Physiol*, 257:H1471–H1479, 1989a.
- R. Krams, P. Sipkema, J. Zegers, and N. Westerhof. Contractility is the main determinant of coronary systolic flow impediment. *Am J Physiol*, 257:H1936–H1944, 1989b.
- R. Krams, A.C.T.A. van Haelst, P. Sipkema, and N. Westerhof. Can coronary systolic-diastolic flow differences be predicted by left-ventricular pressure or time-varying intramyocardial elastance? *Basic Res Cardiol*, 84:149–159, 1989c.
- M.A. L ev eque. Transmission de chaleur par convection. *Ann Mines*, 13:283–362, 1928.
- D.R. Lide, editor. *CRC Handbook of chemistry and physics: a ready-reference book of chemical and physical data*. CRC Press, 87th edition, 2006.
- W.C. Little, M. Constantinescu, R.J. Applegate, M.A. Kutcher, P.A. Burrows, F.R. Kahl, and W.P. Santamore. Can coronary angiography predict the site of a subsequent myocardial infarction in patients with mild-to-moderate coronary artery disease? *Circulation*, 78:1157–1166, 1988.
- M. Marzilli, G. Sambuceti, S. Fedele, and A. L'Abbate. Coronary microcirculatory vasoconstriction during ischemia in patients with unstable angina. *J Am Coll Cardiol*, 35:327–334, 2000.
- K. Matthys, S. Carlier, P. Segers, J. Ligthart, G. Sianos, P. Serrano, P.R. Verdonck, and P.W. Serruys. In vitro study of FFR, QCA, and IVUS for the assessment of optimal stent deployment. *Cathet Cardiovasc Intervent*, 54:363–375, 2001.
- P. Meier and K.L. Zierler. On the theory of the indicator-dilution method for measurement of blood flow and volume. *J Appl Physiol*, 6:731–744, 1954.
- M. Meuwissen, M. Siebes, J.A.E. Spaan, and J.J. Piek. Rationale of combined intracoronary pressure and flow velocity measurements. *Z Kardiol*, 91:III108–III112, 2002.
- R.M. Nerem, J.A. Rumberger, D.R. Gross, W.W. Muir, and G.L. Geiger. Hot film coronary artery velocity measurements in horses. *Cardiovasc Res*, 3:301–313, 1976.
- M.K.C. Ng, A.C. Yeung, and W.F. Fearon. Invasive assessment of the coronary microcirculation: superior reproducibility and less hemodynamic dependence of index of microcirculatory resistance compared with coronary flow reserve. *Circulation*, 113:2054–2061, 2006.

- S.P. Nolan. The normal mitral valve: patterns of instantaneous mitral valve flow and the atrial contribution to ventricular filling. In D. Kalmanson, editor, *The Mitral Valve: a Pluridisciplinary Approach, Proc. 1st Int. Symp. on the Mitral Valve (Paris, 1975)*, page 139, London, 1976. Arnold.
- P.H. Oosthuizen and D. Naylor. *An introduction to convective heat transfer analysis*. McGraw-Hill, New York, 1999.
- P.K. Paulsen. The hot-film anemometer - a method for blood velocity determination. I. In vitro comparison with the electromagnetic blood flowmeter. *Eur Surg Res*, 12: 140–148, 1980a.
- P.K. Paulsen. The hot-film anemometer - a method for blood velocity determination. II. In vivo comparison with the electromagnetic blood flow meter. *Eur Surg Res*, 12: 149–158, 1980b.
- D. Pavin, J. Delonca, M. Siegenthaler, M. Doat, W. Rudishauser, and A. Righetti. Long-term (10 years) prognostic value of a normal thallium-201 myocardial exercise scintigraphy in patients with coronary artery disease documented by angiography. *Eur Heart J*, 18:69–77, 1997.
- T.J. Pedley. On the forced heat transfer from a hot film embedded in the wall in two-dimensional unsteady flow. *J Fluid Mech*, 55:329–357, 1972a.
- T.J. Pedley. Two-dimensional boundary layers in a free stream which oscillates without reversing. *J Fluid Mech*, 55:359–383, 1972b.
- T.J. Pedley. Heat transfer from a hot-film in reversing shear flow. *J Fluid Mech*, 78: 513–534, 1976.
- N.H.J. Pijls, W.R. Aengevaeren, G.J. Uijen, A. Hoevelaken, T. Pijnenburg, K. van Leeuwen, and T. van der Werf. Concept of maximal flow ratio for immediate evaluation of percutaneous transluminal coronary angioplasty result by videodensitometry. *Circulation*, 83:854–865, 1991.
- N.H.J. Pijls, B. De Bruyne, G.J.W. Bech, F. Liistro, G.R. Heyndrickx, H.J. Bonnier, and J.J. Koolen. Coronary pressure measurement to assess the hemodynamic significance of serial stenoses within one coronary artery: validation in humans. *Circulation*, 102:2371–2377, 2000.
- N.H.J. Pijls, B. De Bruyne, L. Smith, W. Aarnoudse, E. Barbato, J. Bartunek, G.J.W. Bech, and F.N. van de Vosse. Coronary thermodilution to assess flow reserve: validation in humans. *Circulation*, 105:2482–2486, 2002.
- N.H.J. Pijls, B van Gelder, P. van der Voort, K. Peels, F.A.L.E. Bracke, H.J.R.M. Bonnier, and M.I.H. El Gamal. Fractional flow reserve. A useful index to evaluate the influence of an epicardial coronary stenosis on myocardial blood flow. *Circulation*, 92:3183–3193, 1995.
- N.H.J. Pijls, J.A.M. van Son, R.L. Kirkeeide, B. De Bruyne, and K.L. Gould. Experimental basis of determining maximum coronary, myocardial, and collateral blood flow by pressure measurements for assessing functional stenosis severity before and after Percutaneous Transluminal Coronary Angioplasty. *Circulation*, 86: 1354–1367, 1993.

- N.H.J. Pijls, M. van 't Veer, J. ter Woorst, W. Aarnoudse, E. van Hagen, M.C.F. Geven, M.C.M. Rutten, B. De Bruyne, and F.N. van de Vosse. Direct volumetric blood flow measurement in coronary arteries by thermodilution: Part I: experimental validation. *J Am Coll Cardiol*, 49:in press, 2007.
- W.T. Porter. The influence of the heart-beat on the flow of blood through the walls of the heart. *Am J Physiol*, 1:145–163, 1898.
- R. Putz and R. Pabst. *Atlas of human anatomy*. Urban and Schwarzenberg, Munich, Germany, 1994.
- S.A. Rebergen, E.E. van der Wall, J. Doornbos, and A. de Roos. Magnetic resonance measurement of velocity and flow: Technique, validation, and cardiovascular applications. *Am Heart J*, 126:1439–1456, 1993.
- H. Sakuma, L.M. Blake, T.M. Amidon, M. O'Sullivan, D.H. Szolar, A.P. Furber, M.A. Bernstein, T.K. Foo, and C.B. Higgins. Coronary flow reserve: noninvasive measurement in humans with breath-hold velocity-encoded cine MR imaging. *Radiology*, 198:745–750, 1996.
- G. Sambuceti, M. Marzilli, S. Fedele, C. Marini, and A. L'Abbate. Paradoxical increase in microvascular resistance during tachycardia downstream from a severe stenosis in patients with coronary artery disease. *Circulation*, 103:2352–2360, 2001.
- W. Schaper, G. Gorge, B. Winkler, and J. Schaper. The collateral circulation of the heart. *Prog Cardiovasc Dis*, 31:57–77, 1988.
- H. Schelbert, G. Wisenberg, M. Phelps, K. Gould, H. Eberhard, E. Hoffman, A. Gormesm, and D. Kuhl. Noninvasive assessment of coronary stenosis by myocardial imaging during pharmacologic coronary vasodilation. VI. Detection of coronary artery disease in man with intravenous [¹³N]*ammonia and positron computed tomography. *Am J Cardiol*, 49:1197, 1982.
- H. Schlichting and K. Gersten. *Boundary layer theory*. Springer-Verlag, Heidelberg, 8th edition, 2000.
- M. Schwaiger and O. Muzik. Assessment of myocardial perfusion by positron emission tomography. *Am J Cardiol*, 67:35D–43D, 1991.
- W.A. Seed and N.B. Wood. An apparatus for calibrating velocity probes in liquids. *J Phys E Sci Instrum*, 2:896–898, 1969.
- W.A. Seed and N.B. Wood. Development and evaluation of a hot-film velocity probe for cardiovascular studies. *Cardiovascular Research*, 4:253–263, 1970a.
- W.A. Seed and N.B. Wood. Use of a hot-film velocity probe for cardiovascular studies. *J Phys E Sci Instrum*, 3:377–384, 1970b.
- W.A. Seed and N.B. Wood. Application of constant temperature anemometry in measurement of intra-arterial blood flow velocity. *Int J Engng Sci*, 10:1009–1021, 1972.
- P. Segers, G. Fostier, J. Neckebroek, and P. Verdonck. Assessing coronary artery stenosis severity: in vitro validation of the concept of fractional flow reserve. *Cathet Cardiovasc Intervent*, 46:375–379, 1999.

- PK. Shah. Mechanisms of plaque vulnerability and rupture. *J Am Coll Cardiol*, 41: 15–22, 2003.
- M. Siebes, B.-J. Verhoeff, M. Meuwissen, R.J. de Winter, J.A.E. Spaan, and J.J. Piek. Single-wire pressure and flow velocity measurement to quantify coronary stenosis hemodynamics and effects of percutaneous interventions. *Circulation*, 109:756–762, 2004.
- F.M. Sones and E.K. Shirey. Cine coronary arteriography. *Med Concepts Cardiovasc Dis*, 31:735–738, 1962.
- J.A.E. Spaan, N.P.W. Breuls, and J.D. Laird. Diastolic and systolic coronary flow differences are caused by intramyocardial pump action in the unanesthetized dog. *Circ Res*, 49:584–593, 1981.
- N. Stergiopoulos, B. Westerhof, and N. Westerhof. Total arterial inertance as the fourth element of the windkessel model. *Am J Physiol*, 276:H81–H88, 1999.
- H. Suga, K. Sakawa, and A.A. Shoukas. Load independence of the instantaneous pressure-volume ratio of the canine left ventricle and effects of epinephrine and heart rate on the ratio. *Circ Res*, 32:314–322, 1973.
- A.A. van Steenhoven and F.J.H.M. van de Beucken. Dynamical analysis of electrochemical wall shear rate measurements. *J Fluid Mech*, 231:599–614, 1991.
- J.-L.J. Vanoverschelde, W. Wijns, C. Depre, B. Essamri, G.R. Heyndrickx, M. Borgers, A. Bol, and J.A. Melin. Mechanisms of chronic regional posts ischemic dysfunction in humans: new insights from the study of noninfarcted collateral-dependent myocardium. *Circulation*, pages 1513–1523, 1993.
- G. Vassalli and O.M. Hess. Measurement of coronary flow reserve and its role in patient care. *Basic Res Cardiol*, 93:339–353, 1998.
- C.W. White. Clinical applications of Doppler coronary flow reserve measurements. *Am J Cardiol*, 71:10D–16D, 1993.
- R.F. Wilson. Looks aren't everything: FFR B4 U PTCA. *Circulation*, 103:2873–2875, 2001.
- R.F. Wilson, D.E. Laughlin, P.H. Ackell, W.M. Chilian, M.D. Holida, C.J. Hartley, M.L. Armstrong, M.L. Marcus, and C.W. White. Transluminal, subselective measurement of coronary artery blood flow velocity and vasodilator reserve in man. *Circulation*, 72:82–92, 1985.
- D. Zinemanas, R. Beyar, and S. Sideman. Relating mechanics, blood flow and mass transport in the cardiac muscle. *Int J Heat Mass Transfer*, 37:191–205, 1994.

Samenvatting

Het vaatstelsel dat de hartspier van bloed voorziet, wordt de coronaire circulatie genoemd. Overal in de coronaire circulatie, van de grote epicardiale kransslagaders buiten op het hart tot de kleinste capillairen in het hartspierweefsel, kunnen aandoeningen voorkomen die de bloedstroom belemmeren. Als ten gevolge van zo'n aandoening de weerstand ernstig toegenomen is, kan door de ontoereikende doorbloeding een tekort aan zuurstof en voedingsstoffen ontstaan in het hartspierweefsel. Dit wordt ischemie genoemd. In de catheterisatiekamer wordt bij patiënten met ischemie de coronaire circulatie in eerste instantie onderzocht met behulp van angiografie. Een angiogram is een röntgenfilmpje waarbij de coronairen zichtbaar worden gemaakt door het inspuiten van contrastvloeistof door een catheter die is ingebracht via de lies. Een nadeel van deze methode is dat alleen een kwalitatieve diagnose kan worden gesteld op basis van een twee-dimensionale projectie van een wellicht grillig gevormde vernauwing. Zo wordt de fysiologische ernst van de vernauwing gemakkelijk over- of onderschat. Om direct inzicht te krijgen in de toegenomen weerstand in het vat, is kwantitatieve informatie nodig over de bloeddruk en bloedvolumestroom. Druk en stroming kunnen worden gemeten tijdens catheterisatie met voedraden waarop sensoren zijn gemonteerd. Vanuit praktisch oogpunt is het wenselijk om één voedraad te hebben waarmee tegelijkertijd druk en stroming kan worden gemeten.

Het belangrijkste doel van de in dit proefschrift beschreven studies was het ontwikkelen van een methode om tegelijkertijd coronaire druk en bloedvolumestroom te meten met één enkele voedraad, de PressureWire (Radi Medical Systems, Uppsala, Zweden), waarop al een druk- en temperatuursensor aanwezig is. Tijdens de ontwikkeling moet de methode onder goed gecontroleerde omstandigheden getest worden. Bij *in-vivo* experimenten kunnen de omstandigheden vaak niet voldoende worden beheerst en vanuit ethisch oogpunt zijn alternatieven voor dieren- en patiëntenstudies zeer wenselijk. Een tweede doel van deze studie was dan ook het ontwikkelen van een alternatief in de vorm van een *in-vitro* model voor de coronaire circulatie.

Het ontwerp van het *in-vitro* model was gebaseerd op het gebruik van fysiologisch representatieve functionele elementen voor de verschillende componenten van de circulatie, ten aanzien van geometrie en functie. Het model bestond uit een computergestuurde pomp voor de linker ventrikel, een systemische en een coronaire circulatie. Met de systemische circulatie werd een fysiologische aortadruk gecreëerd,

als drijvende kracht voor de coronaire circulatie. Na het epicardiale vat splitste het model in een subendo- en subepicardiale tak. Het effect van het samentrekken van de hartspier op de weerstands- en volumeverandering in de subepicardiale tak werd nagebootst door een samendrukbaar slangetje. Dat werd door de linker ventrikel geleid en kon worden samengedrukt door de ventrikulaire druk tijdens de systole, de samentrekkingsfase van de ventrikels. Het model is getest op twee manieren. Als eerste werden de druk- en stromingsmetingen in het model vergeleken met (reeds bekende) metingen in mensen. Hierbij was een goede overeenkomst tussen de twee te zien. Ten tweede werden twee goed gevalideerde klinische meetmethoden waarbij gebruik wordt gemaakt van de PressureWire toegepast in het model (FFR en IMR bepaling). De twee methoden karakteriseren respectievelijk epicardiale en microvasculaire aandoeningen en resultaten van beide kwamen overeen met uitkomsten in de kliniek. Daarmee was aangetoond dat het model goed toepasbaar is voor de ontwikkeling van nieuwe coronaire meetmethoden waarbij een voerdraad met sensor wordt gebruikt.

Vervolgens werden twee meetmethoden voor het onderzoeken van coronaire bloedstroom ge-introduceerd en in eerste instantie *in-vitro* getest. De eerste was coronaire bloedstroommeting door continue infusie. Als een koude zoutoplossing continue wordt ge-infundeerd in de kransslagader, kan de bloedvolumestroom berekend worden uit de temperatuur van het bloed, de zoutoplossing, en het mengsel van de twee stroomafwaarts van de infusie, gecombineerd met de bekende infusievolumestroom. Het meetprincipe is ge-evalueerd, gebruikmakend van het *in-vitro* model van de coronaire circulatie. Hierbij is gekeken naar de bepalende randvoorwaarden voor coronaire stroommeting, met betrekking tot het ontwerp van de infusiecatheter, de grootte van de infusiestroom en de optimale posities voor het infunderen en meten van de temperatuur. Het bleek dat, als een goede catheter (met infusie door zijgaatjes) en een voldoende hoge infusiestroom worden gebruikt, de gemiddelde bloedstroom in de kransslagader voor de toepassing voldoende nauwkeurig bepaald kan worden.

Gebruikmakend van continue infusie kan de gemiddelde volumestroom worden bepaald, maar ook het fasisch patroon van de stroming in de coronairarteriën is klinisch interessant. Bovendien moet een klinische methode zo eenvoudig mogelijk te gebruiken zijn, terwijl voor continue infusie een uitgebreid protocol voor het infunderen en meten van de temperaturen moet worden gevolgd. Om beter in te spelen op deze klinische wensen, is een tweede methode voor stroommeting met de PressureWire ontwikkeld, de thermoconvectie-methode.

Thermoconvectie-stroommeting is gebaseerd op het principe van de hittefilm-anemometrie. Een weerstand op de sensor van de PressureWire wordt verwarmd tot een constante temperatuur boven de omgevingstemperatuur. Het elektrisch vermogen dat nodig is om dat temperatuurverschil te handhaven, kan gerelateerd worden aan de lokale volumestroom. De theoretische relatie tussen het elektrisch vermogen en de stroom is gebruikt om de sensor te kalibreren in stationaire en gemiddelde instationaire stroming in een glazen buis en in het model van de coronaire circulatie. Kalibratie voor gemiddelde stroming kon succesvol worden uitgevoerd: de stroming kon met een vergelijkbare nauwkeurigheid worden bepaald

als bij de continue infusie methode. Voor de dynamische respons in instationaire stroming is de geschatte stroming bepaald uit het elektrisch vermogen in de tijd, met behulp van de stationaire kalibratiecurve. Het fasische stromingspatroon was steeds duidelijk herkenbaar, maar verder onderzoek, bijvoorbeeld met numerieke simulaties, is nodig om de precieze overdracht tussen geschatte en werkelijke stroming te bepalen.

De thermoconvectie-methode is ook toegepast tijdens een dierstudie. Drie Yorkshire varkens werden ge-instrumenteerd met een epicardiale bloedstroommeter en de metingen van elektrisch vermogen en referentiestroming werden tegelijkertijd uitgevoerd. De kalibratiecurves uit de *in-vitro* experimenten werden ook toepasbaar bevonden in de *in-vivo* situatie, de nauwkeurigheid van de bepaling van de gemiddelde bloedstroom was vergelijkbaar met de *in-vitro* resultaten.

Samenvattend zijn in dit proefschrift de ontwikkeling en evaluatie van twee nieuwe methoden voor coronaire bloedstroommeting beschreven. Hierbij is gebruik gemaakt van een speciaal ontwikkeld *in-vitro* model van de coronaire circulatie. De eerste methode, continue infusie, behelst een ingewikkeld protocol en is afhankelijk van een goede keuze van randvoorwaarden, maar kan direct worden toegepast in de kliniek. De tweede methode, thermoconvectie, is erg gemakkelijk toe te passen en potentieel te gebruiken voor het meten van gemiddelde en fasische coronaire stroming in de catheterisatiekamer. Voorafgaand aan de werkelijke klinische toepassing moet nog verder numeriek, *in-vitro* en *in-vivo* onderzoek gedaan worden.

Dankwoord

Met veel plezier heb ik tijdens de afgelopen weken af en toe het lijstje van niet-vergeten-te-bedanken-mensen achter in mijn agenda bekeken en aangevuld. Nu het werk (grotendeels) gedaan is, is het prettig terugkijken op de afgelopen jaren.

Allereerst natuurlijk een woord van dank aan mijn promotoren, Frans van de Vosse en Nico Pijls. Jullie samenwerking is voor mij hét voorbeeld van hoe BMT-onderzoek uitgevoerd kan worden op het snijvlak tussen technologie en geneeskunde. Frans, bedankt voor je rustige en analytische kijk op het onderzoek en mij als onderzoeker. Ik vond het erg prettig dat je deur altijd openstond en dat je niet alleen de grote lijn goed in de gaten hield, maar ook meedacht met de vele inhoudelijke problemen en probleempjes. Nico, vaak heb ik me afgevraagd waar je de tijd en energie vandaan haalde om zo betrokken te zijn bij alles wat er in het onderzoek gebeurt. Mijn dank voor alle kansen, je ideeën en inhoudelijke verbeteringen van het werk, voor je betrokkenheid en voor de vasthoudendheid waarmee je me steeds herinnerde aan de klinische toepasbaarheid. Het begeleidingsteam werd gecompleteerd door mijn copromotor Marcel Rutten. Marcel, veel dank voor je begeleiding in alle opzichten, van de inhoudelijke besprekingen van alles wat in dit proefschrift beschreven staat en het ontwerp van de nieuwe versie van het coronairmodel, tot je vertrouwen in de goede afloop en het ondervangen van mijn onhandigheid in het lab.

Wilbert Aarnoudse was mijn klinische collega-promovendus binnen het project. Wilbert, een fijnere collega had ik me niet kunnen wensen. Bedankt voor onze samenwerking en de gezelligheid buiten het werk, ik heb veel van je geleerd. Ook veel dank aan Marcel van 't Veer, medisch ingenieur en promovendus in het ziekenhuis, voor je hulp, het overleg over alle aspecten van onze projecten en de minder werkgerelateerde gesprekken.

De mensen van Radi Medical Systems hebben steeds een grote bijdrage geleverd. In Nederland Huub Oomes en Monique van den Broek. Huub, dank voor je ondersteuning van het onderzoek, maar ik waardeer vooral ook je persoonlijke betrokkenheid. I would like to thank Lars Tenerz, Leif Smith, Mattias Tullberg, and Johan Svanerud of Radi Medical Systems, Uppsala, Sweden, for the inventive support in the project, and for the warm hospitality during my visits to Uppsala.

For the opportunity to perform the animal study, I would like to thank William Fearon and Yen-Dong Ho of Stanford University. I greatly enjoyed working with you, and your enthusiasm for the thermoconvection method was very motivating during the final phase of the project. Yen, thanks for making me feel at home during my stay

in Palo Alto.

De samenwerking met het Catharinaziekenhuis was onmisbaar en erg motiverend. De cardiologen en verpleegkundigen in het cathlab en Ingrid Aarts, bedankt voor jullie interesse en medewerking.

Een groot aantal stagiaires en afstudeerders heeft een bijdrage geleverd aan het onderzoek. Erwin, Fleur, Chantal, Leon, Ivo, Ferry, Marcel en Arjen, je zult niet allemaal direct je werk terugvinden in dit boekje, maar elk van jullie projecten heeft zeker zijn waarde gehad. Arjen, zonder jou ook in dit proefschrift geen hoofdstuk 5. Ik vind het erg leuk dat je je afstudeerwerk wilde voorzetten in een promotie-onderzoek.

Rens Kodde, Peter Hamels en Harrie van de Loo, bedankt voor het meedenken over en maken van de circuitjes en andere elektronica. Patrick van Brakel en Leo Wouters, wat ben ik blij dat jullie altijd klaarstonden om computers weer te laten doen wat ik wilde. Alice van Litsenburg, dankjewel voor de gezelligheid en alle keren dat ik rennend bij je binnen kwam en rustig weer naar buiten liep omdat het probleem was opgelost.

Collega's van vloer 4, bedankt voor de gezelligheid tijdens de koffiepauzes. Met zijn drieën is natuurlijk beter dan alleen: dank aan alle kamergenoten van de afgelopen jaren, Angélique, Ingrid, Yvonne, Christa en Roel. Sjoerd, ik hoop nog veel meer lief en leed met je te delen en natuurlijk nog vaak de slappe lach met je te hebben. Leonie, ik heb genoten van onze vakanties en hoop dat we nooit uitgepraat raken. Het lezen en corrigeren van het hele proefschrift was vast een hele klus voor iemand die niet betrokken was bij het onderzoek: Paul, bedankt.

Gelukkig had ik naast het werk op de TU een belangrijke uitlaatklep bij ESR Thêta. Vanaf het begin bij Dames 2003 (meiden, bedankt voor jullie enthousiasme en vriendschap!) heb ik me daar bijzonder thuis gevoeld. Veel dank dan ook aan alle roeiers, coaches, stuurtjes en anderen met wie ik heb samengewerkt. Rutger, bedankt dat je vaak mijn dag hebt goedgeemaakt door een goede training of wedstrijd te varen.

Hans, Marijke, Renske en Thijs, wat fijn dat jullie zo meelevén. Bart, ik ben blij dat jij mijn broertje bent. Pap en mam, jullie vinden het gewoon, maar voor mij is het toch heel bijzonder: bedankt voor jullie onvoorwaardelijke vertrouwen en steun vanaf het allereerste begin. Wat er ook gebeurt, jullie zullen altijd een thuis voor me blijven. Lieve Jeroen, door jouw rust en begrip was het een stuk gemakkelijker het werk af te maken. Met het verbouwen van ons huis moest ik je nog even in de steek laten, nu staan we gelukkig overal weer samen voor.

Maartje

Utrecht, augustus 2007

Curriculum Vitae

Maartje Geven werd geboren op 7 september 1979 in Geldrop. In 1997 behaalde zij haar gymnasium-diploma aan het Rythovius College in Eersel. Aansluitend studeerde zij Biomedische Technologie aan de Technische Universiteit Eindhoven, deel uitmakend van de eerste lichting studenten van deze nieuwe opleiding. Haar afstudeerwerk heeft zij uitgevoerd bij de sectie Cardiovasculaire Biomechanica binnen het project "Evaluation of the coronary circulation by guidewire-mounted sensors" in samenwerking met Radi Medical Systems en de afdeling cardiologie van het Catharinaziekenhuis. Na haar afstuderen, cum laude, begin 2003 heeft zij het werk binnen dat project voortgezet in een promotie-onderzoek, resulterend in dit proefschrift.

September 7, 1979	Born in Geldrop, The Netherlands
1991 - 1997	Secondary education, Rythovius College, Eersel
1997 - 2003	Master's degree (cum laude), Biomedical Engineering, Eindhoven University of Technology
2003 - 2007	PhD, Biomedical Engineering, Eindhoven University of Technology